

DEVELOPMENT OF A siRNA DELIVERY SYSTEM  
FOR THE TREATMENT OF OSTEOPOROSIS

A THESIS SUBMITTED TO  
THE GRADUATE SCHOOL OF NATURAL AND APPLIED SCIENCES  
OF  
MIDDLE EAST TECHNICAL UNIVERSITY

BY  
DENİZ SEZLEV BİLECEN

IN PARTIAL FULFILLMENT OF THE REQUIREMENTS  
FOR  
THE DEGREE OF DOCTOR OF PHILOSOPHY  
IN  
BIOTECHNOLOGY

MAY 2018



Approval of the thesis:

**DEVELOPMENT OF A siRNA DELIVERY SYSTEM FOR THE  
TREATMENT OF OSTEOPOROSIS**

submitted by **DENİZ SEZLEV BİLECEN** in partial fulfillment of the requirements  
for the degree of **Doctor of Philosophy in Biotechnology Department, Middle  
East Technical University** by,

Prof. Dr. Halil Kalıpçılar  
Dean, Graduate School of **Natural and Applied Sciences**

Assoc. Prof. Dr. Can Özen  
Head of Department, **Biotechnology, METU**

Prof. Dr. Vasıf Hasırcı  
Supervisor, **Dept. of Biological Sciences, METU**

Prof. Dr. Hasan Uludağ  
Co-supervisor, **Dept. of Chemical and Materials  
Engineering, University of Alberta**

**Examining Committee Members:**

Assoc. Prof. Dr. Ayşe Elif Erson Bensen  
Dept. of Biological Sciences, METU

Prof. Dr. Vasıf Hasırcı  
Dept. of Biological Sciences, METU

Assoc. Prof. Dr. Çağdaş Son  
Dept. of Biological Sciences, METU

Assoc. Prof. Dr. Güvem Gümüş Akay  
Brain Research Center, Ankara University

Asst. Prof. Dr. Yıldız Özalp  
Dept. of Pharmaceutical Technology,  
Near East University

Date: 02/05/2018

**I hereby declare that all information in this document has been obtained and presented in accordance with academic rules and ethical conduct. I also declare that, as required by these rules and conduct, I have fully cited and referenced all material and results that are not original to this work.**

Name, Last Name: Deniz SEZLEV BİLECEN

Signature:

## **ABSTRACT**

### **DEVELOPMENT OF A siRNA DELIVERY SYSTEM FOR THE TREATMENT OF OSTEOPOROSIS**

Sezlev Bilecen, Deniz

Ph.D., Department of Biotechnology

Supervisor: Prof. Dr. Vasıf Hasırcı

Co-Supervisor: Prof. Dr. Hasan Uludağ

May 2018, 118 pages

Osteoporosis, the most common disease of bone, is a skeletal disorder associated with low bone mass, increase in bone fragility and in susceptibility to fractures. The high bone resorption rate is shown to be due to increased number and activity of the osteoclasts. Receptor Activator of Nuclear Factor kappa B (RANK)/ Receptor Activator of Nuclear Factor kappa B Ligand (RANKL) system plays a crucial role in osteoclast differentiation and bone remodeling. RANKL participates in differentiation and activation of osteoclasts by binding to its receptor RANK expressed on osteoclast progenitors and mature osteoclasts. The currently used drugs for osteoporosis, such as use of bisphosphonates, Denosumab and teriparatide, have low bioavailability, long-term safety concerns and cause gastric problems. This led to the need for delivering the drugs in carrier systems to increase their bioavailability and decrease their side effects. In recent years, however, the increased understanding of molecular background of bone pathology, the use of RNA interference (RNAi) gained interest in developing new treatment strategies for the disease. Small interfering RNA (siRNA) is a double stranded RNA (dsRNA) molecule which is used in this context to inhibit the translation of abnormal gene expression in cells.

In this study, we developed a potentially intravenously injectable siRNA-delivery system that can target osteoclasts in bone tissue for the treatment of osteoporosis. Polyethyleneimine (PEI), a polycationic molecule, was used as a complex with RANK siRNA which was then loaded into poly(lactic acid-co-glycolic acid) (PLGA) nanocapsules. The loaded nanocapsules were coated with a genetically engineered osteoconductive polypeptide, Elastin like recombinamer (ELR) designed to attach especially to bone minerals, to specifically target the drug loaded nanocapsules to the bone tissue. The carrier system constructed was studied by Scanning Electron Microscopy (SEM), (Transmission Electron Microscopy) TEM and X-Ray Photoelectron Spectroscopy (XPS) to show the ELR coat on the capsules. Different nitrogen to phosphate ratios (N/P) (presenting PEI and siRNA, respectively) for the PEI:RANK siRNA complexes were studied to determine the least toxic and most effective complex which would lead to satisfactory RANK mRNA inhibition. As a result of that study, the N/P ratio of 20 was chosen to construct the complex to be loaded in the PLGA nanocapsules. The encapsulation efficiency of the PEI:RANK siRNA complex (N/P 20) into PLGA nanocapsules were 48% and its release kinetics followed the Higuchi kinetics for 15 days. The PEI:RANK siRNA loaded PLGA nanocapsules significantly inhibited RANK mRNA (53 %) in an osteoclast precursor cell line. The differentiation of the precursors into mature osteoclasts was also suppressed by the delivery system. Treatment of differentiating osteoclasts with the PEI:RANK siRNA loaded PLGA nanocapsules inhibited their osteoclastic activity. In conclusion, the delivery system designed has the potential to serve as an alternative treatment method for use in the treatment of osteoporosis.

**Keywords:** Osteoporosis, targeted delivery system, siRNA, Receptor Activator of Nuclear Factor kappa B (RANK), poly(lactic acid-co-glycolic acid) (PLGA).

## ÖZ

### KEMİK ERİMESİ TEDAVİSİ İÇİN BİR siRNA SALIM SİSTEMİ GELİŞTİRİLMESİ

Sezlev Bilecen, Deniz

Doktora., Biyoteknoloji Bölümü

Tez yöneticisi: Prof. Dr. Vasıf Hasırcı

Ortak tez yöneticisi: Prof. Dr. Hasan Uludağ

Mayıs 2018, 118 sayfa

En sık görülen kemik hastalığı olan kemik erimesi (osteoporoz), düşük kemik kütlesi ile karakterize edilen, kemik kırılabilirliğinin ve kırılmalara karşı duyarlılığın artmasından kaynaklanan bir iskelet sistemi hastalığıdır. Hastalıkta görülen yüksek kemik yıkımının sebebinin osteoklastların sayısal ve işlevsel olarak artmasından kaynaklı olduğu bilinmektedir. Osteoklast farklılaşması ve kemik yenilenmesinde reseptör aktivatör nükleer faktör kapp B (RANK)/reseptör aktivatör nükleer faktör kapp B ligandı (RANKL) sistemi çok önemli bir rol oynamaktadır. RANKL, osteoklast öncülerinin ve osteoklastların hücre zarları üzerinde bulunan RANK reseptörüne bağlanarak, bu öncülerin osteoklasta farklılaşmasında ve farklılaşmış olan osteoklastların işlevlerinin artmasında görev almaktadır. Günümüzde kullanılan bisfosfonatlar, Denasumab ve teriparatit gibi tedavi yöntemlerinin düşük biyoyararlanımlığı, yol açtığı mide problemleri ve uzun süreli kullanımlarda ortaya çıkan güvenilirlik sorunlarının olması, bu ilaçların salım sistemleri içerisinde uygulanması gerekliliğini doğurmuştur. Son yıllarda yapılan araştırmalar sonucunda kemik patolojisinin moleküler altyapısının çok daha iyi anlaşılmasıyla, yeni tedavi yöntemlerinin geliştirilmesinde, RNA interferans (RNAi) yaklaşımının kullanımı önem kazanmıştır. Küçük interferans RNA (siRNA) çift zincirli bir RNA molekülü olup, hücre içerisinde gen ifadesini baskılamak için kullanılmaktadır.

Bu çalışmada, kemik erimesi tedavisi için kullanılmak üzere, kemik dokusuna hedeflenmiş ve intravenöz olarak enjekte edilebilecek bir siRNA salım sistemi geliştirilmiştir. Polietilenimin (PEI) (polikasyonik molekül) ve RANK siRNA kullanılarak oluşturulan kompleksler poli(laktik asit-ko-glikolik asit) nanokapsüllerinin içerisine yüklenmiştir. Kemik hedeflemesinin yapılabilmesi için, oluşturulan kapsüller, osteokondüktif bir sekans olan, elastin benzeri rekombinamer (ELR) ile kaplanmıştır. Kapsüller üzerindeki ELR kaplaması, Taramalı Elektron Mikroskopu (SEM), Geçirimli Elektron Mikroskopu (TEM) ve X-Işını Fotoelektron Spektroskopisi (XPS) yöntemleri kullanılarak gösterilmiştir. Ayrıca, düşük toksisite ve en yüksek etkiyi gösteren nitrojen fosfat oranına (N/P oranı; sırasıyla PEI ve siRNA) sahip olan PEI:RANK siRNA kompleksi belirlenmiştir. Bu çalışmanın sonucuna göre, N/P 20 oranına sahip olan PEI:RANK siRNA kompleksleri PLGA nanokapsüllerinin içerisine yüklenmiştir ve enkapsülasyon verimliliği % 48 olarak hesaplanmıştır. Bu komplekslerin kapsüllerden salım kinetiği ise 15 gün boyunca çalışılmış ve Higuchi salım kinetiğine uyduğu gösterilmiştir. Bu kapsüller osteoklast öncü hücrelerine uygulanmış ve RANK mRNA seviyelerinin istatistiksel olarak anlamlı bir şekilde azaldığı gösterilmiştir (53%). Ek olarak, uygulanan salım sistemi sayesinde osteoklast öncülerinin osteoklasta farklılaşması da baskılanmıştır. Osteoklast öncülerinin farklılaşmaları sırasında PEI:RANK siRNA yüklü PLGA nanokapsülleri ile muamele edilmesi osteoklastik aktivitenin de azalmasına yol açmıştır. Sonuç olarak, oluşturulan salım sistemi kemik erimesi tedavisinde kullanılacak alternatif bir tedavi yöntemi olma potansiyeli taşımaktadır.

**Anahtar Kelimeler:** Osteoporoz, hedeflenmiş salım sistemi, siRNA, reseptör aktivatör nükleer faktör kappa B (RANK), poli(laktik asit-ko-glikolik asit) (PLGA).



*Dedicated to my beloved family*

## ACKNOWLEDGEMENTS

I would first like to thank my supervisor, Prof. Dr. Vasıf HASIRCI for his encouraging guidance and support throughout my PhD. I have always felt very lucky to find the chance of working under his supervision. He was not only a great mentor but also showed me great patience even when I knocked on his door at the end of the day with my results on my hands. He is, has been and will be the person to ask for advice. Thank you for being with me.

I would also give my thanks to my co-advisor Prof. Dr. Hasan ULUDAĞ, whose comments and help gave a clear view on critical points in this study.

I am also grateful to my thesis committee members Assoc. Dr. A. Elif ERSON BENSAN and Assoc. Dr. Güvem GÜMÜŞ AKAY for their guidance and support.

I would like to acknowledge TUBITAK for their support through BİDEB 2211-C Scholarship.

Throughout my graduate life in BIOMATEN, Center of Excellence in Biomaterials and Tissue Engineering, I was surrounded by helpful and supportive people, Ayşe Selcen ALAGÖZ, Esen SAYIN, Tuğba DURSUN, Dilara TAMAY, Arda and Senem BÜYÜKSUNGUR, Cemile BEKTAŞ, Gökhan BAHÇECİOĞLU, Emre ERGENE and Elbay Malikmammadov and our technician and big brother Zeynel AKIN, and people in our support units Yüksel GÜNEŞ and Ramazan KAVAK.

Assoc. Dr. Pınar YILGÖR HURİ, has been especially very helpful, supportive, understanding, and friendly. Thank you for all of it.

Aylin KÖMEZ, Ezgi ANTMEN, Çağla MİRASYEDİOĞLU and Gözde EKE were very supportive, encouraging, and friendly throughout my years in BIOMATEN. Menekşe ERMİŞ ŞEN, thank you for being so patience and friendly. I know that you will be with me whenever I need. Canan KURŞUNGÖZ, my former lab mate and one of my best friends always knew her place in my life and never bothered me with unnecessary details. We will always start from where we left off. Thank you for being so great.

Every little thing changes in life, but the things that matter are the ones which are the building blocks of one's life. Kıvanç BİLECEN, thank you for being one of them. No need to be worried about anything when I have you by my side. Bora BİLECEN, our new family member, thank you for just being healthy. Having you gives us great peace.

Nothing would have been meaningful without sharing with them; my family. My parents Uğur and Macit SEZLEV were always supportive for every second of my life with all my decisions. I would not have accomplished this much without their endless help and encouragement. I am very thankful for having them as my parents. I would also like to thank to my sister, Pınar SEZLEV YILMAZ, her husband, Adnan YILMAZ and my little nephew, Onur YILMAZ for always being there for me and agreeing not to see me while these endless pages were being written. I am grateful for all the support and encouragement that I have received from my parents-in-law Leyla and Basri BİLECEN and my brother-in-law, Uluç BİLECEN who always knew how to cheer me up when I am down.

## TABLE OF CONTENTS

ABSTRACT .....	v
ÖZ.....	vii
ACKNOWLEDGEMENTS .....	x
TABLE OF CONTENTS .....	xii
LIST OF TABLES .....	xvii
LIST OF FIGURES .....	xviii
CHAPTERS.....	1
1 INTRODUCTION .....	1
1.1 Structure and Physiology of Bone.....	1
1.1.1 Structure of Bone .....	1
1.1.2 Physiology of Bone .....	3
1.1.2.1 Osteoblasts .....	3
1.1.2.2 Osteoclasts .....	3
1.1.2.2.1 Receptor Activator of Nuclear Factor $\kappa$ B (RANK).....	5
1.1.3 Bone Remodeling.....	7
1.1.3.1 Mechanism of Bone Resorption .....	9
1.2 Bone Diseases.....	10
1.2.1 Osteoporosis.....	11
1.2.1.1 Pathogenesis of Osteoporosis .....	12
1.2.2 Treatment of Osteoporosis .....	13
1.2.2.1 Conventional Treatment of Osteoporosis .....	13

1.2.2.2	Advanced Therapies for Osteoporosis .....	14
1.2.2.2.1	Controlled Delivery of Conventional Drugs with Carriers .....	14
1.2.2.2.2	Types of Carriers Used in the Treatment of Osteoporosis .....	15
1.2.2.2.3	Targeted Drug Delivery to Bone Tissue .....	17
1.2.3	RNA Interference for the Treatment of Osteoporosis .....	18
1.2.3.1	Mechanism of RNA Interference .....	18
1.2.3.2	siRNA as a Therapeutic Agent for Osteoporosis Treatment.....	20
1.3	Aim, Approach and Novelty of the Study .....	23
2	MATERIALS AND METHODS .....	27
2.1	Materials .....	27
2.2	Methods.....	28
2.2.1	Preparation and Characterization of PEI:Nucleic Acid Complexes .....	28
2.2.1.1	Measurement of Zeta Potential and Condensation of PEI:Nucleic Acid Complexes .....	29
2.2.2	Preparation of PLGA Nanocapsules .....	30
2.2.2.1	Specificity of the ELR Towards Hydroxyapatite .....	31
2.2.2.2	Preferential Binding of ELR Coated Nanocapsules on CaP Surface .....	31
2.2.3	Characterization of Nanocapsules .....	31
2.2.3.1	Loading and Encapsulation Efficiency of PEI:DNAoligo in PLGA Nanocapsules .....	31
2.2.3.2	In Situ Release of PEI:DNAoligo Complex from the PLGA Nanocapsules .....	32
2.2.3.3	In Situ Degradation of PLGA Nanocapsules .....	33
2.2.3.4	Detection of ELR on PLGA Nanocapsules .....	33
2.2.3.4.1	Nanocapsule Topography with SEM .....	33
2.2.3.4.2	Detection of ELR on Nanocapsules with TEM and XPS.....	33
2.2.3.5	Particle Size Distribution .....	34
2.2.4	Cell Culture Studies .....	34
2.2.4.1	RAW264.7 Cell Line: In Vitro Culture and Differentiation .....	34

2.2.4.2	Determination of Cell Viability .....	34
2.2.4.3	Internalization of the Nanocapsules by the Cells .....	35
2.2.4.4	Treatment with the Delivery System .....	36
2.2.5	Gene Expression Studies.....	37
2.2.5.1	Efficiency of RANK siRNA Sequence in Gene Silencing .....	37
2.2.5.2	Quantitative Real Time PCR (qRT-PCR).....	38
2.2.5.3	Inhibition of RANK mRNA with Varying N/P ratios .....	39
2.2.5.4	Inhibition of RANK mRNA in Nanocapsule Transfected Cells .....	40
2.2.6	Inhibition of Osteoclast Differentiation and Activity .....	40
2.2.6.1	Inhibition of Osteoclast Differentiation.....	40
2.2.6.2	Inhibition of Osteoclastic Activity.....	41
2.2.7	Statistical Analysis .....	41
3	RESULTS AND DISCUSSION .....	43
3.1	Characterization of PEI:DNAoligo Complexes .....	43
3.1.1	Zeta Potential of PEI:DNAoligo Complexes .....	43
3.1.2	Condensation of PEI:Nucleic Acid Complexes .....	45
3.2	Characterization of Nanocapsules .....	47
3.2.1	Loading and Encapsulation Efficiency of PEI:DNAoligo in PLGA Nanocapsules .....	47
3.2.2	<i>In Situ</i> Degradation of PLGA Nanocapsules .....	48
3.2.3	<i>In Situ</i> Release of PEI:DNAoligo Complex from the PLGA Nanocapsules 50	
3.2.4	Determination of Affinity of the ELR Towards Hydroxyapatite with Fourier Transform Infrared (FTIR) Spectroscopy .....	52
3.2.5	Preferential Binding of ELR Coated Nanocapsules on CaP Surface .....	54
3.2.6	Detection of ELR on PLGA Nanocapsules.....	56
3.2.6.1	Study of Nanocapsule Topography with SEM .....	56
3.2.6.1.1	Detection of ELR on Nanocapsules with TEM and XPS .....	58
3.2.7	Particle Size Distribution Analysis .....	62

3.3	<i>In Vitro</i> Cell Culture Studies.....	64
3.3.1	RAW264.7 Cell Line: Culture and Differentiation .....	64
3.3.2	Determination of Cell Viability .....	66
3.3.3	Internalization of PLGA Nanocapsules .....	67
3.4	Gene Expression Studies.....	70
3.4.1	Efficiency of RANK siRNA Sequence in Gene Silencing.....	70
3.4.2	Inhibition of RANK mRNA with Varying N/P Ratios.....	72
3.4.3	Inhibition of RANK mRNA in Nanocapsule Transfected Cells .....	75
3.5	Inhibition of Osteoclast Differentiation and Activity .....	77
3.5.1	Inhibition of Osteoclast Differentiation.....	77
3.5.2	Inhibition of Osteoclastic Activity .....	80
4	CONCLUSIONS .....	83
	REFERENCES .....	85
	APPENDICES .....	105
A.	OPTIMIZATION OF QUANTITATIVE REAL TIME POLYMERASE CHAIN REACTION (qRT-PCR).....	105
	RNA Isolation.....	105
	DNase I Treatment .....	105
	First Strand cDNA Synthesis .....	106
	Optimization of Primers for qRT-PCR .....	107
	RANK Primer .....	107
	GAPDH Primer .....	109
B.	RAW 264.7 PRE-OSTEOCLAST CELL LINE ALAMAR BLUE CALIBRATION CURVE.....	113
C.	PEI:FAM-LABELLED DNAOLIGO FLUORESCENCE INTENSITY CALIBRATION CURVE.....	115

CURRICULUM VITAE .....	117
------------------------	-----



## LIST OF TABLES

### TABLES

Table 1: RANK siRNA Sequences Used in the Study.....	37
Table 2: qRT-PCR Primers and the Amplicon Sizes .....	38
Table 3: qRT-PCR Cycling Conditions for the Primers. ....	38
Table 4: FTIR Peak Intensity Ratios (C=O to P-O) and (N-H to P-O).....	54
Table 5: Diameter and PDI Values of Empty, PEI:DNAoligo (20:1) Loaded and ELR Coated PEI:DNAoligo (20:1) Loaded PLGA Nanocapsules .....	62

## LIST OF FIGURES

### FIGURES

Figure 1: Structure of bone.....	2
Figure 2: Schematic presentation of intracellular signals for osteoclastic differentiation. ....	4
Figure 3: RANK mediated osteoclast differentiation and function. RANK .....	6
Figure 4: Sequential phases of bone remodeling in basic multicellular units .....	8
Figure 5: Mechanism of bone resorption by osteoclasts. ....	10
Figure 6: Scanning electron micrographs of biopsies of human normal bone and osteoporotic bone .....	12
Figure 7: Schematic presentation of siRNA mediated RNAi mechanism. ....	19
Figure 8: Approach of the study.....	24
Figure 9: Schematic presentation of PEI:nucleic acid complex.....	28
Figure 10: Zeta potential of PEI:DNAoligo complexes with different N/P ratios.....	44
Figure 11: Electrophoretic mobility assay of PEI:nucleic acid complexes in Agarose gel.. ....	46
Figure 12: SEM micrographs of PLGA nanocapsules during 21 days of incubation in TE buffer (A, B). ....	49
Figure 13: Release of PEI: DNAoligo from PLGA nanocapsules (pH 7.4).....	51
Figure 14: FTIR-ATR spectra of HAp and polypeptide interaction. ....	53
Figure 15: Confocal micrographs of PLGA nanocapsules.....	55
Figure 16: SEM micrographs of PLGA nanocapsules.. ....	57
Figure 17: TEM micrographs of PLGA nanocapsules.....	59

Figure 18: XPS spectra of PLGA nanocapsules. (A) Uncoated, (B) ELR coated PLGA nanocapsules.....	61
Figure 19: Representative graphs of particle size distribution.....	63
Figure 20: Representative microscopy images of undifferentiated and differentiated cells used in the study.. .....	65
Figure 21: Effect of PLGA nanocapsules on viability of RAW264.7 cells as determined by Alamar Blue cell viability assay. ....	66
Figure 22: Confocal laser scanning micrograph of Nile Red loaded PLGA nanocapsules (pink) in RAW264.7 cells 48 h post transfection. ....	68
Figure 23: Fold change of RANK mRNA expression in mock (HiPerfect Transfection Reagent), scrambled, and RANK siRNA#1 transfected cells. ....	71
Figure 24: Fold change of RANK mRNA expression in mock (HiPerfect Transfection Reagent), scrambled, and RANK siRNA#2 transfected cells.. ....	72
Figure 25: Inhibition of RANK mRNA expression with N/P ratios of 6, 20, 25, 30, 60 (A, B). ....	74
Figure 26: Fold change of RANK mRNA at 3 and 5 days post transfection with PLGA nanocapsules carrying different cargo (n=3). ....	76
Figure 27: Representative images of staining of TRAP in differentiating RAW264.7 cells transfected with empty nanocapsules, PEI:Scrambled siRNA and PEI:RANK siRNA loaded PLGA nanocapsules. ....	78
Figure 28: Inhibition of differentiation in empty nanocapsule, PEI:Scrambled and PEI:RANK siRNA loaded nanocapsule transfected cells.....	79
Figure 29: Osteoclastic activity determined by pit formation assay.....	81
Figure 30: The amplification of RANK amplicon .....	107
Figure 31: The melt curve of RANK amplicons.....	108
Figure 32: The standard curve of RANK primer. ....	108

Figure 33: The amplification of GAPDH amplicons. ....	109
Figure 34: The melt curve of GAPDH amplicons.....	109
Figure 35: The standard curve of GAPDH primer. ....	110
Figure 36: Agarose gel electrophoresis of PCR products. ....	111
Figure 37: Amplification of DNaseI treated RNA sample (No-RT control) and NTC (No-Template Control).....	112
Figure 38: Melt Curves of No-RT control or NTC.. ....	112
Figure 39: Alamar Blue calibration curve of RAW264.7 preosteoclast cell line.....	113
Figure 40: Calibration curve of PEI:FAM labelled DNAoligo complex .....	115

## **CHAPTER 1**

### **INTRODUCTION**

Bone is an organ which is responsible for support and protection of other organs, production of blood cells, storage of minerals and regulation of hormones. Disorders of bone, therefore, cause serious complications and even mortality. Although bone diseases, such as bone cancer, osteoarthritis and osteoporosis, are very important health problems, their effective treatments remain a challenge (Cheng et al., 2017). Osteoporosis affects approximately 200 million people worldwide. It is estimated that in 2050 osteoporotic hip fractures will exceed 21 million (Pisani et al., 2016). In this context, therefore, prevention and treatment of the disease gains significant importance. The researchers studying a treatment strategy for the disease have recently started to focus on the use of RNAi as a therapeutic agent and biomaterials as the carriers. The present work is an example of the development of such a delivery system to be used in the treatment of osteoporosis.

#### **1.1 Structure and Physiology of Bone**

##### **1.1.1 Structure of Bone**

Bone is a type of connective tissue which structurally supports and protects the organs of the body. It produces blood cells through bone marrow and store minerals such as calcium phosphate (Florencio-Silva et al., 2015). Calcified bone consists of organic matrix (mainly type I collagen) and minerals (hydroxyapatite). The organic matrix also contains osteocalcin, osteopontin and proteoglycans (Morinobu et al., 2003; Lamoureux et al., 2007; Blair et al., 2011).

Crystalline hydroxyapatite (HAp) is made up of calcium and phosphate in its composition  $[\text{Ca}_{10}(\text{PO}_4)_6(\text{OH})_2]$ . Calcium and phosphate is recovered from nutritional sources and deposited on collagen fibrils as HAp which together gives structural integrity to bone (Kini and Nandeesh, 2012).

Bone is mainly composed of two parts; the cortical (compact) bone and trabecular (spongy) bone (Figure 1). The outer dense shell is the cortical bone and it surrounds the bone marrow. It also provides sites for attachment of tendons and muscles. Within the cortical bone, there is the trabecular bone. The periosteum is the fibrous connective tissue that surrounds the cortical bone. It contains blood vessels, nerves and osteoblast precursor cells in its inner layer. The endosteum is the membranous structure surrounding the inner part of the cortical bone and the spongy bone. It contains the blood vessel canals which are called Volkmann's canals. The fundamental unit of cortical bone is the osteon. Each osteon is composed of layers (lamellae) which surround the Haversian canals that contain blood capillaries and nerves (Buckwalter et al., 1995).

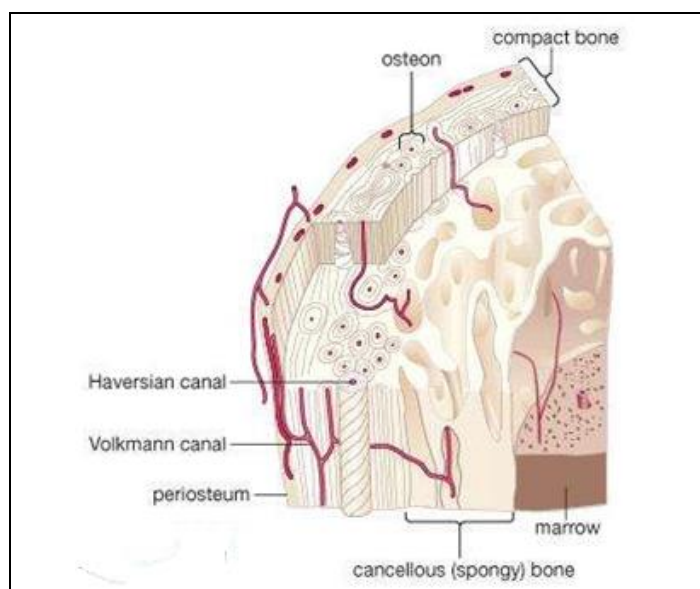


**Figure 1:** Structure of bone. (Bone Anatomy, Encyclopedia Britannica)

### **1.1.2 Physiology of Bone**

Bone is a dynamic tissue which is remodeled throughout life by the coupled activities of bone forming cells, the osteoblast lineage cells, and bone resorbing cells, the osteoclast lineage cells.

#### ***1.1.2.1 Osteoblasts***

Osteoblasts are involved in the formation of bone. They are mononucleated and found on the bone surfaces (Kini and Nandeesh, 2012). Osteoblasts differentiate from mesenchymal stem cells of the bone marrow stroma (osteoprogenitor cells) (Ducy et al., 1997). Mature osteoblasts secrete collagen and chondroitin sulfate, and therefore, the osteoids are formed. They also possess alkaline phosphatase (ALP) activity to hydrolyze the pyrophosphate and increase the concentration of phosphates used in the calcification process (Hessle et al., 2002). After active bone formation, some osteoblasts differentiate into osteocytes and become embedded in the bone matrix and others appear on quiescent bone surfaces and called the bone lining cells (Nakamura H., 2007).

#### ***1.1.2.2 Osteoclasts***

Osteoclasts originate from hematopoietic stem cells (HSC) and go through a series of differentiation stages to become multinucleated, non-dividing and bone resorbing cells (Soysa et al., 2012). Precursors of osteoclasts are found in the bone marrow and circulating blood (Buckwalter et al., 1995; Takahashi et al., 2014)

The differentiation of osteoclast precursors to mature osteoclasts requires their interaction with osteoblasts to activate different pathways in the precursors. Some of these pathways are summarized in Figure 2.

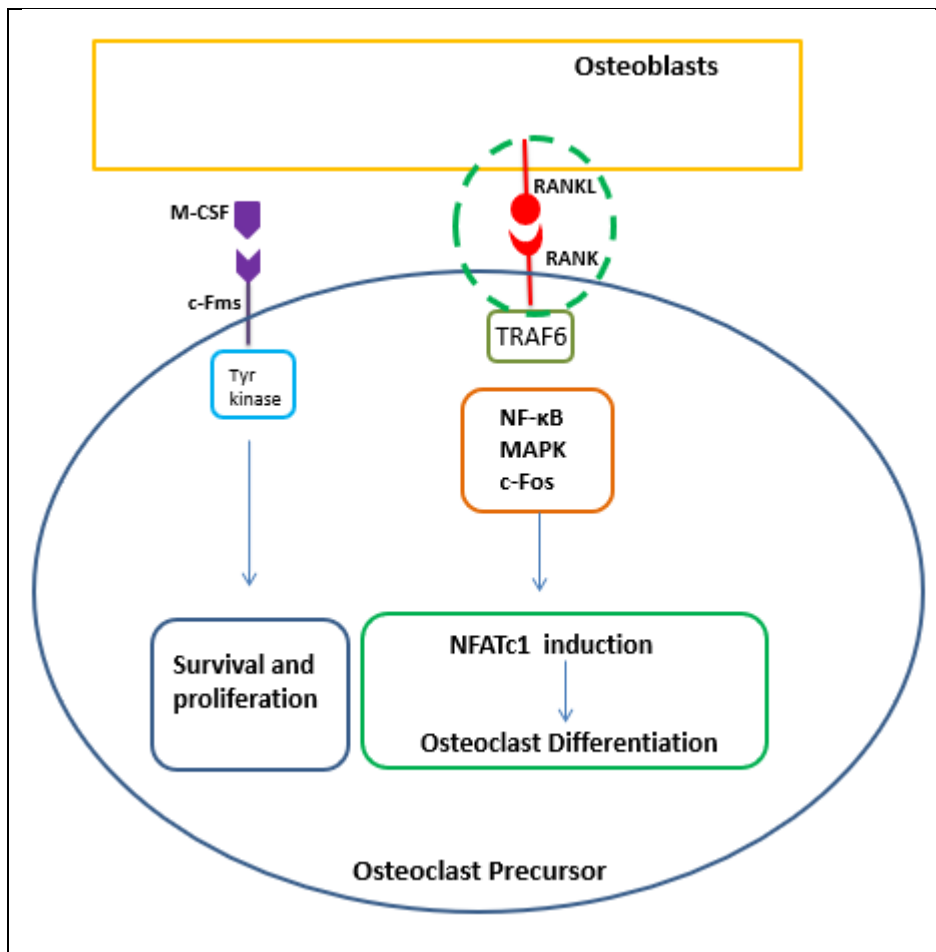


**Figure 2:** Schematic presentation of intracellular signals for osteoclastic differentiation. RANKL: Receptor Activator of Nuclear Factor Kappa B Ligand; RANK: Receptor Activator of Nuclear Factor Kappa B; TRAF6: Tumor Necrosis Factor Receptor 6; NF-κB: Nuclear Factor Kappa B; MAPK: Mitogen Activated Protein Kinase; NFATc1: Nuclear Factor of Activated T cell; M-CSF: Macrophage Colony Stimulating Factor; c-Fms: Colony Stimulating Factor Receptor.

Osteoblasts synthesize and secrete Macrophage Colony Stimulating Factor (M-CSF) (Takahashi et al., 2014). The binding of M-CSF to its receptor (c-Fms) on osteoclast precursors is important in the survival and proliferation of the precursors (Takayanagi H., 2005).



The most important cytokine that is synthesized on osteoblasts for osteoclastic differentiation is the receptor activator of nuclear factor  $\kappa$  B ligand (RANKL). The interaction of RANKL with its only receptor RANK on osteoclast precursor cells is required in the activation of osteoclastogenesis, bone resorption and survival of mature osteoclasts (Boyle et al., 2003). M-CSF also induces the expression of RANK on osteoclast precursor cells to increase the response of RANKL/RANK signaling pathway during osteoclast differentiation (Teti and Rucci, 2010).

The binding of RANKL to RANK causes recruitment of Tumor Necrosis Factor Receptor (TNFR) associated factor 6 (TRAF6) which activates Nuclear Factor Kappa B (NF $\kappa$ B) and Mitogen Activated Protein Kinase (MAP kinase) pathways and other transcription factors such as c-Fos (Kim and Kim, 2014). The increased activity of NF $\kappa$ B results in the enhancement of Nuclear Factor of Activated T cell (NFATc1) expression which is the major transcription factor of osteoclastogenesis. It controls the expression of osteoclast specific genes such as Tartrate Resistant Acid Phosphatase (TRAP), Cathepsin K and Calcitonin receptor (Kim and Kim, 2016).

The RANK/RANKL pathway is regulated by Osteoprotegrin (OPG) which is also secreted by osteoblasts. OPG serves as a decoy receptor. It binds to RANKL, and therefore, prevents the binding of RANKL to RANK which suppresses the differentiation process (Feng X., 2005).

#### **1.1.2.2.1 Receptor Activator of Nuclear Factor $\kappa$ B (RANK)**

Osteoclasts, the bone resorbing cells, are multinucleated giant cells formed by cytoplasmic fusion of their mononuclear precursors from the hematopoietic origin (Udagawa et al., 1990). The differentiation of osteoclasts from their precursors is called osteoclastogenesis. It requires two very important cytokines that are synthesized and secreted from the osteoblasts, namely receptor activator of nuclear factor  $\kappa$  B ligand (RANKL) and macrophage colony stimulating factor (M-CSF) (Boyce and Xing, 2007).

The differentiation of osteoclasts requires the regulation of signaling pathways (discussed in section 1.1.2.2) which are mainly activated by the interaction of RANKL and its receptor RANK (Figure 3).

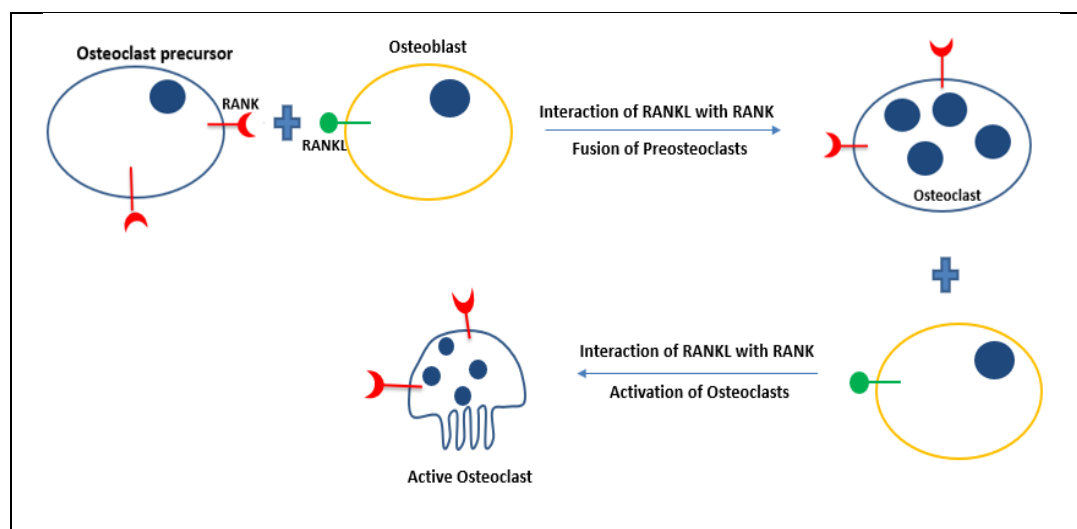


**Figure 3:** RANK mediated osteoclast differentiation and function. RANK: Receptor activator of nuclear factor  $\kappa$ -B; RANKL: Receptor activator of nuclear factor  $\kappa$ -B Ligand.

RANK is a member of tumor necrosis factor (TNF) receptor superfamily (Wada T. et al., 2006). It is a receptor which is expressed on osteoclast precursors and mature osteoclasts (Nakagawa et al., 1998; Feng X., 2005; Dougall W. C., 2012). The interaction of RANKL with its receptor RANK induces the expression of osteoclast specific genes such as TRAP, Calcitonin and Cathepsin K, and thus osteoclastic differentiation and activation (Boyle et al., 2003).

In this study, we chose RANK as the molecular target of the treatment. The number and activity of mature osteoclasts would be suppressed by the use of RNAi pathway through the use of small interfering RNA (siRNA) targeting RANK.

This suppression would lead a decrease in the differentiation of osteoclast precursors to mature osteoclasts which would eventually lead to reduced bone resorption.

### **1.1.3 Bone Remodeling**

Bone remodeling is the process of continuous replacement of old, microdamaged bone with new bone. It is important in the maintenance of the bone strength and calcium homeostasis (Lerner U. H., 2006). The cortical bone has a slower turnover rate than the trabecular bone (Hadjidakis and Androulakis, 2006) thus metabolic bone diseases such as osteoporosis is mainly observed in trabecular bone (Li et al., 2017).

Bone remodeling is performed by the coupled activities of osteoclasts and osteoblasts arranged within temporary structures called “basic multicellular units” (BMUs) over a period of several weeks (Raggatt and Partridge, 2010). Sequential phases of bone remodeling in a BMU are: activation, resorption, reverse, formation and mineralization (Figure 4). Activation, resorption and reversal phases takes about four weeks, while formation and mineralization lasts for 4 months (Lerner U. H., 2006).

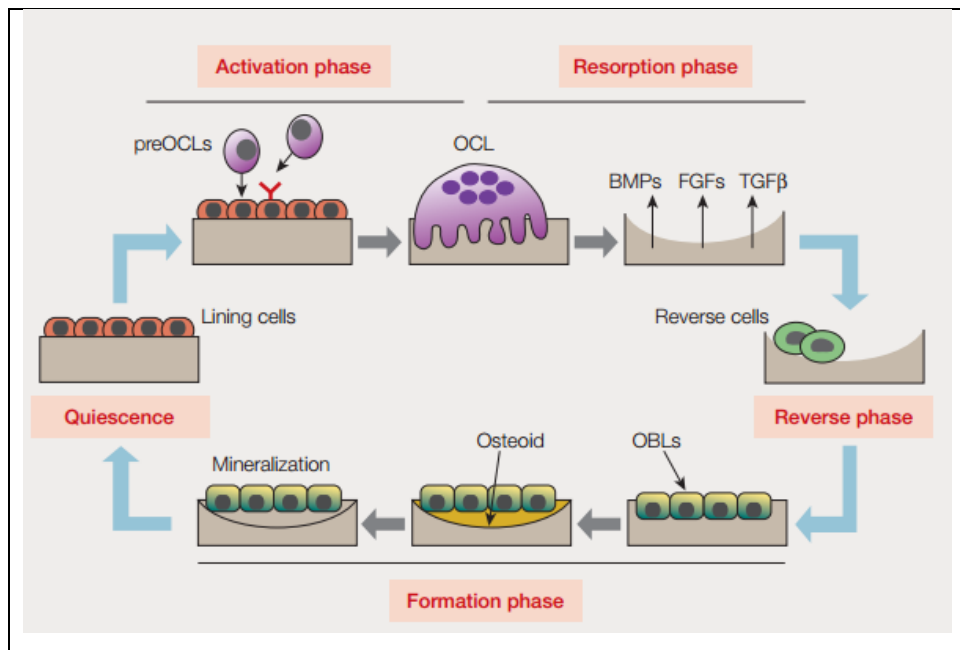


**Figure 4:** Sequential phases of bone remodeling in basic multicellular units (BMUs). (Takayanagi H., 2010). BMP: Bone Morphogenetic Proteins, FGF: Fibroblast Growth Factor; TGF: Transforming growth factor.

The surface of bone tissue is covered with a single layer of osteoblasts. Activation phase starts with a stimulus, such as mechanical strain on bones. The bone lining cells (osteoblasts) produce a chemokine called Monocyte Chemoattractant Protein-1 (MCP-1) which recruits osteoclast precursors to the BMU (Raggatt and Partridge, 2010). Osteoblasts also increase the expression of RANKL and M-CSF and reduce OPG synthesis. By cell-to-cell contact, RANKL interacts with the RANK receptor on osteoclast precursors and preosteoclasts differentiate into active bone resorbing mature osteoclasts (Lerner U. H., 2006). During the resorption phase, several growth factors such as Bone Morphogenetic Proteins (BMPs) or Fibroblast Growth Factor (FGF) stored in bone matrix are released and it is proposed that those factors recruit osteoblastic cells towards to the resorbed area so that bone formation would be initiated (Lajeunesse et al., 2010).

Just before the formation phase, mononuclear cells with no distinct phenotype, the reversal cells, cover the newly exposed bone surface and remove the collagen remnants to prepare it for new bone formation. In the formation phase osteoblasts synthesize osteoid and in the mineralization phase, HAp is deposited onto the synthesized osteoid and then the cycle continues to its final phase, termination phase, in which mature osteoblasts either undergo apoptosis or go back to bone lining phenotype or become embedded into the bone matrix to differentiate into osteocytes. The newly synthesized bone is maintained until the next remodeling cycle is initiated (Raggatt and Partridge, 2010).

#### ***1.1.3.1 Mechanism of Bone Resorption***

During the resorption phase of bone remodeling, osteoclast cell body is polarized and attaches itself to bone tissue through vitronectin receptors found in the clear zone of polarized osteoclast (Figure 5). This attachment is achieved by the interaction of the vitronectin receptors and the Arg-Gly-Asp (RGD) sequences of osteopontin in the bone matrix. After the attachment, osteoclasts form the ruffled border, where the bone resorption pits are formed due to disruption of HAp and collagen (Lerner U. H., 2006).

HAp is decalcified by the acidic environment (pH 4-5) formed by the conversion of  $\text{CO}_2$  and  $\text{H}_2\text{O}$  to  $\text{H}^+$  and  $\text{HCO}_3^-$  by Carbonic Anhydrase II and pumping of  $\text{H}^+$  from the vacuolar type  $\text{H}^+/\text{ATPase}$  in the ruffled border (Nakamura H., 2007). The collagen and other matrix proteins in the demineralized bone matrix is degraded by the enzymes Cathepsin K (Saftig et al., 1998), matrix metalloproteinase-9 (MMP-9) and tartrate resistant acid phosphatase (TRAP) (Hayman A., 2008; Takahashi et al., 2014). Degradation products are then endocytosed by osteoclasts and secreted into extracellular fluid through functional secretory domain (Figure 5).

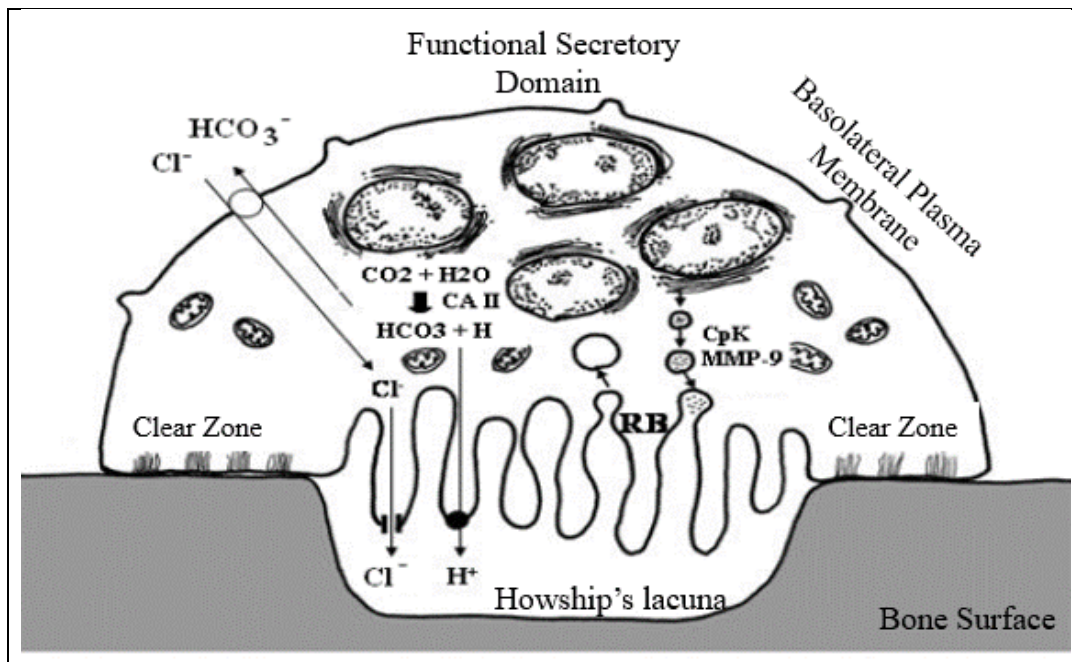


**Figure 5:** Mechanism of bone resorption by osteoclasts.  $H^+$  ions produced by carbonic anhydrase II (CA II) to Howship's lacuna to create the acidic environment for the decalcification of hydroxyapatite. Collagen is degraded by the lysosomal enzymes cathepsin K (CpK) and Matrix metalloproteinase 9 (MMP-9). RB: Ruffled Border (Modified from Nakamura H., 2007).

## 1.2 Bone Diseases

Bone diseases are conditions which lead to impairment of normal bone function and properties. There are many factors that could cause abnormalities in bone development and remodeling. For instance, genetic abnormalities may lead to either very dense or weak bone. Osteogenesis imperfecta, a genetic disorder leading to increased bone fragility, is dominantly caused by a number of mutations in either  $\alpha$ -1 or  $\alpha$ -2 chains of type I collagen (Rauch and Glorieux, 2004), in addition to the mutations in genes for collagen protein folding and osteoblast differentiation (Forlino and Marini, 2016).

Another type of bone disease with genetic origin is osteopetrosis. It leads to increased bone density and mass due to impaired bone resorption as a result of mutations in genes for osteoclast ruffled border formation (Sobacchi et al., 2013).

In addition to genetic abnormalities, environmental factors contribute to diseases of bone. Paget's disease is an example of such a condition. It is characterized by increased bone remodeling in local areas affecting one or more sites throughout the body. Mutations in NF $\kappa$ B signaling proteins or viral infections can cause the disease (Ralston et al., 2008). Nutritional deficiencies, especially vitamin D causes weakened bones (Lips and van Schoor, 2011). The deficiency leads to reduced calcium absorption from the gut, thereby to reduced bone mineralization. Vitamin D deficiency also causes hyperparathyroidism which also increases bone turnover (Lips and van Schoor, 2011) by increasing the expression of RANKL from osteoblasts (Das and Crockett, 2013).

Another type of bone disease is osteoporosis. Due to its importance it is given in a separate section below.

### **1.2.1 Osteoporosis**

Osteoporosis is, by far the most common bone disease and it represents a major health problem. Approximately 200 million people, worldwide, is affected by the disease and the failure in skeleton structure causes increased fracture risks in bone causing 8.9 million fractures every year (Kanis J. A., 2007; Pisani et al., 2016). It is a systemic disease characterized by reduced bone mineral density (BMD), bone mass and strength which leads to increased susceptibility to fractures. The increased bone resorption relative to formation causes the structural failure of the bone tissue (Holroyd et al., 2008). The disease is diagnosed by BMD assessment (Kanis J. A., 2002).

Osteoporosis is mainly observed in spongy bones because the bone turnover is higher in the trabecular bone (Lerner U. H., 2006).

Figure 6 shows the SEM of healthy and osteoporotic spongy bones. As can be seen from the figure normal bone appears strong with interconnected pores however, in the osteoporotic bone thinner, rod-like plates are seen (Dempster et al., 1986).

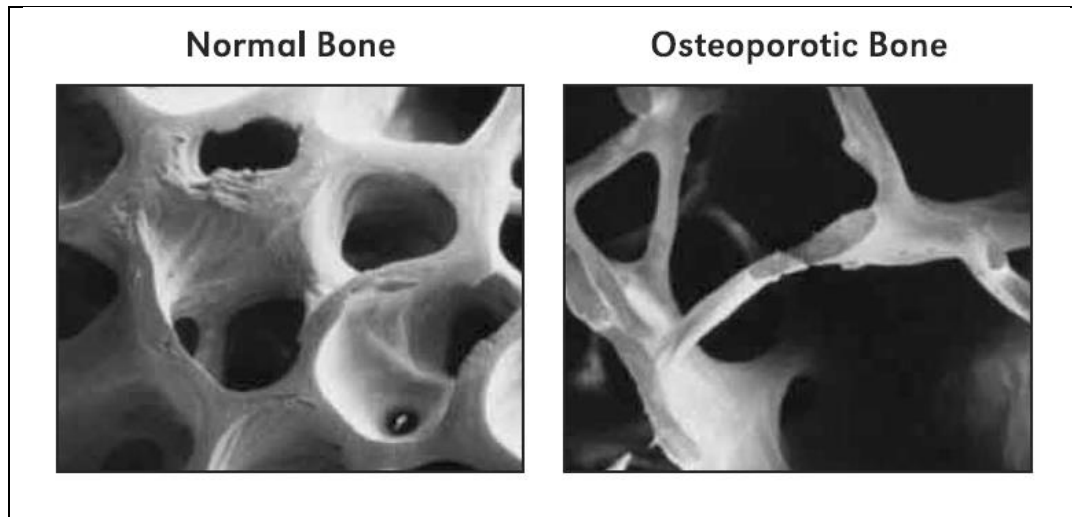


**Figure 6:** Scanning electron micrographs of biopsies of human normal bone and osteoporotic bone (Dempster et al., 1986).

#### ***1.2.1.1 Pathogenesis of Osteoporosis***

The primary cause of osteoporosis is aging. Reduction in estrogen levels in post-menopause, causes increased RANKL levels on the surface of osteoblastic cells (Eghbali-Fatourehchi et al., 2003) which leads to increased bone resorption. The osteoporosis seen in men is believed to be due to increase in sex hormone binding protein leading to reduced estrogen and testosterone levels (Lerner U. H., 2006). The reduction in estrogen is responsible for the increased bone resorption and decreased testosterone level is the cause of reduced bone formation (Willson et al., 2015). In addition to sex hormone deficiency, inflammatory cytokines such as  $\text{TNF}\alpha$  and interleukins are also associated with the pathology of osteoporosis (Yu and Wang, 2016).



Other diseases such as hyperparathyroidism or osteogenesis imperfecta (discussed in section 1.2) are the secondary causes of osteoporosis (Lerner U. H., 2006).

### **1.2.2 Treatment of Osteoporosis**

Being the most common bone related disease, there are a variety of prevention and treatment strategies for osteoporosis. For prevention, although it is less effective, calcium and Vitamin D supplementation is recommended (Chan et al., 2016). The existing treatments are discussed below.

#### ***1.2.2.1 Conventional Treatment of Osteoporosis***

Pharmacological agents used for the treatment of osteoporosis is classified into two groups: agents that suppress bone resorption or those that have anabolic function on new bone formation. Bisphosphonates, strontium ranelate, denosumab, and selective estrogen receptor modulators such as Tamoxifen or Raloxifene are the drugs used to inhibit bone resorption (Das and Crockett, 2013). Bisphosphonates are the most commonly used drugs for the treatment of the disease.

They have the ability to bind to  $\text{Ca}^{+2}$  ions during active bone resorption and endocytosed by osteoclasts. They inhibit the mevalonate pathway, a pathway common to all cell types, causing the apoptosis of osteoclasts. However, the neighboring osteoblasts or stromal cells also internalize the drug especially after a series of bisphosphonate administration (Roelofs et al., 2006) which also causes apoptosis in these cells. Strontium of Strontium Ranelate is incorporated into bone as a substitute for calcium. It also increases OPG and decrease RANKL expression from osteoblasts resulting in reduced osteoclastic activity (Hamdy N., 2009). In 2014, however, the drug was restricted only to people with severe osteoporosis for whom there are no other alternative treatments since it leads to serious cardiovascular problems (Chan et al., 2016). Denosumab is a human RANKL antibody designed to mimic the natural effect of OPG. The drug is generally well tolerated and the uncommon side effect of the drug is osteonecrosis (Bone et al., 2013).

The selective estrogen receptor modulators (SERMs) are used to act as agonist of estrogen in bone and act as an inhibitor of bone resorption (Barrett-Connor et al., 2006; Lerner U. H., 2006). The side effects of the treatment are fatal stroke and thromboembolism.

Teriparatide (recombinant form of PTH) increases calcium absorption from the intestines a process which is important in bone mineralization. The intermittent injections of the drug also suppresses osteoblast apoptosis, stimulates bone matrix production whereas continuous injections cause elevated osteoclast numbers by upregulating RANKL expression (Das and Crockett, 2013; Narayanan et al., 2013).

The other treatment methods that are in development are cathepsin K inhibitors (responsible for the degradation of collagen in bone) and anti-sclerostin antibody (sclerostin is an inhibitor in osteoblastic differentiation) (Chan et al., 2016).

#### ***1.2.2.2 Advanced Therapies for Osteoporosis***

Apart from their side effects, all conventional strategies mentioned above exhibit low bioavailability and patient compliance. The oral formulations such as bisphosphonate or SERM are associated with challenges such as susceptibility to degradation due to enzymes and instability in the gastrointestinal tract, poor permeability across the intestinal epithelium and rapid clearance after they are adsorbed (Zhang et al., 2014). Injections (for denosumab and teriparatide), on the other hand, are less convenient for the patients. To overcome these negative drawbacks, many approaches are now being used to deliver these drugs in carrier systems (Asafo-Adjei et al., 2016).

##### **1.2.2.2.1 Controlled Delivery of Conventional Drugs with Carriers**

The use of carriers as drug delivery systems has some advantages. The therapeutic molecule is protected from early degradation by enzymes and its toxicity is reduced. The distribution of the drug becomes less dependent on its own physicochemical properties and long term release of the drug can be achieved (Miladi et al., 2013). In addition, by using the carrier systems, the drugs can be targeted specifically to bone

tissue where the carrier could release its contents and the therapeutic agents can function with minimal exposure to non-target cells (Dang et al., 2016).

Several studies have been published aiming at increasing the bioavailability of conventional drugs for the treatment of osteoporosis. The drugs are loaded into organic or inorganic nanoparticles to carry them to the bone tissue. In the next section, types of carrier systems for the treatment of the disease will be presented.

#### **1.2.2.2.2 Types of Carriers Used in the Treatment of Osteoporosis**

The types of drug carriers used for the treatment of osteoporosis can be classified into three groups; organic particles from lipids (liposomes), chitosan, and PLGA; inorganic nanoparticles made from silica, metal and hydroxyapatite and finally bone cement (PMMA).

Liposomes are self-assembled lipid structures made from molecules with a hydrophilic head group and a hydrophobic tail. They were used in the treatment of experimental osteoporosis and injected estradiol loaded liposomes to ovariectomized rats (as a model of osteoporosis) (Lu et al., 2011). They showed that bone mineral density and serum ALP levels were increased after one month of treatment. Chitosan is obtained from polysaccharide chitin which is widely available in nature as a primary component of cell walls of fungi and exoskeletons of insects. Chitosan particles loaded with raloxifene (a type of SERM) for intranasal delivery for osteoporosis treatment were administered to Wistar rats and resulted in increased bioavailability of the drug in plasma when compared with oral administration (Saini et al., 2015).

An oral formulation for PTH administration, as an alternative to injection was also developed (Narayanan et al., 2013). PTH was loaded into chitosan nanoparticles and administered to osteoblastic cells and to rats. They found that ALP production was increased and osteocalcin production was slightly elevated. In addition the bioavailability of the drug was found to be higher compared to bare PTH.

Another type of carrier used is PLGA (Poly(lactic acid-co-glycolic acid)). It is a FDA approved, biocompatible and biodegradable synthetic copolymer of lactic and glycolic acids. The degradation rate of the polymer depends on the molar ratio of lactic acid to glycolic acid chains in the copolymer which affects the crystallinity and hydrophobicity of the copolymer (Makadia and Siegel, 2011). Lactic acid is more hydrophobic than glycolic acid, and therefore, lactate rich PLGA polymers, absorb less water and degrade more slowly. PLGA can be functionalized with many different moieties including proteins which is important in targeted drug delivery applications.

PLGA has been widely used in a variety of drug delivery applications (Jung et al., 2009; Kumari et al., 2010; Pradhan et al., 2013). It has also been used in encapsulating the drugs to treat osteoporosis. For instance, PLGA nanoparticles were loaded with estradiol in transdermal delivery for osteoporosis treatment (Takeuchi et al., 2016). Administration of the nanoparticles to rats resulted in increased bone mineral density. In another study, PLGA microspheres were loaded with strontium ranelate to be used in the treatment of osteoporosis (Mao et al., 2017). The particles were administered to a medium of preosteoblastic cell line. The treatment resulted in stimulation in the proliferation of the cells and ALP activity and collagen type I and osteocalcin mRNA expressions were elevated (Mao et al., 2017). In another study, oral administration of PLGA nanoparticles loaded with estradiol increased the bioavailability of the drug in rats (Mittal et al., 2007).

Other types of carriers used in the research for treatment of osteoporosis were metallic (Lee et al., 2016) and inorganic nanoparticles. Using gold nanoparticles coated with alendronate (a type of bisphosphonate), RANKL induced differentiation of bone marrow macrophages to mature osteoclasts were reduced (Lee et al., 2016). Bisphosphonate loaded HAp nanoparticles, on the other hand, increased the bone density and reduced bone porosity in ovariectomized (osteoporotic) rat model (Sahana et al., 2013).

Calcium phosphate cement (CPC) is another inorganic carrier used in the treatment of experimental osteoporosis (Wei et al., 2016). They showed that introduction of bisphosphonates into these bone cements reduced the proliferation of osteoclasts by inducing their apoptosis (Panzavolta et al., 2010).

#### **1.2.2.2.3 Targeted Drug Delivery to Bone Tissue**

Delivery systems mentioned above deliver drugs at controlled rates, but they are not designed to control the site where the drug would be bioavailable once it enters the body. Targeting systems are used to concentrate the drug release in a preselected site to improve drug safety and efficacy (Singh and Lillard, 2009).

The high amount of HAp mineral in bone tissue makes it a possible target for moieties that have high affinity towards HAp (Mora-Raimundo et al., 2017). There are two general approaches to drug targeting towards the skeletal system: targeting the systemic skeletal system and targeting a specific cell type within the skeletal system. Tetracyclines (Neale et al., 2009; Wang et al., 2015), bisphosphonates (Doschak et al., 2009; Cong et al., 2015) and oligopeptides (Sekido et al., 2001; Jiang et al., 2014) are used to target the entire skeletal system since they target HAp crystals in bone tissue. In a study, PLGA nanoparticles were grafted with tetracycline and the accumulation of particles in the skeleton was shown, *in vivo* (Wang et al., 2015). In another study, OPG was conjugated with bisphosphonate and intravenous injections to Sprague-Dawley rats resulted in increased deposition of OPG in tibia and femur (Doschak et al., 2009). In addition, conjugation of (L-Asp)<sub>6</sub> with estradiol and injection to mice through tail vein resulted in accumulation of fluorescently tagged (L-Asp)<sub>6</sub> in tibia and caused elevation in bone mineral density in ovariectomized mice (Sekido et al., 2001).

The second approach is to selectively target cells within the skeleton (Zhang et al., 2012). All the clinical drugs used for osteoporosis treatment have severe off-target effects such as increased risk of breast cancer, thromboembolism, nausea and diarrhea, therefore, specific cell targeted systems are required (Sun et al., 2016).

Gene therapy might be considered as a type of cell targeting approach. It is a promising method for effective and selective treatment for diseases. It involves the delivery of small nucleic acids, such as short interfering RNA (siRNA) or micro RNA (miRNA), which need sequence similarity to exert their functions. This requirement makes the siRNA delivery systems a route for cell specific targeting.

### **1.2.3 RNA Interference for the Treatment of Osteoporosis**

Advances in understanding the molecular pathways involved in bone pathology lead to the identification of new molecular targets. Abnormal expression of those molecular targets can be suppressed by the use of RNA interference (RNAi) for treatment of bone diseases (Liu X., 2016). RNAi is a natural process used by the cells to silence gene expression through degradation of mRNA. Delivery of small interfering RNA (siRNA) mimics this natural process and is used to silence expression any disease-causing gene (Wang and Grainger, 2012).

#### ***1.2.3.1 Mechanism of RNA Interference***

Mechanism of RNAi through siRNA starts with the introduction of exogenous long dsRNA or synthetic siRNA into the cells (Figure 7). After Dicer mediated cleavage of long dsRNA, siRNA duplexes of 21-25 nucleotides are formed. The guide strand of siRNA duplex is loaded on to Argonaute family proteins of the RNA-induced silencing complex (RISC) and the other strand is dispensed. RISC uses the guide strand to target mRNA with full complementarity, for the cleavage). If full complementarity is not achieved, sometimes the translation of the mRNA could be repressed (Carthew and Sontheimer, 2009).

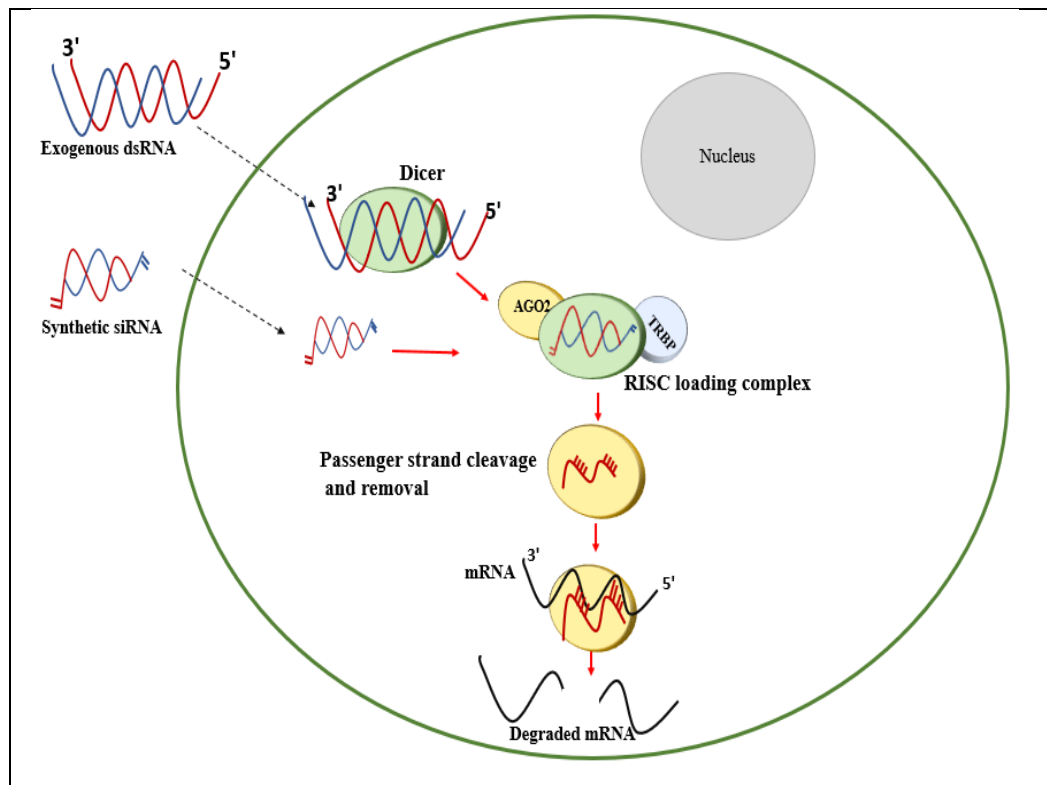


**Figure 7:** Schematic presentation of siRNA mediated RNAi mechanism. dsRNA: double stranded RNA; siRNA: small interfering RNA; AGO2: Argonaute protein 2; TRBP: Human Immunodeficiency virus (HIV)-1 transactivating response (TAR) RNA-binding protein; RISC: RNA-induced silencing complex.

The RISC loading complex consists of Argonaute protein, Dicer and the dsRNA binding protein TRBP. TRBP is a RNA binding protein and it is involved in the recruitment of Argonaute proteins to Dicer (Chendrimada et al., 2005). The Argonaute protein is responsible for the unwinding of siRNA, cleaving and ejecting the passenger strand and guiding the siRNA to specific mRNA for gene silencing.

### ***1.2.3.2 siRNA as a Therapeutic Agent for Osteoporosis Treatment***

Effective delivery of siRNA to desired tissue or cells *in vivo* is very challenging due to high molecular weight (approximately 13 kDa), negative charge and instability of siRNA. Once siRNA is in the body, it is rapidly degraded by nucleases (half life of 6 min in rats) (Soutschek et al., 2004) and removed from the circulation by the reticuloendothelial system (RES), namely macrophages and Kupffer cells of liver. The excretion and degradation cause very small amount of siRNA to reach the targeted cell. In addition, once in the target cell, their cellular localization and degradation in the lysosomes are very important parameters to be considered to reach the highest efficacy (Whitehead et al., 2009). Due to these problems, many strategies are being developed to protect the siRNA and increase its circulation time. For this purpose, the delivery of RNAi with non-viral carrier systems such as liposomes, polymeric and inorganic (calcium phosphate) nanoparticles are becoming promising approaches for the treatment of some diseases such as osteoporosis (Liu X., 2016).

The studies concerning the treatment of osteoporosis using siRNA as a therapeutic agent focus on either suppression of osteoclastogenesis or induction of osteogenesis. These studies are generally limited to *in vitro* applications by using commercially available transfection reagents (Fahid et al., 2008; Wang and Grainger, 2010), or non-viral carriers such as polyethyleneimine (PEI) (Nguyen et al., 2014). Local delivery of siRNA to bone tissue has also been studied by using scaffolds (Zhang et al., 2016) or CPC cements (Wang et al., 2012).

Delivery of siRNA to bone tissue for the treatment of osteoporosis *in vivo* has just started (Zhang et al., 2012; Liang et al., 2015; Zhang et al., 2015; Sun et al., 2016). In one study, cationic liposomes were conjugated with a peptide of six repetitive sequences of three aminoacids; aspartate-serine-serine ((AspSerSer)<sub>6</sub>) for selective delivery of siRNA to bone forming surfaces (Zhang et al., 2012). Systemic delivery of the system to osteoporotic rats increased the accumulation of the delivery system in osteoblasts prompting bone formation.



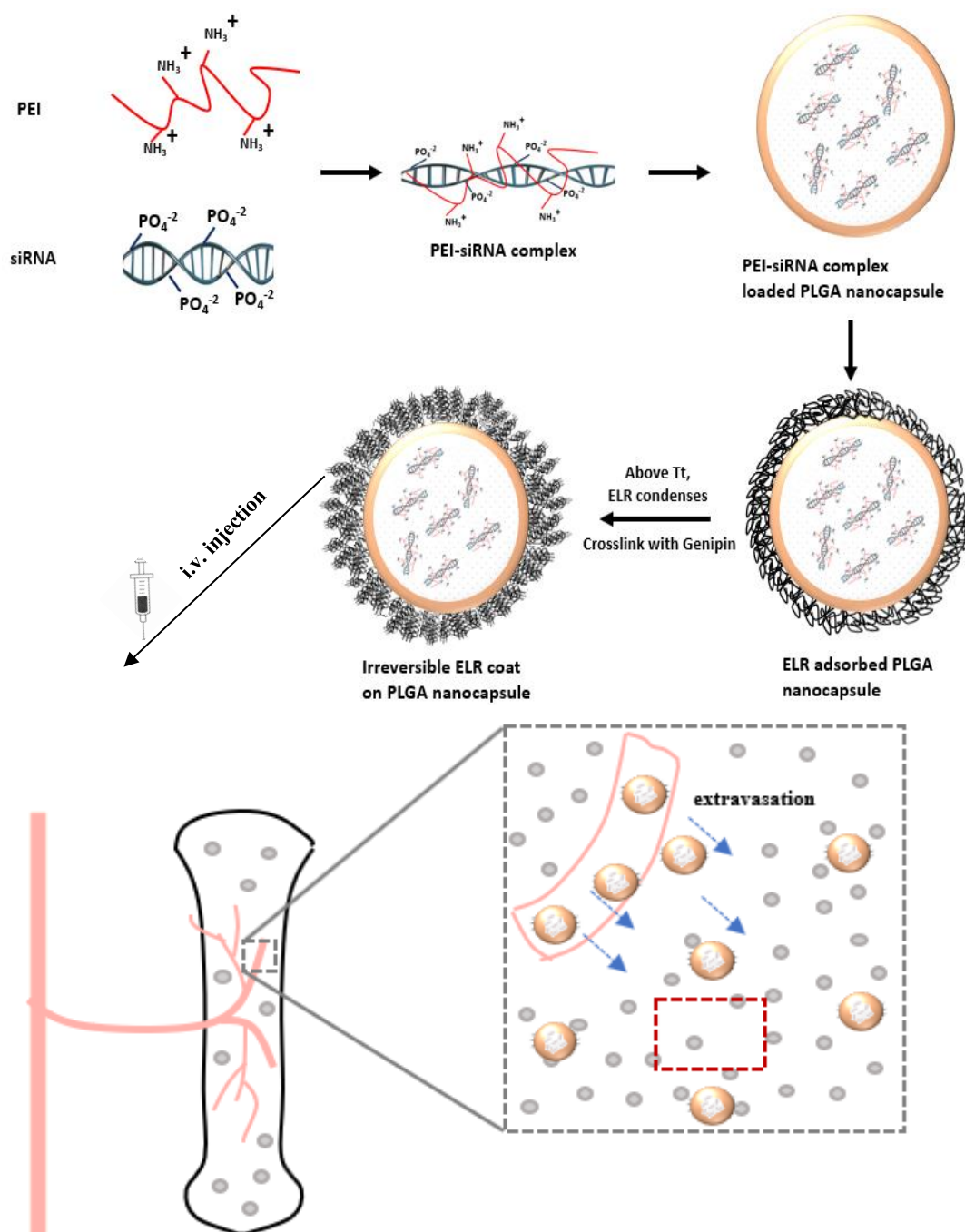
In another study, N-(2-hydroxypropyl) methacrylamide (HPMA) polymer was attached with (L-Asp)<sub>8</sub> to target bone surfaces (Zhang et al., 2015). Intravenous injections of the delivery system to ovariectomized rats increased the number of osteoblasts which led to increase in bone volume. In another study, osteoblasts on bone forming surfaces were targeted by using aptamer conjugated cationic liposomes (Liang et al., 2015). The system was administered to osteopenic rats and their bone mass was increased.

One of the non-viral carriers, polyethyleneimine (PEI) is widely used in the delivery of plasmid DNA and siRNA both *in vitro* (Richards et al., 2006) and *in vivo* (Bonnet et al., 2008). PEI is a cationic polymer which can form complexes with anionic nucleic acids. The capability of PEI to condense the nucleic acids in physiological and acidic conditions makes them efficient carriers for cellular uptake of siRNA (Utsuno and Uludag, 2010) because this complexation protects the siRNA from extracellular nucleases and neutralizes its negative charge. PEI is also known to exert proton sponge effect. In this approach, the proton absorbance capability of PEI, prevents the acidification of endosomes which leads to H<sup>+</sup> ion influx. This influx results in the accumulation of Cl<sup>-</sup> ions and water penetration into the endosomes, thus rupturing of endosomes and eventual leakage of the polyplex into the cytosol (Dominska and Dykxhoorn, 2010).

In siRNA delivery applications, generally branched PEI is used because linear PEI has lower folding capability when complexing with siRNA than the branched PEI, therefore, siRNAs from complexes with linear PEI are released more easily (Demadis et al., 2011). PEI is used either in the form of a complex with siRNA and loaded into the carriers or it is used together with the carriers to encapsulate naked siRNA for increasing the encapsulation of siRNA into the carriers (Patil and Panyam, 2009; Shen et al., 2015). During nanoparticle preparation, addition of PEI into the inner core has also been shown to decrease the initial burst release of siRNA from the particles due to the ionic interactions of PEI:siRNA complex with negatively charged polymers forming the shell (Murata et al., 2008).

Despite its mentioned advantages in gene delivery applications PEI, especially the branched form, exhibits high toxicity. The branched PEI causes apoptosis in transfected cells in a concentration and time dependent manner (Hall et al., 2013), therefore, loading the PEI-siRNA complex into the carriers reduces the toxicity of PEI (Alshamsan et al., 2010; Brunner et al., 2010).

### 1.3 Aim, Approach and Novelty of the Study



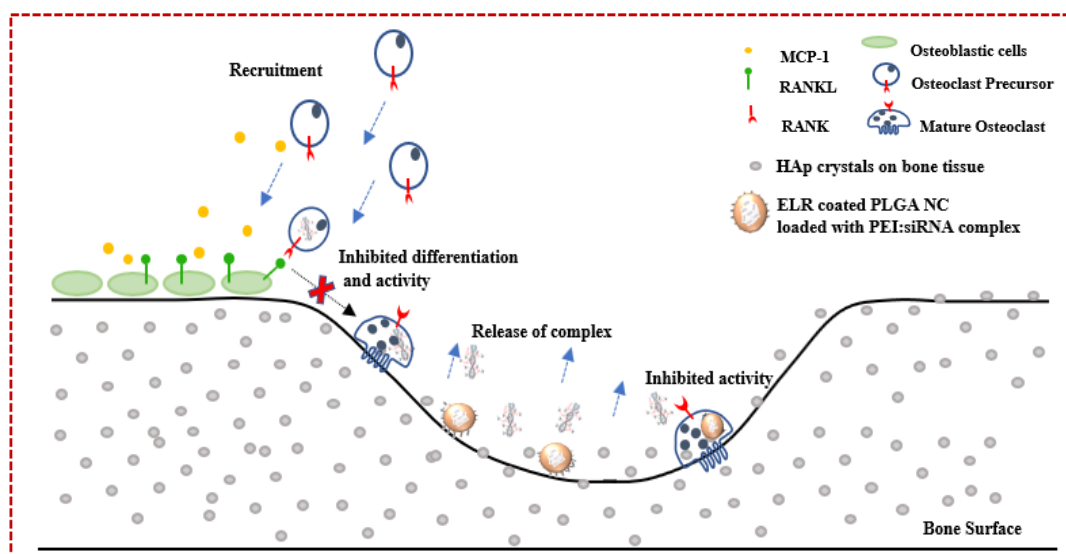


**Figure 8:** Approach of the study.

The aim of this study was to develop an injectable siRNA delivery system targeted to concentrate on the bone minerals to be used in the treatment of osteoporosis. The schematic presentation of the delivery system shows the intended route of administration and the possible working mechanism of the *in vivo* delivery system (Figure 8).

Branched PEI (section 1.2.3.2) was complexed with RANK siRNA because of its capability to protect the siRNA in extra and intracellular environments and its proton sponge property. The toxicity of PEI was reduced by encapsulating the complex in PLGA nanocapsules (section 1.2.2.2.2) which is a FDA approved polymer with good biocompatibility. PLGA is very suitable for nucleic acid delivery applications because PLGA nanocapsules can be internalized by the cells, escape from the endosomes, accumulate in the cytoplasm and act as drug depots to release their content into the cytoplasm where siRNA should function (Panyam et al., 2002; Vasir and Labhasetwar, 2007).

PLGA nanocapsules loaded with PEI:siRNA complex were then coated with a genetically engineered polypeptide, Elastin-Like Recombinamer (ELR) to target the nanocapsules specifically to bone tissue. The specific ELR used in this study is reported to contain a sequence which presents high affinity towards HAP minerals in bone tissue (Barbosa et al., 2009; Tejeda-Montes et al., 2014). ELR has a thermoresponsive property called inverse transition temperature (ITT). Below the transition temperature ( $T_i$ ) the free chains exist as random coils in solution in their hydrated form. Above the  $T_i$ , however, the chains fold which leads to aggregation of the chains (Rodriguez-Cabello et al., 2007). The ITT property of ELR was used in coating the ELR on PLGA nanocapsules for targeting.

Once operational, after the i.v. injection of the constructed delivery system, the nanocapsules are expected to extravasate from the fenestrations of the epithelium in the bone marrow. Due to existence of the ELR on them, the capsules will attach themselves to the extracellular matrix of the bone tissue where HAP is located and will start to release their content. During bone remodeling process at BMUs, the osteoclast precursors and mature osteoclasts will internalize either the released PEI:RANK siRNA complex or PLGA nanocapsules loaded with the complex, thereby osteoclastic differentiation and their activity will be diminished (Figure 8). This would eventually lead to reduced bone resorption and thus increased bone mass.

In the present study, ELR coated PLGA nanocapsules loaded with PEI:siRNA complex were prepared and *in situ* and *in vitro* studies were performed. The ELR coating, topography, encapsulation efficiency, release behavior and particle size distribution of these nanocapsules were studied. The efficacy of the PEI:RANK siRNA loaded PLGA nanocapsules were determined *in vitro* by analyzing RANK mRNA levels. Moreover, the effect of PEI:RANK siRNA loaded nanocapsules on the inhibition of differentiation of osteoclast precursors to mature osteoclast and suppression in their activity were studied.

To our knowledge, there is no study in the literature that has developed a bone targeted and systemic delivery of PLGA based siRNA delivery system to suppress RANK mRNA for the treatment of osteoporosis. The constructed delivery system is, therefore, a novel approach.

## CHAPTER 2

### MATERIALS AND METHODS

#### 2.1 Materials

For nanocapsule preparation, poly(lactic acid-co-glycolic acid) (PLGA) (50:50) was purchased from Corbion Purac Biomaterials (Netherlands). bPEI (25 kDa) was from Sigma (Germany). Targeting polypeptide, Elastin-like recombinamer (ELR) was synthesized in the laboratory of Prof. Dr. J. Carlos Rodriguez-Cabello, University of Valladolid (Spain). The Inverse Temperature Transition (ITT) of ELR sequence was around 34 °C and its molecular weight is 31,877 kDa. Hydroxyapatite (HAp), and polyvinylalcohol (PVA) was purchased from Sigma (Germany) and crosslinker genipin was purchased from Wako Chemicals (USA). RANK siRNA was purchased from Ambion (USA). DNA substitute for the siRNA molecule (DNAoligo) was purchased from Iontek (Turkey). In the cell culture studies, murine RAW 264.7 macrophage cell line was used (ATCC, UK). Dulbecco's Modified Eagle Medium (DMEM)-high glucose (glucose concentration: 4.5 g/L), DMEM-high glucose colorless, fetal bovine serum (FBS) was obtained from Biological Industries (USA). Penicillin/streptomycin (100 units/mL-100 µg/mL) and bovine serum albumin (BSA) were purchased from Fluka (Switzerland). Hiperfect Transfection Reagent was purchased from Qiagen, (Germany). TRAP staining kit was purchased from Sigma (Germany). RIPA buffer and BCA protein assay kit were purchased from Millipore (USA) and proteinase inhibitory cocktail was purchased from Thermo Scientific (Germany). RANK primary (4845s),  $\beta$ -actin primary (4970s; 1:1000 dilution in 5% skimmed milk) and Anti-rabbit IgG HRP conjugated secondary antibodies (7074s) were from Cell Signaling Technologies (USA).

## 2.2 Methods

### 2.2.1 Preparation and Characterization of PEI:Nucleic Acid Complexes

In the *in situ* studies DNAoligo was used as a substitute for siRNA. The formation of complex of nucleic acids (DNAoligo and siRNA) and PEI is achieved due to the ionic interactions of negatively charged phosphates in nucleic acids and positively charged amino groups in PEI (Figure 9).

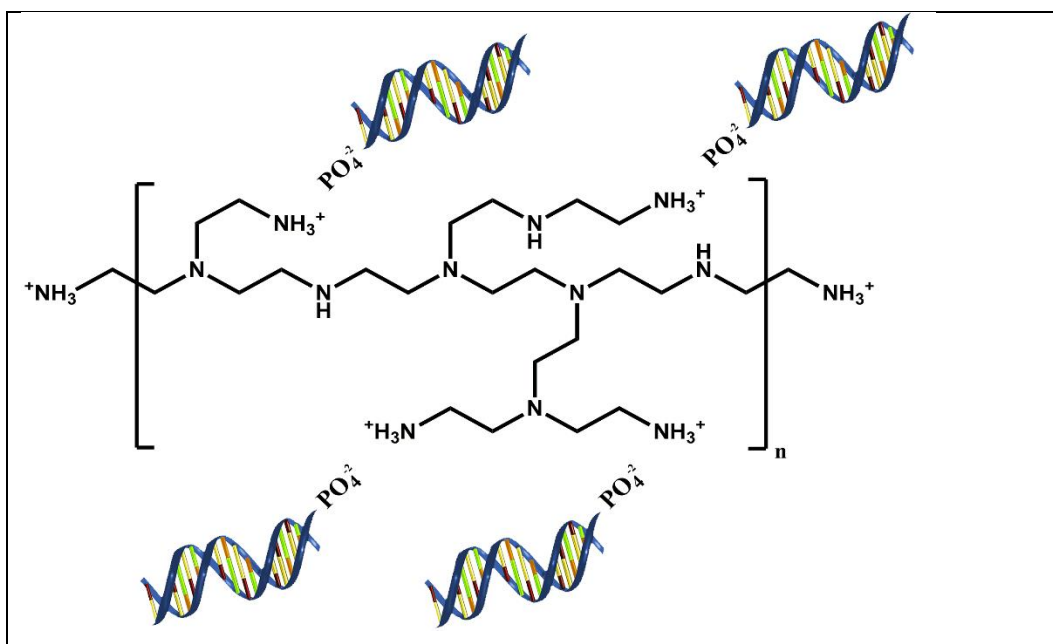


**Figure 9:** Schematic presentation of PEI:nucleic acid complex. The complexes are formed by the ionic interaction of the positive charged amino groups of PEI ( $\text{-NH}_3^+$ ) and negative charged phosphates in the nucleic acids ( $\text{-PO}_4^{2-}$ ).



The DNAoligo or siRNA sequences are 21 nucleotides long and therefore contain 42 phosphate groups (P). One PEI molecule contains 53 repeating units containing 11 nitrogen atoms (N). Therefore, N/P ratio was calculated by the following equation:

$$\text{N/P ratio} = \frac{\text{number of moles of N in PEI} \times 583}{\text{number of moles of P in siRNA} \times 42}$$

PEI:nucleic acid complexes with varying nitrogen-to-phosphate ratios (N/P) were prepared in 1X Tris-EDTA (TE) buffer, pH 7.4. For complex formation, DNAoligo (10  $\mu$ M, 2  $\mu$ L) or siRNA (10  $\mu$ M, 2  $\mu$ L) were mixed with aqueous PEI solutions (starting PEI solution concentration 175 ng/ $\mu$ L) to yield final N/P atomic ratios of 1, 2, 3, 4, 5, 6 and 10. The mixtures were incubated for 20 min at room temperature. The formed complexes were subjected to agarose gel electrophoresis (2%, 100 V, 20 min) and visualized under UV light (UVP GelDoc Imaging System, USA).

#### ***2.2.1.1 Measurement of Zeta Potential and Condensation of PEI:Nucleic Acid Complexes***

The zeta potential of PEI:DNAoligo complexes with varying N/P atomic ratios (0-20) were measured by Zeta Sizer (Malvern Nano ZS90, UK). DNAoligo (10  $\mu$ M, 6  $\mu$ L, in TE buffer pH 7.4) and aqueous PEI solutions (6  $\mu$ L) were mixed to form complexes with N/P ratios of 0, 1, 2, 3, 4, 5, 6, 10 and 20. The mixtures were incubated for 20 min at room temperature and diluted in nuclease-free dH<sub>2</sub>O water (1 mL).

For visualization of migration and analyzing the condensation of PEI:nucleic acid complexes, the complexes were stained with EtBr during agarose gel electrophoresis. Complexes of different N/P ratios (section 2.2.1), were loaded in EtBr stained agarose gel (2%) and run for 20 min at 100 V in 1X TAE buffer (pH 8). The gel was visualized under UV exposure (ChemiDoc UVP, Germany).

### 2.2.2 Preparation of PLGA Nanocapsules

Nanocapsules were prepared by water-oil-water (w/o/w) double emulsion method. Briefly, PLGA (50:50) (50 mg) was dissolved in DCM (0.5 mL), PEI:siRNA complexes (150  $\mu$ L) were added and probe sonicated for 30 s at 50 W. This emulsion was added into PVA solution (3 mL, 4%) and sonicated. This double emulsion was added into PVA solution (7.5 mL 0.3%) and mixed vigorously for three hours with a magnetic stirrer at room temperature for evaporation of DCM. Nanocapsules were centrifuged (18,000 rpm, 10 min, RT). The pellet was washed twice with 3 mL nuclease free water. Nanocapsules were resuspended in 5 mL dH<sub>2</sub>O and lyophilized for 8 h.

In order to coat ELR onto PLGA nanocapsules, inverse temperature transition (ITT) property of the recombinamer was used. Due to ITT, the solubility of ELR decreases above the transition temperature ( $T_t$ ) which causes the aggregation of the recombinamer (Rodriguez-Cabello et al., 2007). The  $T_t$  of ELR used in this study has around 34 °C (Barbosa et al., 2009). As a crosslinking agent, genipin was used (Chang et al., 2003).

PLGA nanocapsules (10 mg) were added into ELR solution (1 mL, 10 mg/mL) for physical adsorption of ELR on the nanocapsules. This suspension was incubated at 25°C in a sonication bath for 1 h then the volume was increased to 10 mL PBS solution in a volumetric flask. The temperature was raised to 37°C and maintained for 20 min which causes the ELR to aggregate on the nanocapsules. The capsules were centrifuged (18,000 rpm, 10 min, 37°C) to remove the free ELR and the pellet was resuspended in 10 mL PBS (37°C) to which genipin solution (1 mL, 10 mg/mL) was added. The suspension was incubated at 37°C for 6 h, centrifuged and washed. As a control, the same procedure was performed for 10 mg PLGA nanocapsules and 1 mL genipin solution addition (10 mg/mL).

#### ***2.2.2.1 Specificity of the ELR Towards Hydroxyapatite***

The specificity of ELR to HAp was determined by Fourier Transform Infrared (FTIR) spectroscopy. Disks of HAp crystal (diameter 13 mm) were prepared by compression. Aqueous ELR solution (5 %, 50  $\mu$ L) was added onto the HAp disk and incubated for 1 h at 25<sup>0</sup>C. The HAp disk was washed three times with dH<sub>2</sub>O (3 mL) and allowed to dry. As a blank, a HAp disk was produced as mentioned above, wetted with dH<sub>2</sub>O (50  $\mu$ L) and air dried before FTIR. As a control of protein adhesion, a HAp disk was treated with aqueous BSA solution (5 %, 50  $\mu$ L) and air dried. The FTIR of the samples were obtained in the range 4000-400 cm<sup>-1</sup> using a FTIR spectrophotometer (PerkinElmer, PIKE GladiATR, USA).

#### ***2.2.2.2 Preferential Binding of ELR Coated Nanocapsules on CaP Surface***

Suspensions of Nile Red loaded uncoated and ELR coated PLGA nanocapsules (1 mg NC/5 mL dH<sub>2</sub>O) were added in CaP coated Osteoassay Surface Plates (Corning, USA) and incubated for 1 h at 25<sup>0</sup>C. The plates were then washed three times with dH<sub>2</sub>O (200  $\mu$ L) and allowed to dry. The nanocapsules remained on the CaP coated surface were visualized with Confocal Laser Scanning Microscopy (Zeiss LSM800, Germany).

### **2.2.3 Characterization of Nanocapsules**

#### ***2.2.3.1 Loading and Encapsulation Efficiency of PEI:DNAoligo in PLGA Nanocapsules***

Encapsulation efficiency of PEI:DNAoligo complex within the PLGA nanocapsules were studied by using the fluorescence intensity (FI) of FAM-labelled DNA-oligo measured with a spectrofluorometer ( $\lambda_{\text{ex}}$ : 494 nm,  $\lambda_{\text{em}}$ : 524 nm) (SpectraMax M2e, Molecular Devices, USA). A calibration curve constructed with empty nanocapsules (1 mg in 200  $\mu$ L 1X TE buffer) which are mixed with known amounts of PEI:FAM labelled DNAoligo complexes (N/P 20) (0.1, 0.2, 0.4, 0.6, 0.8  $\mu$ g FAM-labelled DNAoligo) was used for the calculations.

PLGA nanocapsules (1 mg), which were prepared with an input of 20 µg FAM-labelled DNAoligo (N/P 20), were suspended in 1X TE buffer (200 µL). The amount of complex encapsulated in the nanocapsules were calculated from the calibration curve. The loading and encapsulation efficiency was calculated using the following equations:

$$\text{Loading} = \frac{\text{Amount of encapsulated complex (}\mu\text{g)}}{\text{Amount of nanocapsule (g)}}$$

$$\text{E. E. (\%)} = \frac{\text{Amount of encapsulated complex (g)}}{\text{Input amount of complex (g)}} \times 100$$

### ***2.2.3.2 In Situ Release of PEI:DNAoligo Complex from the PLGA Nanocapsules***

In order to study the release of the PEI:FAM-labelled DNAoligo (N/P 20) complex from PLGA nanocapsules, the capsules (1 mg) were suspended in TE buffer (200 µL) in an Eppendorf tube and kept at 37°C under constant shaking for 15 days. On Days 1, 3, 5, 7, 10 and 15, suspensions were centrifuged (18,000 g, 20 min). The pellet was resuspended in fresh TE buffer (200 µL) and the FI was measured by using a spectrofluorometer ( $\lambda_{\text{ex}}$  494 nm,  $\lambda_{\text{em}}$  524 nm) (SpectraMax M2e, Molecular Devices, USA). The amount of complex remained in the capsules was calculated by using FI obtained from the nanocapsules at each time point. The data is presented as “cumulative complex released vs time” and treated according to Higuchi equation

$$\left(\frac{[M]_t}{[M]_{\infty}} \text{ vs } t^{1/2}\right).$$

#### ***2.2.3.3 In Situ Degradation of PLGA Nanocapsules***

The degradation of PLGA nanocapsules were studied with SEM. Nanocapsules (1 mg) were suspended in 1X TE buffer (pH 7.4, 200  $\mu$ L) in Eppendorf tube and incubated at 37<sup>0</sup>C under constant shaking for 21 days. On Days 1, 3, 5, 7, 10, 15 and 21, the suspension was centrifuged and the pellet was resuspended in TE buffer (200  $\mu$ L). 20  $\mu$ L of this suspension was diluted with dH<sub>2</sub>O (80  $\mu$ L) and dried overnight on SEM stubs. Stubs were coated with Au–Pd in a sputter coater. SEM images were obtained at 10 kV with QUANTA 400F Field Emission SEM (Netherland) at the Central Laboratory (METU).

#### ***2.2.3.4 Detection of ELR on PLGA Nanocapsules***

##### **2.2.3.4.1 Nanocapsule Topography with SEM**

Control PLGA and the ELR coated PLGA nanocapsule suspensions were added on a carbon tapes (Electron Microscopy Sciences, USA) attached to Scanning Electron Microscopy (SEM) stubs, air dried overnight and coated with Au–Pd in a sputter coater. SEM images were obtained at 10 kV. Nanocapsule topography was studied with SEM (QUANTA 400F Field Emission SEM, Netherland) at the Central Laboratory (METU).

##### **2.2.3.4.2 Detection of ELR on Nanocapsules with TEM and XPS**

For TEM analysis, control PLGA and the ELR coated PLGA nanocapsules were suspended in ethanol and air dried on TEM grids. TEM (FEI Technai G2 Spirit Biotwin, USA) images were obtained at the Central Laboratory (METU).

For XPS analyses, both control PLGA and the ELR coated PLGA nanocapsules were lyophilized and analyzed with XPS (PHI 5000 VersaProbe) for presence of nitrogen as an indicator of the ELR (protein) existence. XPS analyses was performed at the Central Laboratory (METU).

#### **2.2.3.5 Particle Size Distribution**

Size distribution of the PLGA nanocapsules were determined using a suspension of PLGA nanocapsules in dH<sub>2</sub>O (ca. 1 mg PLGA/5 mL) with Zeta Sizer (Malvern Nano ZS90, UK). For each sample, 3 measurements were performed, 12 runs each, in order to obtain the final size distribution.

#### **2.2.4 Cell Culture Studies**

##### **2.2.4.1 RAW264.7 Cell Line: In Vitro Culture and Differentiation**

In the *in vitro* studies, commonly used murine macrophage RAW 264.7 cell line (ATCC, UK) was used as preosteoclasts (Pre-OC) (Hsu et al., 1999). The cells were cultured in Dulbecco's Modified Eagle's Medium (DMEM) supplemented with 1% penicillin-streptomycin, and 10 % FBS. The cells were incubated at 5 % CO<sub>2</sub>, at 37°C.

For differentiation of RAW264.7 cells to osteoclasts, RAW cells ( $1.4 \times 10^4$ ) were mixed with RANKL (100 ng/mL, Peprotech, USA) and M-CSF (20 ng/mL, R&D Systems, USA) and seeded on TCPS slides (2.8 cm<sup>2</sup>). Differentiation was monitored by Acid Phosphatase Leukocyte (TRAP) Kit (Sigma, Germany) according to manufacturer's protocol. TRAP-positive and multinucleated cells containing three or more nuclei were counted as osteoclasts under a light microscope by using ImageJ Analysis Software (NIH, USA).

##### **2.2.4.2 Determination of Cell Viability**

Pre-OC cells ( $5 \times 10^3$ ) were seeded on 96-well plates (30 µL). PLGA nanocapsules (0.5 mg) diluted in OptiMEM (30 µL) was added on to the cell suspension and incubated for 6 h (37°C in 5% CO<sub>2</sub> incubator). Then DMEM high full medium supplemented with 10% FBS was added onto the cells (140 µL). The cell viability was measured for 5 days with Alamar Blue Cell Viability assay. The medium was refreshed after 3 days.

At each time point, the medium was removed and 10% Alamar Blue solution in colorless DMEM (200 µL) was added onto the cells and incubated for 150 min. The optical density was measured at 570 nm and 595 nm with a microplate reader (SpectraMax M2, Molecular Devices, U.S.A.).

From these optical density values, percent reduction and cell numbers were calculated by using a calibration curve for the cell line (Appendix B) plotted from the percent reductions and corresponding cell number, with the following equation:

$$Reduction (\%) = \frac{((\epsilon_{ox})_{\lambda_2} \times A_{\lambda_1}) - ((\epsilon_{ox})_{\lambda_1} \times A_{\lambda_2})}{((\epsilon_{red})_{\lambda_1} \times A'_{\lambda_2}) - ((\epsilon_{red})_{\lambda_2} \times A'_{\lambda_1})} \times 100$$

where,  $\lambda_1 = 570 \text{ nm}$  and  $\lambda_2 = 595 \text{ nm}$

$A_{\lambda_1}$  and  $A_{\lambda_2}$  = Absorbance of test well

$A'_{\lambda_2}$  and  $A'_{\lambda_1}$  = Absorbance of negative control well (blank)

Molar Extinction Coefficients

$(\epsilon_{ox})_{\lambda_2} = 117.216$        $(\epsilon_{red})_{\lambda_1} = 155.677$

$(\epsilon_{ox})_{\lambda_1} = 80.586$        $(\epsilon_{red})_{\lambda_2} = 14.652$

#### **2.2.4.3 Internalization of the Nanocapsules by the Cells**

For imaging the localization of PLGA nanocapsules in cells, PLGA nanocapsules stained with Nile Red (6 mg) were resuspended in OptiMEM (200 µL) and added onto RAW264.7 cell ( $1.2 \times 10^5$ ) suspension in an Eppendorf tube. The mixture was seeded on TCPS slides, incubated for 6 h (37°C in 5% CO<sub>2</sub> incubator) for complete attachment and full medium was added (3 mL). 48 h post transfection, cells were fixed with PFA (4% w/v) for 15 min at room temperature. Cell membranes were permeabilized with Triton X-100 (0.1% v/v in 10 mM Tris-HCl buffer) for 5 min at room temperature.

After washing with PBS, cells were incubated in BSA (1% w/v in PBS) at 37°C for 1 h to prevent non-specific binding. Then, they were incubated in Alexa 488-labelled Phalloidin (1:50 dilution in 0.1% BSA in PBS) for 1 h and incubated with DRAQ5 (1:1000 dilution in PBS) for 30 min at 37°C. Cells were washed twice with PBS and visualized by confocal laser scanning microscopy (Leica DM2500, Germany).

#### **2.2.4.4 Treatment with the Delivery System**

For the mRNA inhibition studies, PLGA nanocapsules containing PEI:RANK siRNA (6 mg) was resuspended in OptiMEM (200 µL).  $1.2 \times 10^5$  RAW264.7 osteoclast precursor cells were seeded in 12-well plates and the capsules were added dropwise onto the cell suspension (200 µL). The cells were incubated (37°C in 5% CO<sub>2</sub> incubator) for 6 h. At the end of 6 h growth medium (800 µL) (DMEM supplemented with 10 % FBS) was added very gently. Gene silencing was monitored at 3 and 5 days post transfection (Section 2.2.5). The controls of the study were empty nanocapsule and PEI:Scrambled siRNA loaded nanocapsule transfected cells.

For the inhibition of differentiation of RAW264.7 preosteoclastic cell line into mature osteoclasts, RAW cells ( $5 \times 10^3$  cells/cm<sup>2</sup> in DMEM high full medium, 50 µL) were mixed with RANKL (100 ng/mL), M-CSF (20 ng/mL) and PLGA nanocapsules (0.7 mg of either empty, PEI:scrambled siRNA or PEI:RANK siRNA loaded nanocapsules in OptiMEM, 50 µL). The cell suspensions together with the nanocapsules were seeded onto TCPS slides (2.8 cm<sup>2</sup>) and incubated 3 h for cell attachment. Then, full medium was added (3 mL) and incubated for 5 days (37°C in 5% CO<sub>2</sub> incubator) with a medium change at the 3rd day. On Days 3 and 5, the cells were fixed with PFA (4% w/v) and washed twice with PBS. Then, TRAP staining was performed by Acid Phosphatase Leukocyte (TRAP) Kit (Sigma, Germany) according to manufacturer's protocol. Multinucleated cells were counted as osteoclasts under light microscope by using ImageJ Analysis Software (NIH, USA) (Section 2.2.6.1).



## 2.2.5 Gene Expression Studies

### 2.2.5.1 Efficiency of RANK siRNA Sequence in Gene Silencing

In order to determine the efficiency of siRNAs to knockdown the target gene RANK and to understand the time interval that indicates the maximum inhibition, two RANK siRNA sequences were studied (RANK siRNA #1, RANK siRNA #2, Table 1).

**Table 1:** RANK siRNA Sequences Used in the Study

	Sequences	
RANK siRNA Type	Sense	Antisense
RANK siRNA#1 (5'->3')	GCAGUAGUCUAAGUG GAAATT	UUUCCACUUAGACUAC UGCAA
RANK siRNA#2 (5'->3')	GGAGAGGCAUUAUG AGCAUTT	AUGCUCAUAAUGCCUC UCCTG

For the transfection of siRNA into the cells, HiPerfect Transfection Reagent was used with a fast-forward transfection protocol as follows: 28 pmol siRNA (375 ng, final concentration 23 nM) was diluted in Opti-MEM (200  $\mu$ L) and vortexed. HiPerfect transfection reagent (6  $\mu$ L) was added to the siRNA solution, mixed and incubated for 10 min at room temperature to allow the formation of transfection complexes. Meanwhile,  $1.2 \times 10^5$  RAW264.7 osteoclast precursor cells were seeded on 12-well plates. The complexes were added drop-wise onto the cell suspension (200  $\mu$ L). The cells with transfection complexes were incubated (37°C in 5% CO<sub>2</sub> incubator) for 6 h and 800  $\mu$ L of growth medium (DMEM supplemented with 10 % FBS) was added very gently. Gene silencing was monitored at 24, 48 and 72 h post transfection.

### 2.2.5.2 Quantitative Real Time PCR (qRT-PCR)

For the determination of RANK mRNA inhibition through siRNA transfection, qRT-PCR studies were performed. The primer pairs (Table 2) used to analyze the fold change of RANK were designed according to mRNA sequences of *Mus musculus* (NCBI accession numbers: RANK; NM\_009399 and GAPDH; NM\_001289726).

**Table 2:** qRT-PCR Primers and the Amplicon Sizes

	Primers (5'-3')	Sequence	Amplicon size (bp)
<b>RANK</b>	<b>Forward</b>	AGAGGGGAGCCTCAGGGTCC	112
	<b>Reverse</b>	AAGTTCATCACCTGCCCGCTAGA	
<b>GAPDH</b>	<b>Forward</b>	TGCACCACCAACTGCTTAGC	87
	<b>Reverse</b>	GGCATGGACTGTGGTCATGAG	

The optimization studies performed for the primers are presented in Appendix A. The qRT-PCR cycling conditions for both RANK and GAPDH primers are given in (Table 3).

**Table 3:** qRT-PCR Cycling Conditions for the Primers.

Process	Conditions
Initial Denaturation	95 <sup>0</sup> C, 5 min
Denaturation	95 <sup>0</sup> C, 5 s } 35 cycle 60 <sup>0</sup> C, 10 s }
Annealing and Extension	
Melt	50 <sup>0</sup> C-99 <sup>0</sup> C; 1 <sup>0</sup> C/1 cycle

The amount of RANK mRNA normalized to the housekeeping gene GAPDH and relative to control (the fold change of RANK) was calculated using the  $2^{-\Delta\Delta C_t}$  relative expression equation:

$\Delta C_t (\text{treated}) = C_t (\text{target gene}) - C_t (\text{reference gene})$	Eq. 1
$\Delta C_t (\text{control}) = C_t (\text{target gene}) - C_t (\text{reference gene})$	Eq. 2
$\Delta\Delta C_t = \Delta C_t (\text{treated}) - \Delta C_t (\text{control})$	Eq. 3
Amount of target normalized to reference gene and relative to control (Fold Change) = $2^{-\Delta\Delta C_t}$	Eq. 4

where,

Treated sample	siRNA treated sample
Control sample	Untransfected sample
Target gene	RANK
Reference gene	GAPDH

At 24, 48 and 72 h, RNA was isolated from the cells, treated with DNase I in order to remove the DNA contamination from the isolated RNA solution. DNase I treated RNA samples were then converted into cDNA (Appendix A) and finally qRT-PCR was performed.

Fold changes of mock (only HiPerfect transfection reagent treated cells) and scrambled siRNA transfected cells and RANK siRNA transfected cells were normalized to that of untransfected cells.

### **2.2.5.3 Inhibition of RANK mRNA with Varying N/P ratios**

In order to determine the efficient N/P ratio of PEI:siRNA complexes which is not toxic and would lead to inhibition of the expression of RANK, qPCR studies were performed with the complexes of N/P ratios of 6, 20, 25, 30 and 60. For this purpose, the known amount of siRNA (375 ng/well, 23 nM) was complexed with PEI, so that the mentioned N/P ratios were achieved.

The complexes were diluted in OptiMEM (200  $\mu$ L) and were added onto the cell suspension ( $1.2 \times 10^5$  RAW264.7 cells). The cells with the complexes were incubated ( $37^\circ\text{C}$  in 5%  $\text{CO}_2$  incubator) for 6 h and 800  $\mu$ L of growth medium (DMEM supplemented with 10 % FBS) was added very gently. Gene silencing was monitored at 24, 48 and 72h post transfection. The amount of siRNA was determined according to previous studies (section 2.2.5.1) which led to significant inhibition in RANK mRNA expression. The controls of the study were, untransfected cells, PEI transfected cells (Mock) and PEI:scrambled siRNA complex transfected cells.

#### ***2.2.5.4 Inhibition of RANK mRNA in Nanocapsule Transfected Cells***

RAW264.7 ( $1.2 \times 10^5$ ) cells were transfected with either empty, PEI:Scrambled siRNA loaded (N/P 20) or PEI:RANK siRNA complex loaded (N/P 20) PLGA nanocapsules (6 mg). On Days 3 and 5, the cells were washed with PBS to remove the dead cells, RNA isolation and then qRT-PCR were performed.

### **2.2.6 Inhibition of Osteoclast Differentiation and Activity**

#### ***2.2.6.1 Inhibition of Osteoclast Differentiation***

RAW cells ( $5 \times 10^3$  cells/ $\text{cm}^2$ ) were mixed with RANKL (100 ng/mL), M-CSF (20 ng/mL) and PLGA nanocapsules (0.7 mg of either empty, PEI:Scrambled siRNA or PEI:RANK siRNA loaded nanocapsules). The cell suspensions were seeded onto TCPS slides ( $2.8 \text{ cm}^2$ ). On Days 3 and 5, the cells were fixed with PFA (4% w/v) and washed twice with PBS. Then, TRAP staining was performed by Acid Phosphatase Leukocyte (TRAP) Kit (Sigma, Germany) according to manufacturer's protocol. The entire images of three TCPS slides from separate runs were obtained by Zeiss Brightfield MosaiX Protocol (Zeiss Axio Imager M2, Germany). Multinucleated cells were counted as osteoclasts under microscope by using ImageJ Analysis Software (NIH, USA).

#### **2.2.6.2 Inhibition of Osteoclastic Activity**

For the determination of inhibition of osteoclastic activity pit formation assay was performed on 96 well Osteoassay surface plates (Corning, USA).

For the study, RAW264.7 cells ( $5 \times 10^3$  in DMEM high full medium, 50  $\mu$ L) were mixed with RANKL (100 ng/mL), M-CSF (20 ng/mL) and PLGA nanocapsules (0.4 mg of either empty, PEI:Scrambled siRNA or PEI:RANK siRNA loaded nanocapsules, 50  $\mu$ L).

After complete attachment of cells, the medium was completed to 200  $\mu$ L with DMEM high full medium. The cells were differentiated for 5 days, with a medium change on Day 3. At the end of Day 5, the medium was removed and cells were treated with bleach solution (10 %, 100  $\mu$ L) for 5 min at room temperature. Then, the wells were washed twice with distilled water and allowed to dry. The resorption pits were visualized under light microscope at 20 X magnification. The fraction of resorbed surface area was quantified by using 15 images from each group (n=3) by using Image J software (NIH, USA).

#### **2.2.7 Statistical Analysis**

All quantitative data presented in the study were expressed by mean  $\pm$  standard deviations. Statistical differences among groups were assessed by two-way ANOVA (analysis of variance) with Tukey's post-hoc analysis except for pit formation assay which was assessed by one-way ANOVA (analysis of variance).  $p$  value  $\leq 0.05$  was considered to be statistically significant. Analysis was performed via GraphPad Prism v6.0.



## CHAPTER 3

### RESULTS AND DISCUSSION

#### 3.1 Characterization of PEI:DNAoligo Complexes

##### 3.1.1 Zeta Potential of PEI:DNAoligo Complexes

In order to determine the complete complexation of PEI with DNAoligo or siRNA, the zeta potential of the PEI:DNAoligo complexes was measured. Zeta potential is a function of surface charge of a particle in a test solution and the ionic strength of the test solution is important in the measurement of the zeta potential (Sze et al., 2003). The nucleic acids are negatively charged due to the phosphate groups they carry on their backbone and PEI is positively charged because of its primary, secondary and tertiary amino groups. When PEI and nucleic acids interact, the charges are neutralized.

For the measurement, equal volumes of PEI (starting PEI concentration 175 ng/ $\mu$ L) and DNAoligo (10  $\mu$ M) were mixed, incubated at room temperature, and diluted in nuclease free dH<sub>2</sub>O to form complexes of N/P ratios of 1, 2, 3, 4, 5, 6, 10 and 20. The zeta potentials of the PEI:DNAoligo complexes with N/P ratios of 0–20 are presented in Figure 10.

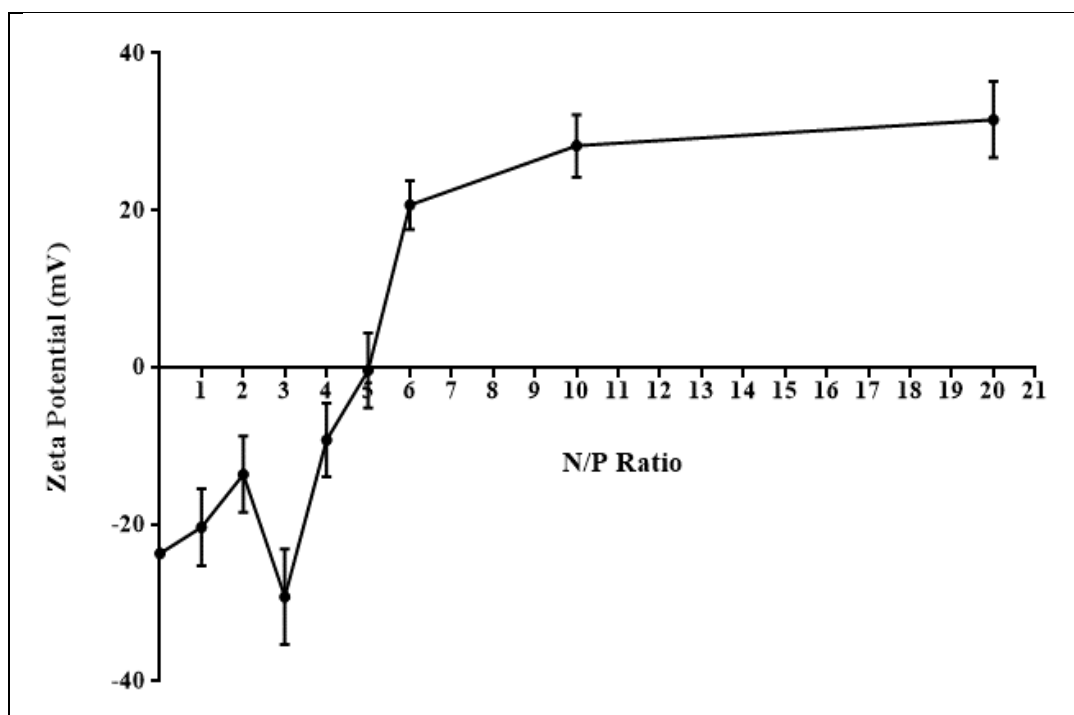


**Figure 10:** Zeta potential of PEI:DNAoligo complexes with different N/P ratios. Complexes with up to N/P ratio of 5 presented negative zeta potentials. The charge of the complexes shifted to positive values after N/P 5 which indicates that all the DNAoligo was in complexed form with PEI.

As can be seen from the figure, up to the N/P ratio of 5, the zeta potential of the complexes was negative. This may be explained by the steric availability of  $\text{PO}_4^{2-}$  groups which were not neutralized. After that point, where the PEI amount is much higher than the nucleic acids, the zeta potential of the complexes shifts to positive values. These results are consistent with the literature. Wagner et al., studied the complexation and zeta potentials of PEI:siRNA complexes (Wagner et al., 2013). In that study, it was also found that increasing the N/P ratios led to a shift of surface charge from negative to positive values. From these results, it may be concluded that N/P ratio of 5 is needed to bring the zeta potential of the complexes to approximately neutral ( $-0.4 \pm 4.8$  mV). As the PEI proportion increases further, the zeta potential becomes more positive and reaches a plateau after a N/P ratio of 10.



### 3.1.2 Condensation of PEI:Nucleic Acid Complexes

Condensation of nucleic acids with PEI were studied by using electrophoretic mobility assay. In this assay, the migration of the molecules through the matrix of the agarose gel is controlled by the size and charge of the molecules. Complexes of PEI:DNAoligo and PEI:siRNA were prepared and their condensation levels were compared with agarose gel electrophoresis to determine whether DNAoligo can be used as a substitute for siRNA in the encapsulation efficiency and release studies. Complexes of PEI and nucleic acids are formed due to ionic interactions between negatively charged Phosphates of nucleic acids and positively charged Nitrogens of PEI (Figure 9) which neutralize their charges. PEI also condenses the nucleic acids, therefore, both the neutralization and resultant condensation of the complexes lead to reduced electrophoretic migration in agarose gel during electrophoresis.

The migration patterns of the complexes PEI:siRNA and PEI:DNAoligo with N/P ratios of 0–10 on EtBr stained agarose gel (2%) are presented in Figure 11. In complexes with  $N/P \leq 4$ , nucleic acid bands present the uncomplexed form of the nucleic acids that has migrated through the gel. As the N/P increases, the band intensity becomes weaker indicating that lesser amount of nucleic acids which have migrated. When N/P was higher than 5, no electrophoretic movement was observed. This is due to the complexation process, the charge of the complex becomes cationic which prevented their migration through the gel. Since both PEI:siRNA (Figure 11A) and PEI:DNAoligo (Figure 11B) complexes exhibit the same pattern of complexation, we concluded that the DNAoligo could be used as a substitute for siRNA in the optimization of encapsulation efficiency and release studies.

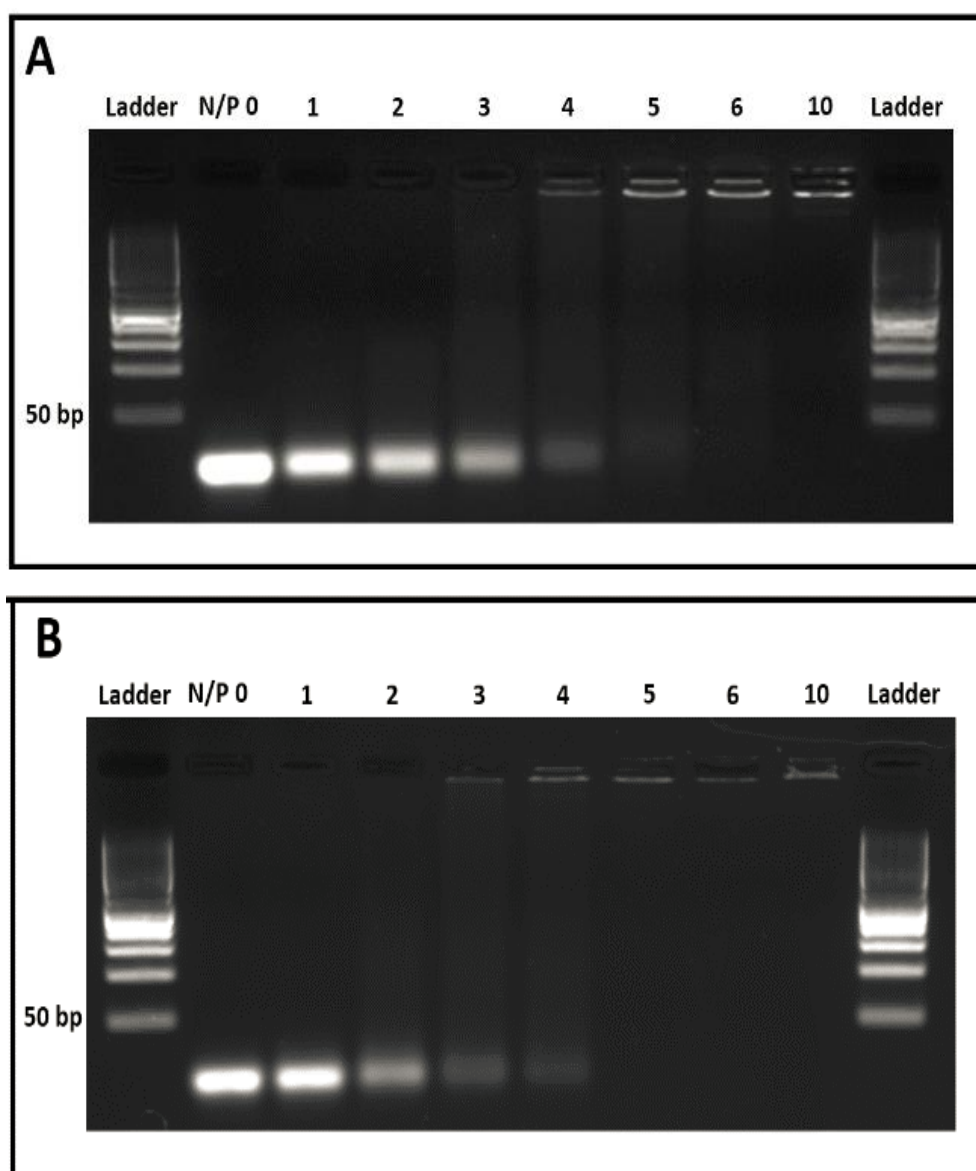


**Figure 11:** Electrophoretic mobility assay of PEI:nucleic acid complexes in Agarose gel. (A) PEI:siRNA, and (B) PEI:DNAoligo complexes with N/P of 0–10. The agarose gel (2%) was run for 20 min at 100 V. Above a N/P ratio of 5, nucleic acid migration was suppressed by charge neutralization through PEI complexation.

## **3.2 Characterization of Nanocapsules**

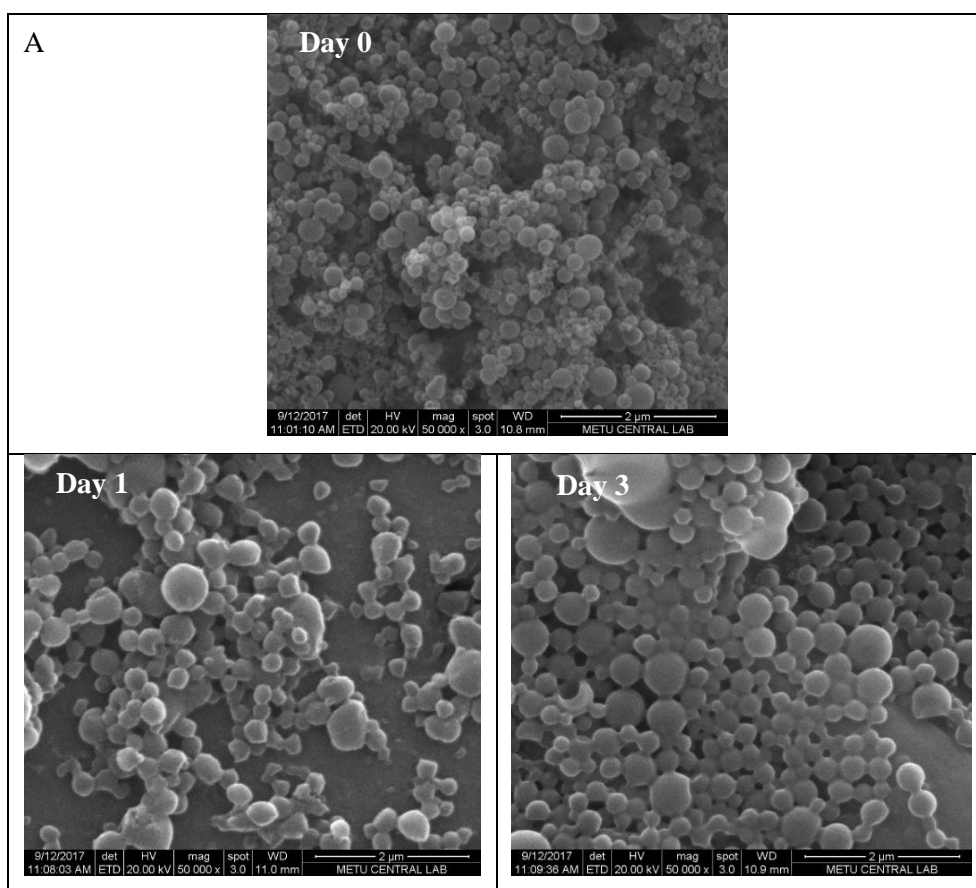
### **3.2.1 Loading and Encapsulation Efficiency of PEI:DNAoligo in PLGA Nanocapsules**

Loading and encapsulation efficiency of therapeutics in carrier systems are two very important parameters in adjusting the dose and the efficacy of the drug delivery system. In the determination of encapsulation efficiency, the fluorescence intensity (FI) obtained from FAM-labelled DNAoligo ( $\lambda_{\text{ex}}$ : 494 nm,  $\lambda_{\text{em}}$ : 524 nm) was used to calculate the amount of complex encapsulated in the PLGA nanocapsules. PEI and FAM-labelled DNAoligo were used at a N/P of 20 in the preparation of PLGA nanocapsules. The amount of the complex encapsulated was calculated from the calibration curve obtained by using empty nanocapsules mixed with known amounts of PEI: FAM-labelled DNAoligo complex (N/P 20) and their corresponding FI values (Appendix D). Based on the parameters for particle preparation used in this study the encapsulation efficiency was calculated to be  $48.1 \pm 1.4\%$  and the loading was  $192 \pm 4 \mu\text{g/g}$  PLGA nanocapsule.

The PLGA polymer used in this study has carboxylic acid end groups and therefore the produced nanoparticles are negatively charged ( $-10.96 \pm 3.84$ ). Encapsulating negatively charged hydrophilic molecules such as siRNA into negatively charged PLGA nanocapsules is challenging mainly due to the electrostatic repulsion between siRNA and PLGA. PEI was used to overcome this drawback by adding positive charged molecules during capsule preparation (Patil and Panyam, 2009). The encapsulation of siRNA into nanometer sized capsules also depends on various parameters such as the volume ratios of aqueous and organic phases, polymer and siRNA concentrations and sonication time (Cun et al., 2010). The encapsulation efficiency obtained in this study was found to be comparable with the literature which ranges between ~20-50 % with changes in the nanocapsule preparation parameters (Alshamsan et al., 2010; Cun et al., 2010; Cun et al., 2011; Hasan et al., 2012).

### 3.2.2 *In Situ* Degradation of PLGA Nanocapsules

PLGA nanocapsules (1 mg) was suspended in 1X TE buffer (pH 7.4, 200  $\mu$ L). On Days 1, 3, 5, 7, 10, 15 and 21 the nanocapsules were centrifuged, resuspended in fresh TE buffer, diluted with dH<sub>2</sub>O, added dropwise onto SEM stubs and air dried. The morphology of PLGA nanocapsules during degradation were analyzed by SEM (Figure 12). SEM micrographs revealed that the nanocapsules initially exhibited a regular spherical shape and smooth surface. With time, agglomeration of particles could be observed (Day 3). In the following days, increasing fractions of degraded nanocapsules were observed (Day 5 to 14). Finally, on Day 21 the spherical morphology of the nanocapsules was completely lost and almost a matrix like structure was observed.



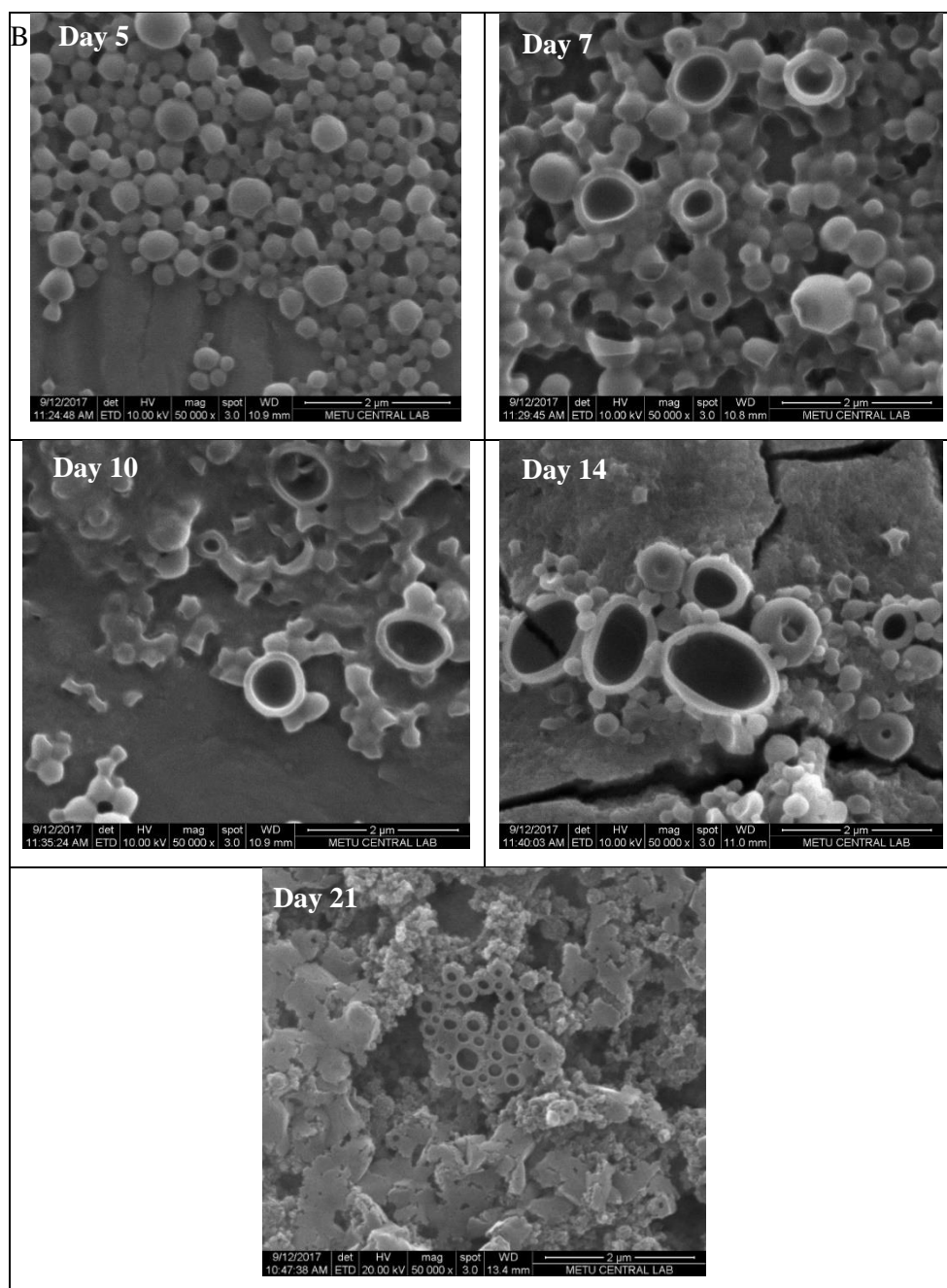


**Figure 12:** SEM micrographs of PLGA nanocapsules during 21 days of incubation in TE buffer (A, B). Scale bar: 2  $\mu\text{m}$ .

### **3.2.3 *In Situ* Release of PEI:DNAoligo Complex from the PLGA Nanocapsules**

In the studies conducted to assess the rate of release of the complex from the PLGA nanocapsules, the amount of complex remaining in the capsules was measured by using the fluorescence of the FAM-labelled DNAoligo and then deducted from the entrapped value to determine the released amount through mass balance (Figure 13). At predetermined time points, the nanocapsules were centrifuged and pellet was resuspended in fresh TE buffer (pH 7.4). The addition of fresh medium created a sink effect and prevented the pH drop by degradation of PLGA through the autocatalytic degradation of PLGA.

On Day 1, capsules released 20% of their content. In the following days, the released amount gradually decreased. On Day 15 the cumulative release was approximately 80%. The release pattern was in accordance with Higuchi model and was in agreement with the literature for PLGA nanocapsules (Murata et al., 2008; Alshamsan et al., 2010; Pantazis et al., 2012).

Drug release from particles is controlled by molecular weight, hydrophobicity, and crystallinity of the polymer used since these properties affect the degradation time of the polymer. High molecular weight, hydrophobic polymers degrade more slowly than low molecular weight and more hydrophilic polymers. The length of chains determines the extent of hydrophobic interactions of the polymer chains with each other, therefore, the release of the drug through long chains becomes difficult resulting in the reduced release rate of the drug (Dinarvand et al., 2011). In this study, PLGA used had a low molecular weight (44 kDa) with a lactic acid to glycolic acid ratio of 50:50, and had a high degradation rate. The burst release on Day 1, could be explained by the release of PEI:siRNA closer to the capsule surface. The following release might be both through diffusion of the complex through the PLGA nanocapsule walls in addition to the degradation of ester linkages between the backbone of PLGA polymer as the time progress (Dinarvand et al., 2011).

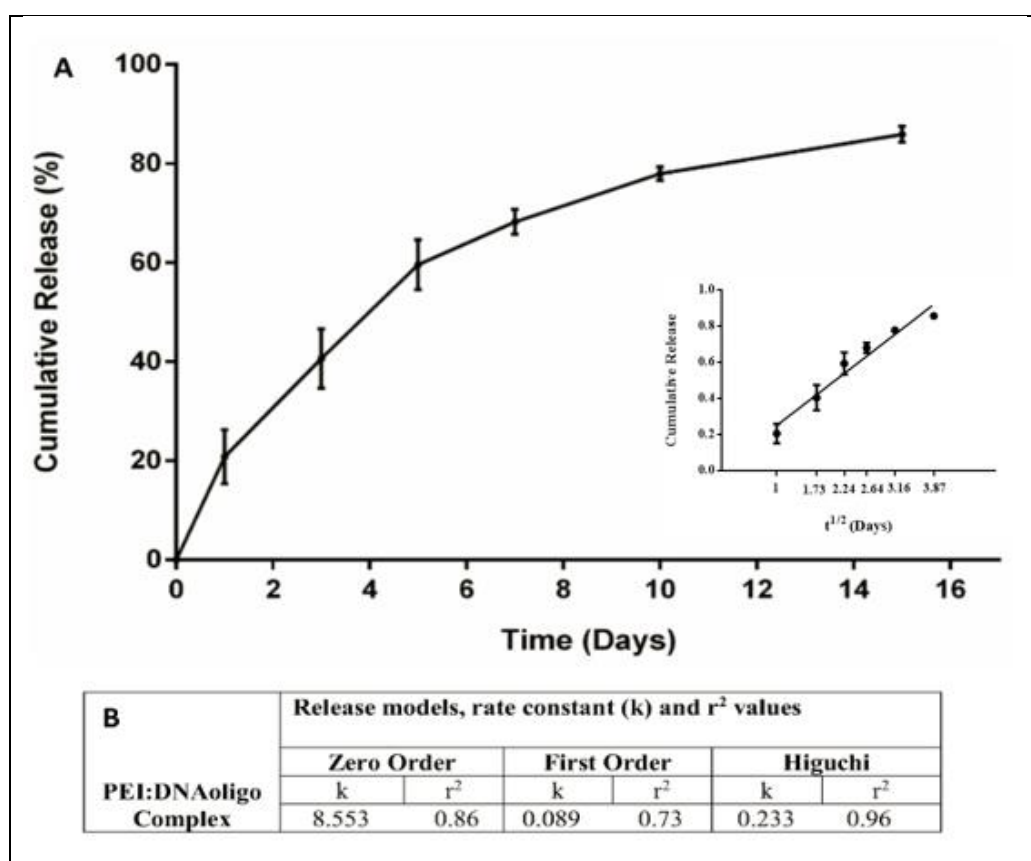


**Figure 13:** Release of PEI: DNAoligo from PLGA nanocapsules (pH 7.4). (A) Cumulative release of PEI:DNAoligo complex from nanocapsules. (B) Release kinetics of PEI:DNAoligo complex. Quantification was done by measuring the fluorescence intensities on Days 1, 3, 5, 7, 10 and 15 ( $n = 3$ ).

The release results obtained in this study were treated according to various rate equations. With the results obtained from the release study, the best fit was obtained with the Higuchi model ( $r^2$  value was higher than 0.9) and not with zeroth (release rate is independent of drug concentration) or first order (release rate is proportional to the drug concentration). Higuchi release kinetics is a mathematical model for drug release based on the principle of the bioactive agent being released by diffusion through the polymeric coat.

It shows the direct proportionality of the cumulative amount of drug released from nanocapsule with the square root of time and is expressed as  $M_t/M_\infty$  vs  $t^{1/2}$  ( $M_t$  = cumulative amount of released drug at certain time (t),  $M_\infty$  = the maximum release at infinite time). There are other studies in the literature that find their results fit best when plotted according to Higuchi release kinetics (Bohr et al., 2012; Eke et al., 2015).

### **3.2.4 Determination of Affinity of the ELR Towards Hydroxyapatite with Fourier Transform Infrared (FTIR) Spectroscopy**

The bioactive epitope present in the ELR sequence used in this study, DDDEEKFLRRIGRFG, is known to have high affinity for hydroxyapatite (Barbosa et al., 2009) (Tejeda-Montes et al., 2014).

In order to check this information in a simple environment and to observe whether the ELR could be used to target the PLGA nanocapsules towards bone tissue, the affinity of ELR to calcium phosphate compared to a standard protein, BSA, was studied by using HAp disks by Fourier transform infrared spectroscopy (FTIR). Figure 14 shows the FTIR spectra of HAp, ELR and BSA adsorbed HAp disks. BSA was used as a control for protein adhesion. As can be observed from the figure both amide I ( $1650\text{ cm}^{-1}$ , C=O bond) and amide II ( $1534\text{ cm}^{-1}$ , N-H bond) bands are visible in ELR adsorbed HAp disk.

The protein absorption peaks observed in the FTIR spectrum are those of amide I and II bands. Amide I results from the vibrational energy of carbonyl (C=O) stretching ( $1600\text{-}1700\text{ cm}^{-1}$ ) and amide II arises from the N-H bending ( $1480\text{-}1575\text{ cm}^{-1}$ ) (Byler and Susi, 1986; Kong and Yu, 2007; Popescu et al., 2010).



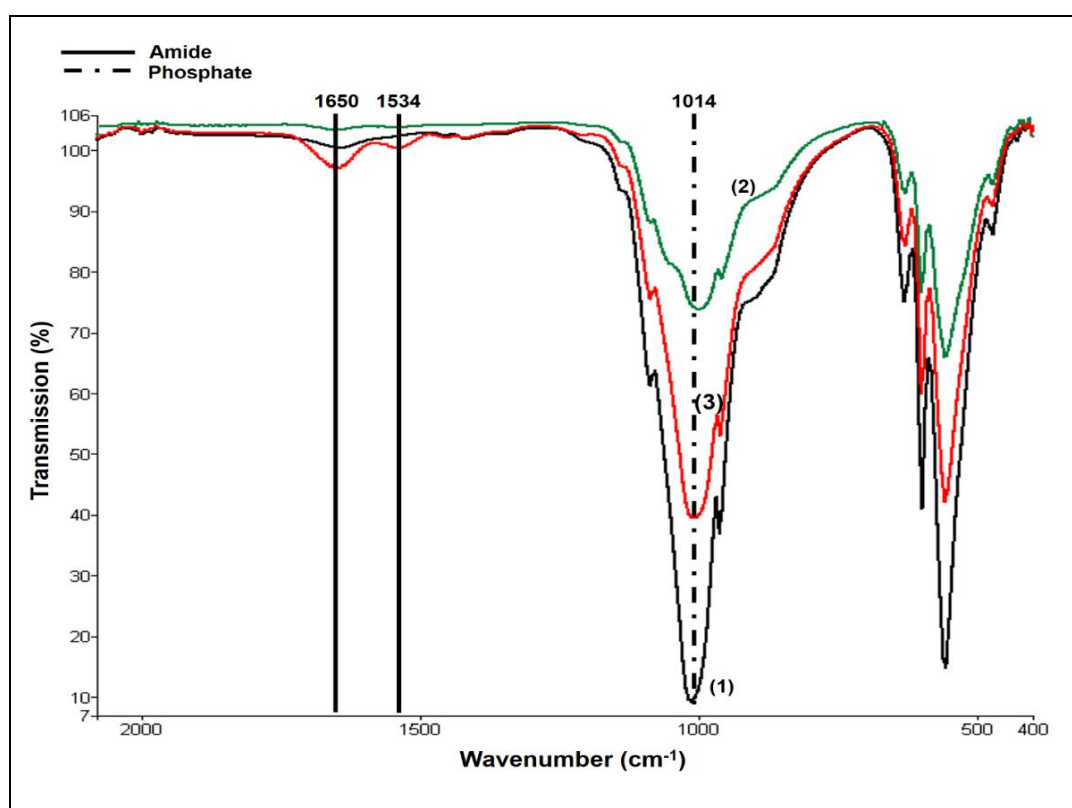


**Figure 14:** FTIR-ATR spectra of HAp and polypeptide interaction. (1) HAp, (2) BSA adsorbed HAp, and (3) ELR adsorbed HAp pellet. Amide I and II bands are visible in the FTIR spectrum of ELR and BSA adsorbed HAp indicating that both proteins were adsorbed on HAp pellets.

The peak intensity of phosphate group ( $\text{PO}_4$ )<sup>-3</sup> group ( $1014 \text{ cm}^{-1}$ ) of HAp (Miller and Wilkins, 1952) was used as a reference for the calculation of peak intensity ratios of amide I and II to phosphate (Table 4). The NH-to-PO peak intensity ratio in ELR-adsorbed HAp ( $2.9 \times 10^{-2}$ ) is higher than that of BSA-adsorbed HAp ( $1.8 \times 10^{-2}$ ). Similarly, the CO-to-PO ratio is much higher in ELR adsorbed HAp when compared with BSA adsorbed HAp. In addition, a peak intensity ratio in the amide I region (C=O/P-O) was observed in HAp pellet treated with water as blank (Table 4) which was thought to be due to water adsorption on the HAp disk (Kong and Yu, 2007).

All together these results suggest that more protein is adsorbed on HAp when ELR is used and implies a higher affinity of ELR towards HAp. Based on the results of this study, it was concluded that ELR could be used as a targeting moiety for PLGA nanocapsules towards HAp crystals present in the bone structure.

**Table 4:** FTIR Peak Intensity Ratios (C=O to P-O) and (N-H to P-O).

<b>FTIR Peak Intensity Ratios</b>	<b>C=O/P-O</b>	<b>N-H/P-O</b>
HAp	$1.7 \times 10^{-2}$	-
HAp-BSA	$3.2 \times 10^{-2}$	$1.8 \times 10^{-2}$
HAp-ELR	$8.4 \times 10^{-2}$	$2.9 \times 10^{-2}$

### 3.2.5 Preferential Binding of ELR Coated Nanocapsules on CaP Surface

After the observation of higher affinity of ELR polypeptide towards HAp, the ELR coated PLGA nanocapsules were used to determine whether these nanocapsules could preferentially accumulate on CaP coated surfaces. Figure 15 shows the confocal micrographs of uncoated and ELR coated PLGA nanocapsules on CaP coated osteoassay surface (Corning, USA). The higher number of ELR coated nanocapsules (Figure 15B) compared to uncoated PLGA nanocapsule clusters (Figure 15A) indicate the preferential binding of the ELR coated nanocapsules onto CaP surfaces.

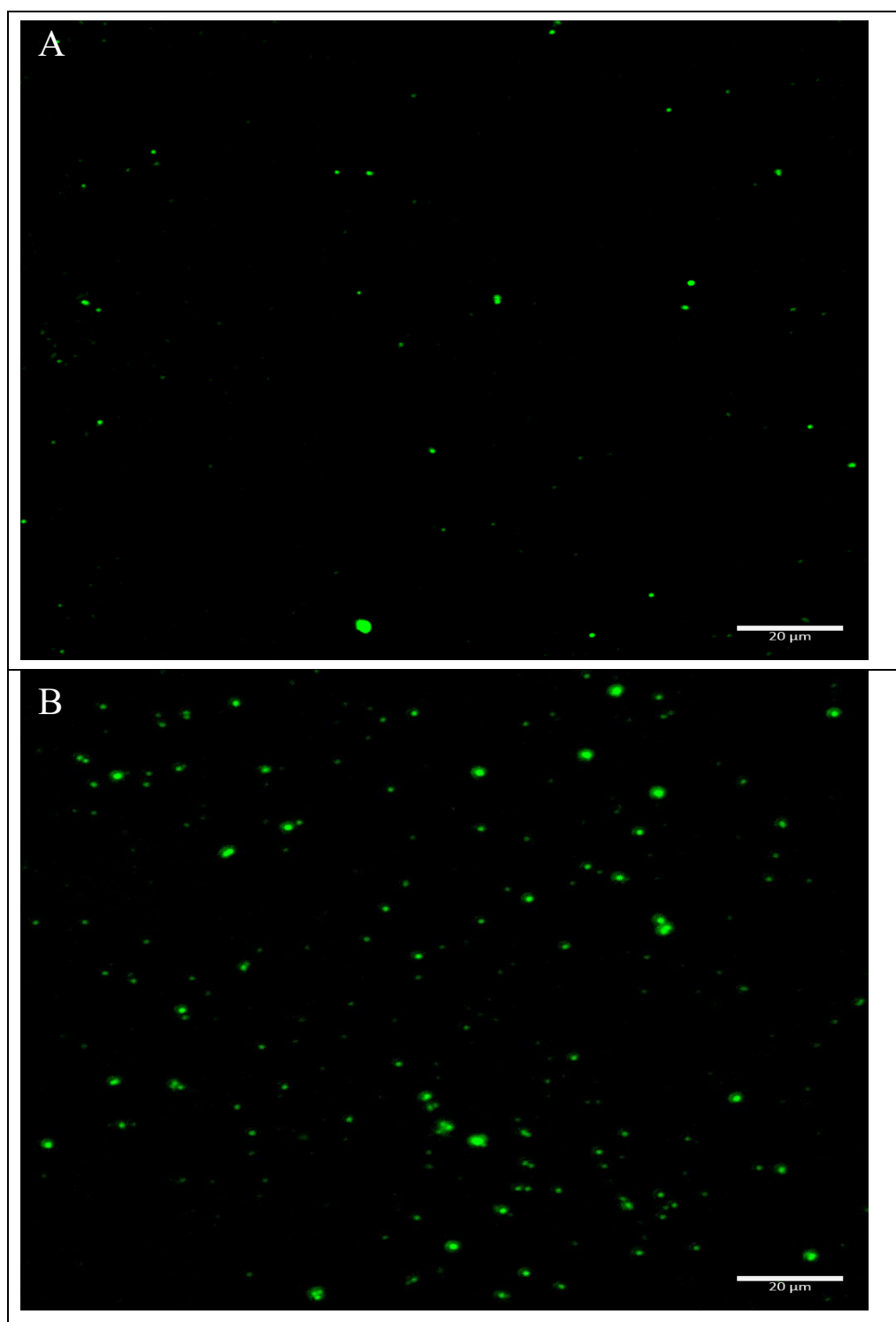


**Figure 15:** Confocal micrographs of PLGA nanocapsules. A) Nile Red Loaded, uncoated, and B) ELR coated PLGA nanocapsules. Scale Bar: 20  $\mu\text{m}$ .

### **3.2.6 Detection of ELR on PLGA Nanocapsules**

#### ***3.2.6.1 Study of Nanocapsule Topography with SEM***

The use of Scanning Electron Microscopy (SEM) to observe and compare the topography of coated and uncoated particles is a common technique (Singh et al., 2005). In this study, the topography of uncoated and coated PLGA nanocapsules were studied by SEM (Figure 16). Uncoated PLGA nanoparticles appeared as smooth and spherical particles (Figure 16A), however, coated nanoparticles had rough surfaces (Figure 16B). The roughness observed on coated PLGA nanocapsules was interpreted to be due to the presence of protein (ELR) coat on the capsules.

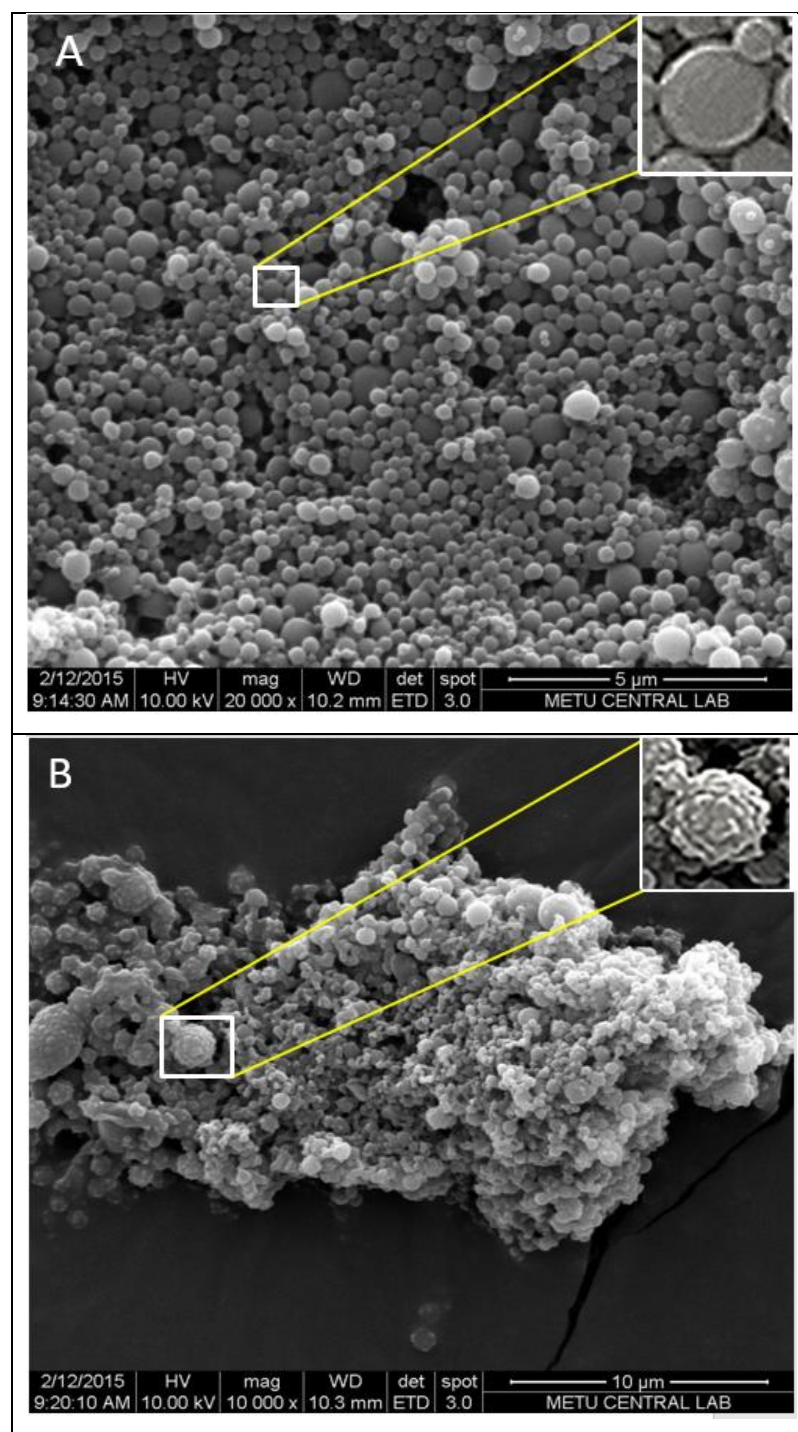


**Figure 16:** SEM micrographs of PLGA nanocapsules. (A) Uncoated, (B) ELR coated PLGA nanocapsules. The rough surface of ELR coated PLGA nanocapsule implies the presence of the protein coat on the capsules.

#### ***1.1.1.1 Detection of ELR on Nanocapsules with TEM and XPS***

PLGA nanocapsules were studied with Transmission Electron Microscopy (TEM) to confirm that the roughness on the capsules observed in SEM micrographs was due to the protein coat on the surface of the capsules (Figure 17). As can be seen from the TEM figure, the uncoated PLGA nanocapsules appear to have a sharp outline (Figure 17A), however, a halo which was interpreted to be a protein coat on the PLGA surface was visible on ELR coated PLGA nanocapsules (Figure 17B).

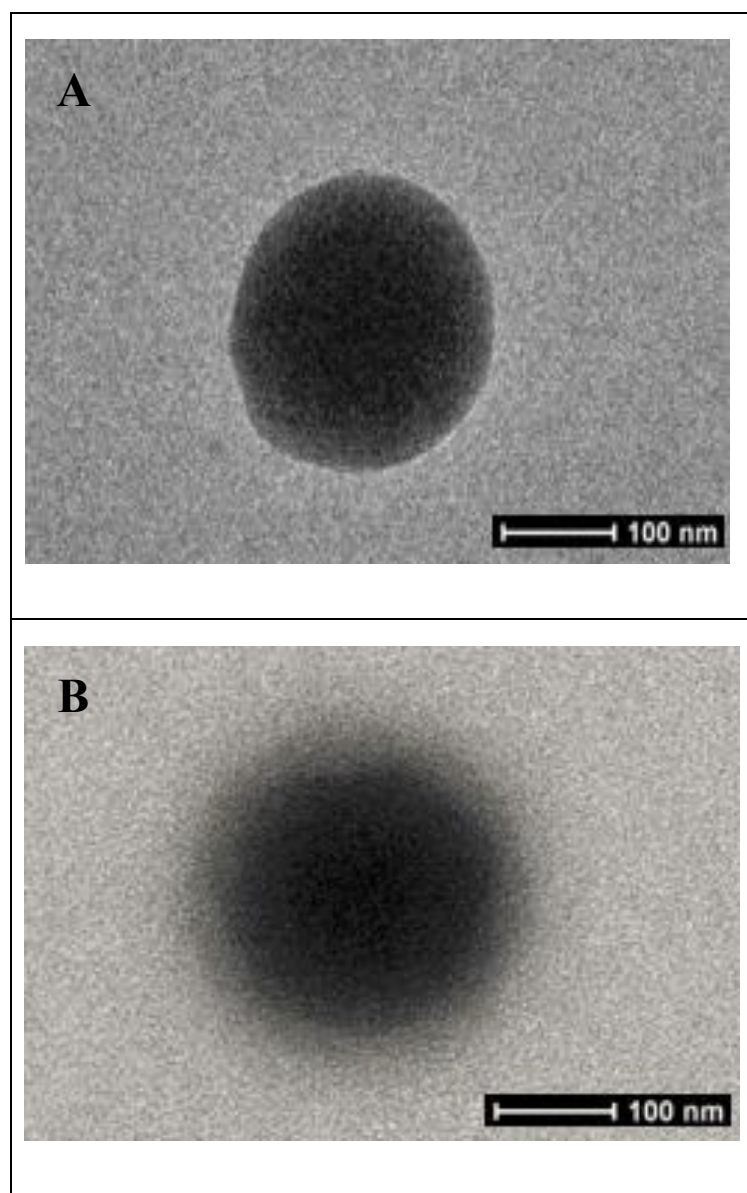


**Figure 17:** TEM micrographs of PLGA nanocapsules. (A) Uncoated, (B) ELR coated PLGA nanoparticle. The fuzzy appearance of the edges of ELR coated PLGA nanocapsule implies the presence of ELR on the surface of PLGA nanocapsules.

The capsules were also studied with X-Ray Photoelectron Spectroscopy (XPS) for nitrogen atom presence to serve as a sign of the protein on the PLGA nanocapsules (Ray and Shard, 2011). As can be seen from Figure 18 no nitrogen atom was detected on the uncoated sample (Figure 18A). In addition, XPS results of the coated PLGA nanocapsules yielded 11.7 % nitrogen atom on the sample (Figure 18B). The nanocapsules used in the XPS analysis were empty nanocapsules, therefore, did not contain any PEI:DNA oligo complex. The source of this nitrogen, therefore, can only be the ELR treatment which supports that ELR was coated on the PLGA nanocapsules.



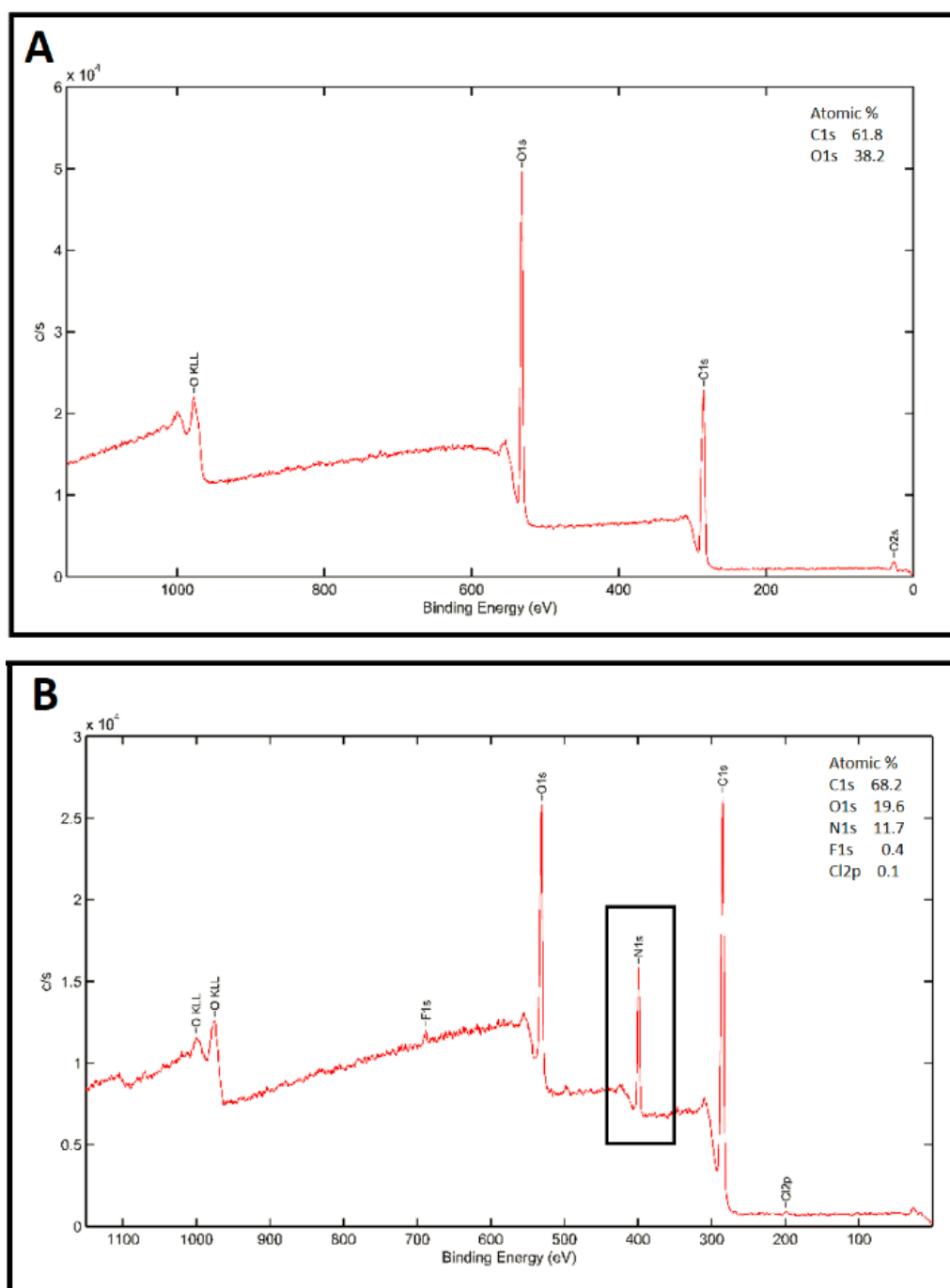


**Figure 18:** XPS spectra of PLGA nanocapsules. (A) Uncoated, (B) ELR coated PLGA nanocapsules. The XPS spectra of the capsules show the presence of nitrogen in the ELR coated PLGA nanocapsules.

### 3.2.7 Particle Size Distribution Analysis

The size relevant properties of the various types of nanocapsules are presented in Table 5 as diameters and PDI values and as particle size distribution in Figure 19. The average diameter of uncoated, empty PLGA nanocapsules produced in this study was  $208 \pm 83$  nm (Table 5). Loading the capsules with PEI:DNAoligo or coating them with ELR did not change the size of the nanocapsules. In addition, polydispersity index (PDI), the measure of particle size distribution, values were between 0.17 and 0.63 representing mid-range size distribution.

**Table 5:** Diameter and PDI Values of Empty, PEI:DNAoligo (20:1) Loaded and ELR Coated PEI:DNAoligo (20:1) Loaded PLGA Nanocapsules

Sample	Diameter (nm)	Polydispersity Index
Empty PLGA nanocapsule	$208 \pm 83$	0.18
PEI:DNAoligo (20:1) loaded PLGA nanocapsule	$197 \pm 76$	0.17
ELR coated PEI:DNAoligo (20:1) loaded PLGA nanocapsule	$220 \pm 81$	0.63

When drug delivery systems are administered in an i.v. manner into the blood stream, they undergo biodistribution. They extravasate from the blood vessel epithelium according to their sizes and are deposited in the tissues. Very small nanoparticles (ca  $<6$  nm) are eliminated by renal excretion (Choi et al., 2007). Particles in the size range of 100-200 nm are deposited in the liver, spleen and bone marrow due to the discontinuous fenestrations of the basal membranes of those tissues (Barua and Mitragotri, 2014). The representative plots of the particle size distribution of empty, uncoated and ELR coated PEI:DNAoligo loaded nanocapsules are presented in Figure 19.

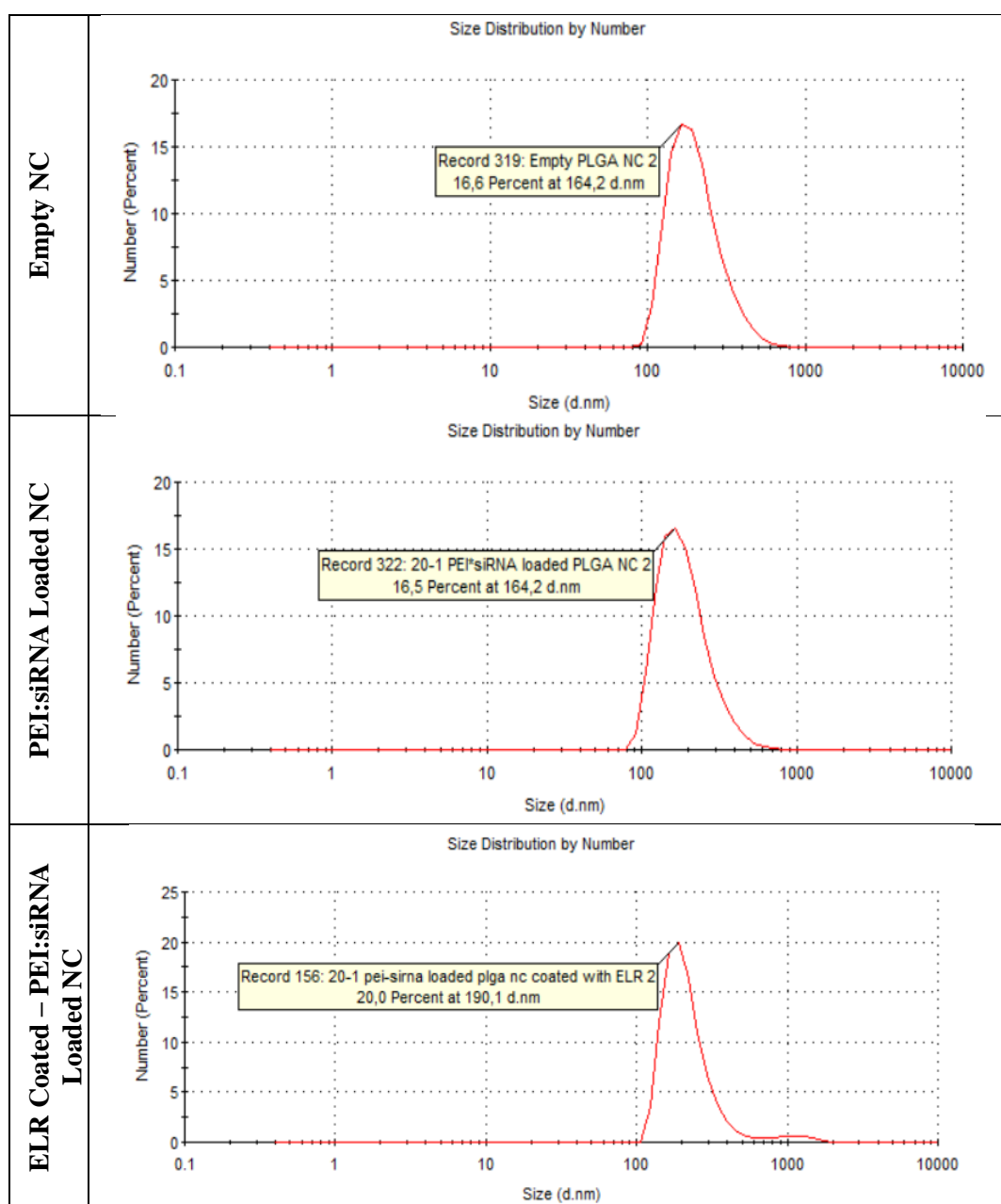


**Figure 19:** Representative graphs of particle size distribution.

In this study 53% of ELR coated and PEI:DNAoligo loaded PLGA nanocapsules had a diameter less than 200 nm. The large fraction of nanoparticles increases the possibility that some might extravasate from the fenestrations in the bone marrow, attach to HAp of the bone tissue and release their content into the basic multicellular units (BMUs) during bone resorption process.

### **3.3 *In Vitro* Cell Culture Studies**

#### **3.3.1 RAW264.7 Cell Line: Culture and Differentiation**

The pre-osteoclastic (pre-OC) cell line, murine macrophage RAW264.7 cells, responds to RANKL stimulation *in vitro* to generate bone resorbing multinucleated osteoclasts and has been widely used in studies of osteoclast differentiation and function (Gan et al., 2016; Zeng et al., 2016; Tanaka et al., 2017). Their origin is a tumor induced by injection of Abelson leukemia virus in a male mouse. However, these cells do not secrete any detectable virus particles (Collin-Osdoby et al., 2012). When these cells are seeded at a low density ( $2 \times 10^4$  cells/cm<sup>2</sup>) their doubling time is 11 h in DMEM medium supplemented with 10% heat inactivated serum (Sakagami et al., 2009). RAW264.7 cells express the receptors c-fms (for M-CSF) and RANK (for RANKL) (Theoleyre et al., 2004; Ohno et al., 2006).

For the differentiation of RAW264.7 pre-OC to mature osteoclasts, the cells were incubated with the cytokines (RANKL and M-CSF) for a total of five days because it is known that RAW264.7 cells can fuse with each other after day 5-6 even in the absence of RANKL (Collin-Osdoby et al., 2012).

Representative images of undifferentiated RAW cells and differentiated RAW-OC are shown in (Figure 20). The image in this figure was obtained on Day 5 of the differentiation procedure, then fixed with PFA (4%) and stained for Tartrate Resistant Acid Phosphatase (TRAP).

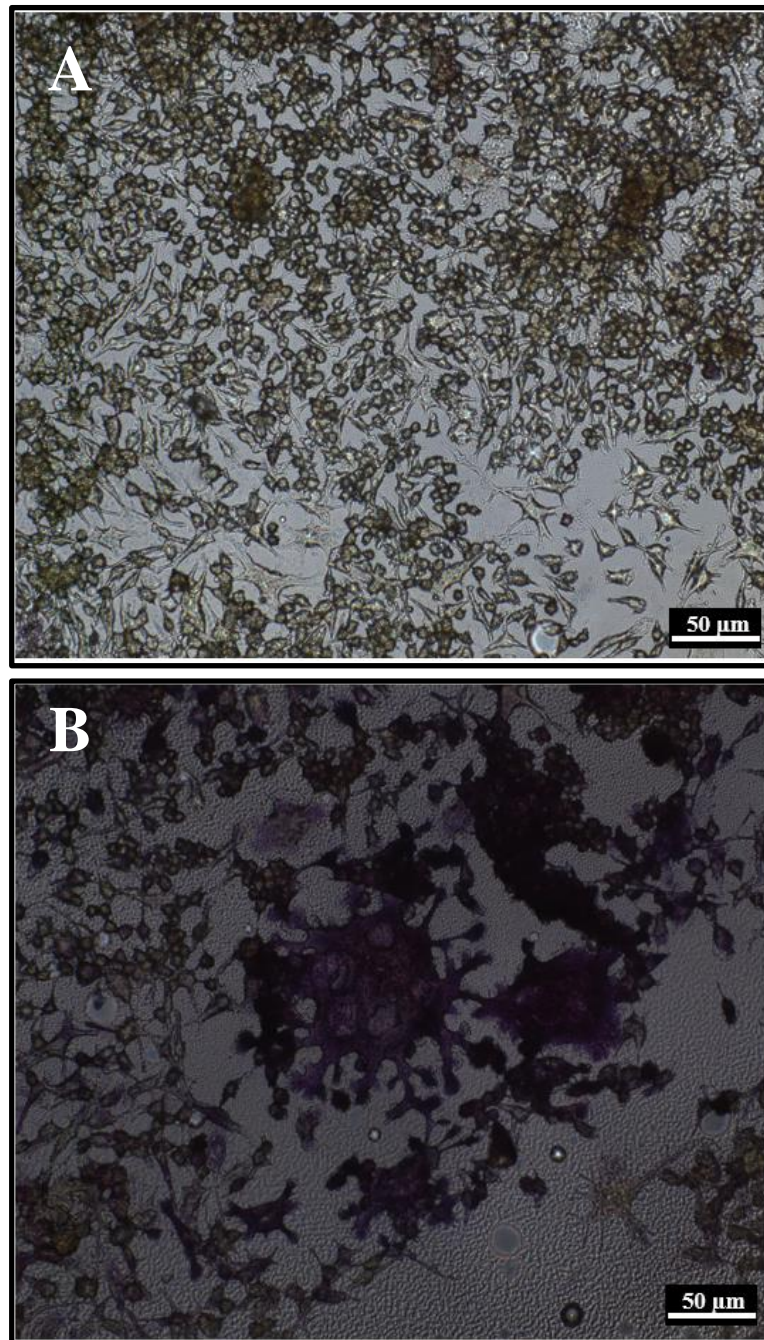


**Figure 20:** Representative microscopy images of undifferentiated and differentiated cells used in the study. A) undifferentiated, B) differentiated RAW264.7 osteoclastic cells. The images were obtained on Day 5 of the differentiation procedure with phase-contrast microscope.

### 3.3.2 Determination of Cell Viability

The possible adverse effect of PLGA nanocapsules on RAW264.7 cell viability was assessed for five days in 96-well plates for  $5 \times 10^3$  cells/0.5 mg NC/well (Figure 21).

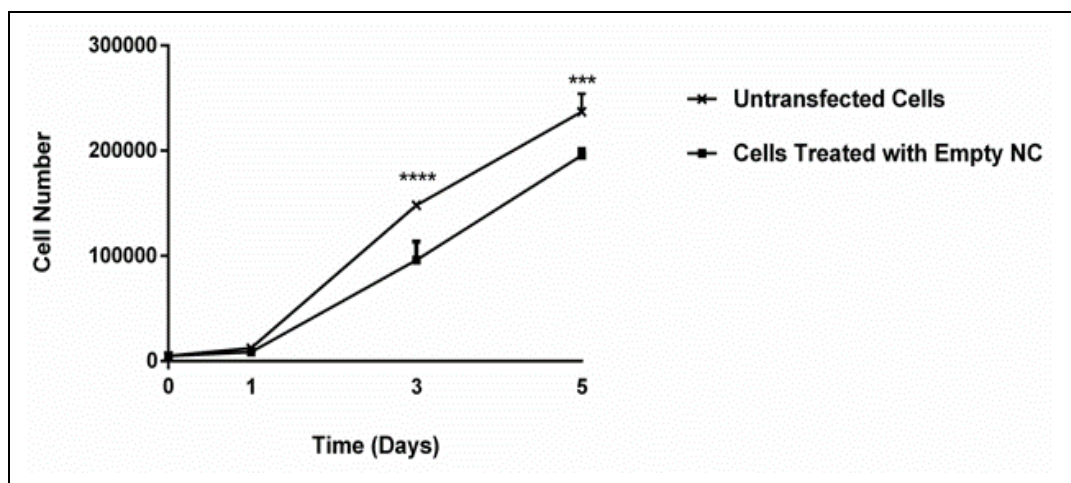


**Figure 21:** Effect of PLGA nanocapsules on viability of RAW264.7 cells as determined by Alamar Blue cell viability assay. The significance values are result from the comparison of untransfected and empty nanocapsule-transfected cells at each time point (n=3). Seeded cell density was  $5 \times 10^3$  cells/well.

On Day 1, no significant effect of nanocapsules was observed on the attachment of the cells compared to the untransfected cells. Between Days 1 and 5, both untransfected and empty nanocapsule-treated cells proliferated approximately with similar rates (4.5 and 5.4; untransfected and nanocapsule treated cells). These indicate that the PLGA nanocapsules do not significantly affect RAW264.7 cell viability. Based on these results, it was concluded that PLGA nanocapsules have no significant toxic effect on the viability of RAW264.7 cells.

### 3.3.3 Internalization of PLGA Nanocapsules

The cellular uptake is a dynamic process where both endocytosis and exocytosis are involved and are concentration, time and energy dependent. The internalization and localization of PLGA nanoparticles within the RAW264.7 cells were studied with confocal laser scanning microscopy. RAW264.7 cell suspension was transfected with Nile Red ( $\lambda_{\text{ex}}=551$  nm,  $\lambda_{\text{em}}=636$  nm) loaded PLGA nanocapsules and seeded on TCPS covers. Two days post transfection, the cells were fixed and stained with DRAQ5 and 488-labelled Phalloidin to stain the nucleus and the actin of the cytoskeleton; respectively (Figure 22). As can be seen from the figure, nanocapsules have crossed the cell membrane (Figure 22A) and are internalized (Figure 22B). This is an indication of the potential of the PLGA NC to be effective in delivering their drug cargo (siRNA) into the cytoplasm where siRNA inhibits the translation of the mRNA. In the cytoplasm, PEI:siRNA loaded PLGA nanocapsules are expected to act as drug depots and release their content, so that siRNA could function once it is dissociated from PEI.



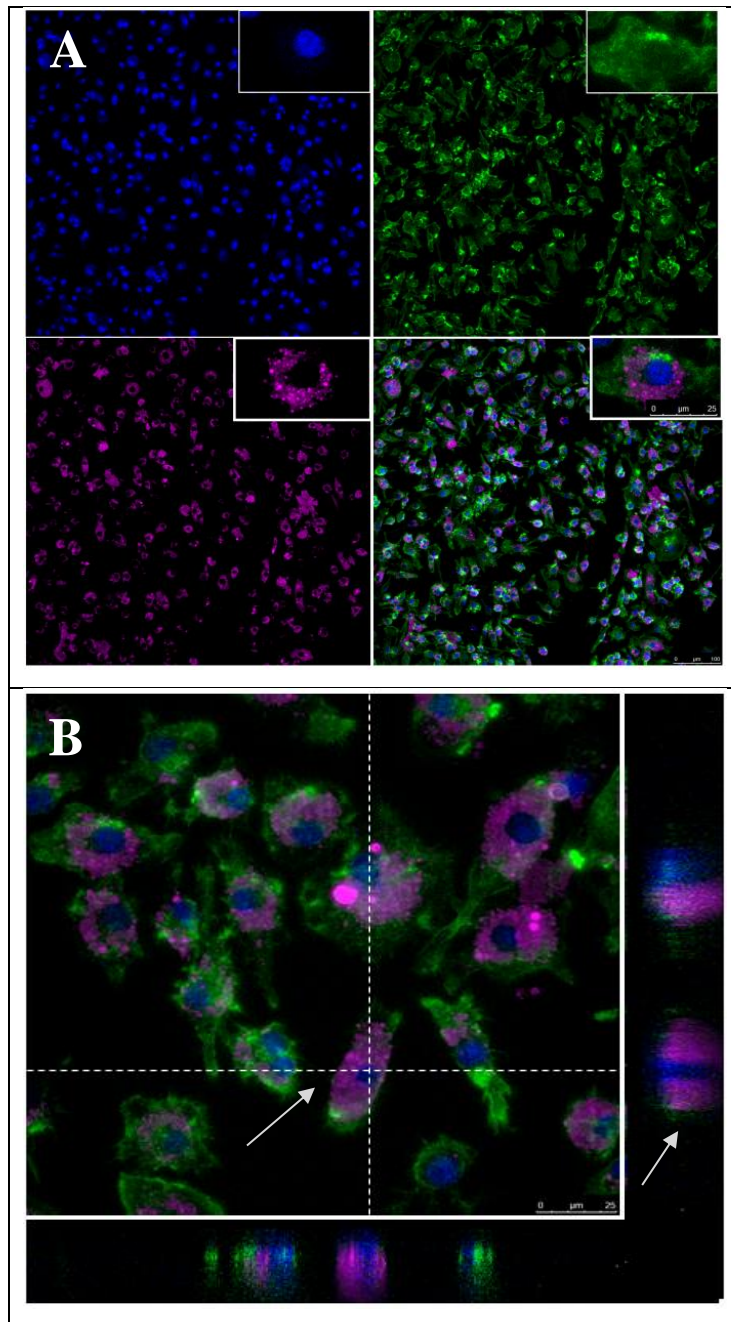


**Figure 22:** Confocal laser scanning micrograph of Nile Red loaded PLGA nanocapsules (pink) in RAW264.7 cells 48 h post transfection. A) The Nile Red loaded PLGA nanocapsules are internalized by the cells. Insets present the 40X magnification. B) The nanocapsules are localized around the nucleus. DRAQ5 stains the nucleus (blue) and Alexa 488-labelled Phalloidin stains the cytoskeleton (green).



The internalization of nanoparticles is initiated when the particle attaches onto the cell membrane. This attachment is affected both by the hydrophobicity and the surface charge of the particulate system (Gratton et al., 2008). Hydrophobicity of the particle increases the possibility of cellular uptake due to increased chance of interaction with hydrophobic cell membrane (Samadi Moghaddam et al., 2015). As for the charge of the particle, positively charged particles are more advantageous than negatively charged carriers as they can attach themselves more efficiently onto the negatively charged cell membrane. They are, however, more toxic to the cells, in a dose dependent manner (Bannunah et al., 2014). The influence of the cell type, on the other hand, can not be ignored. Phagocytic cells are known to interact more with negatively charged particles, in contrast to non-phagocytic cells (Fröhlich E., 2012). Our results show that the particles used in this study were negatively charged (zeta potential  $-10.96 \pm 3.8$ ) and were effectively internalized probably because of cell type. The internalization of negatively charged PLGA microparticles by murine primary monocyte macrophages were also shown by other groups (Wang et al., 2012). In another study, the preferential uptake of the anionic polystyrene nanoparticles (with a size of 116 nm) by human macrophages was also shown (Lunov et al., 2011). In conclusion, the internalization of nanoparticles by the cells is affected mostly by charge and hydrophobicity of the nanocapsules along with the cell type (Mailänder and Landfester, 2009).

### **3.4 Gene Expression Studies**

#### **3.4.1 Efficiency of RANK siRNA Sequence in Gene Silencing**

Knockdown of the target gene RANK was studied using qRT-PCR. For this purpose two siRNAs (RANK siRNA#1 and RANK siRNA#2) (sequences presented in Table 1, Section 2.2.5.1) were used to determine the siRNA which leads to a significant inhibition of the target gene. The amount of RANK mRNA normalized to the housekeeping gene GAPDH and relative to control (the fold change of RANK) was calculated using the  $2^{-\Delta\Delta C_t}$  equation (Section 2.2.5.2).

In order to eliminate the possible interference by mock (only HiPerfect transfection reagent) or scrambled siRNA to RANK mRNA expression in RAW264.7 cells, fold change of RANK in mock and scrambled siRNA transfected cells were calculated by using the untransfected cells as control sample.

In the first 24 h, no significant alteration in RANK fold change was observed in the mock ( $1.01 \pm 0.27$ ) or the scrambled siRNA transfected cells ( $0.98 \pm 0.24$ ) relative to untransfected control (Figure 23). At 24 h post transfection, a significant reduction in the fold change was observed in RANK siRNA transfected samples ( $0.19 \pm 0.08$ ). These reductions in the fold change of RANK in the first 24 h correspond to 80% inhibition.

The inhibition level was reduced to 73% 48 h post transfection. Fold change of RANK in siRNA#1 treated samples were  $0.27 \pm 0.04$ . At 72 h post transfection, fold change of RANK was found to be  $0.26 \pm 0.13$  when compared to untransfected cells. No significant changes of RANK mRNA levels were observed in the mock or scrambled siRNA transfected cells at 48 h ( $0.86 \pm 0.09$ ,  $0.99 \pm 0.32$ ; respectively) or 72 h ( $0.38 \pm 0.23$ ,  $0.73 \pm 0.05$ ) post transfection when compared to untransfected cells.

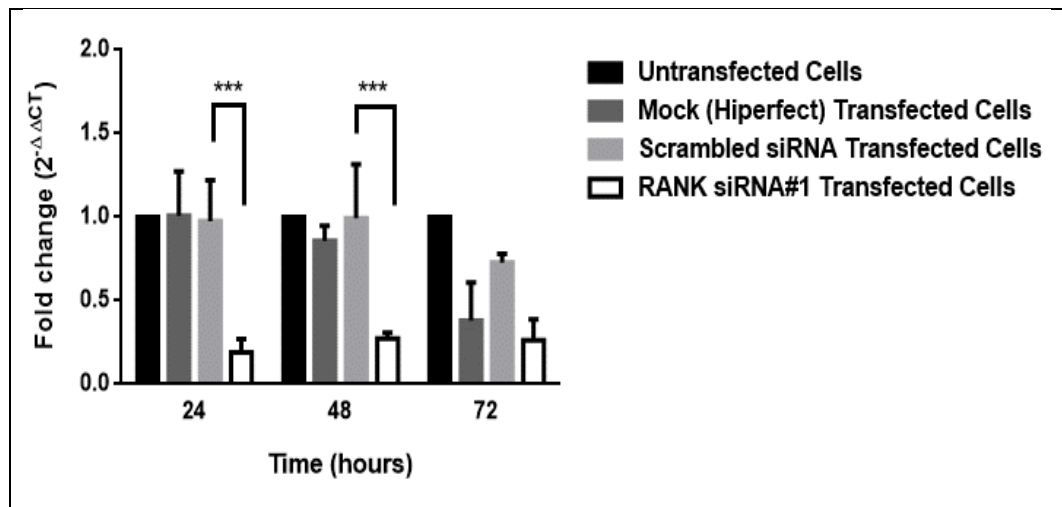


**Figure 23:** Fold change of RANK mRNA expression in mock (HiPerfect Transfection Reagent), scrambled, and RANK siRNA#1 transfected cells. The fold change of RANK expression is presented as mean  $\pm$  STDEV of three individual experiments.

The inhibition in RANK mRNA by the second siRNA (RANK siRNA#2) was also calculated using the same method (Figure 24). No significant reduction was observed at 24, 48 or 72 h post transfection in the fold change of RANK expression;  $1.02 \pm 0.41$ ,  $0.78 \pm 0.12$  and  $0.46 \pm 0.34$ , respectively. The lower levels of RANK mRNA inhibition with the siRNA treatment did not reach to significant levels.

For this reason, RANK siRNA#1 was used in the further experiments.

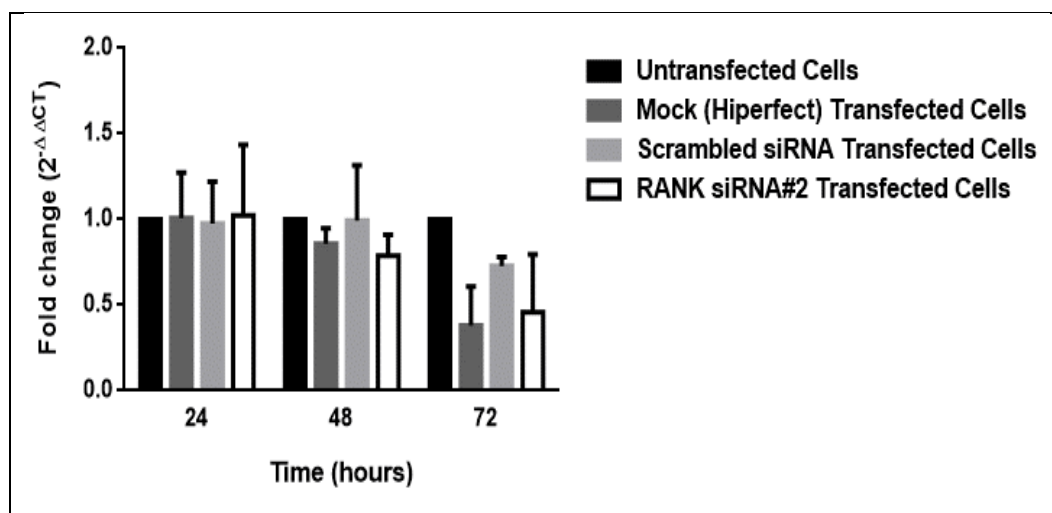
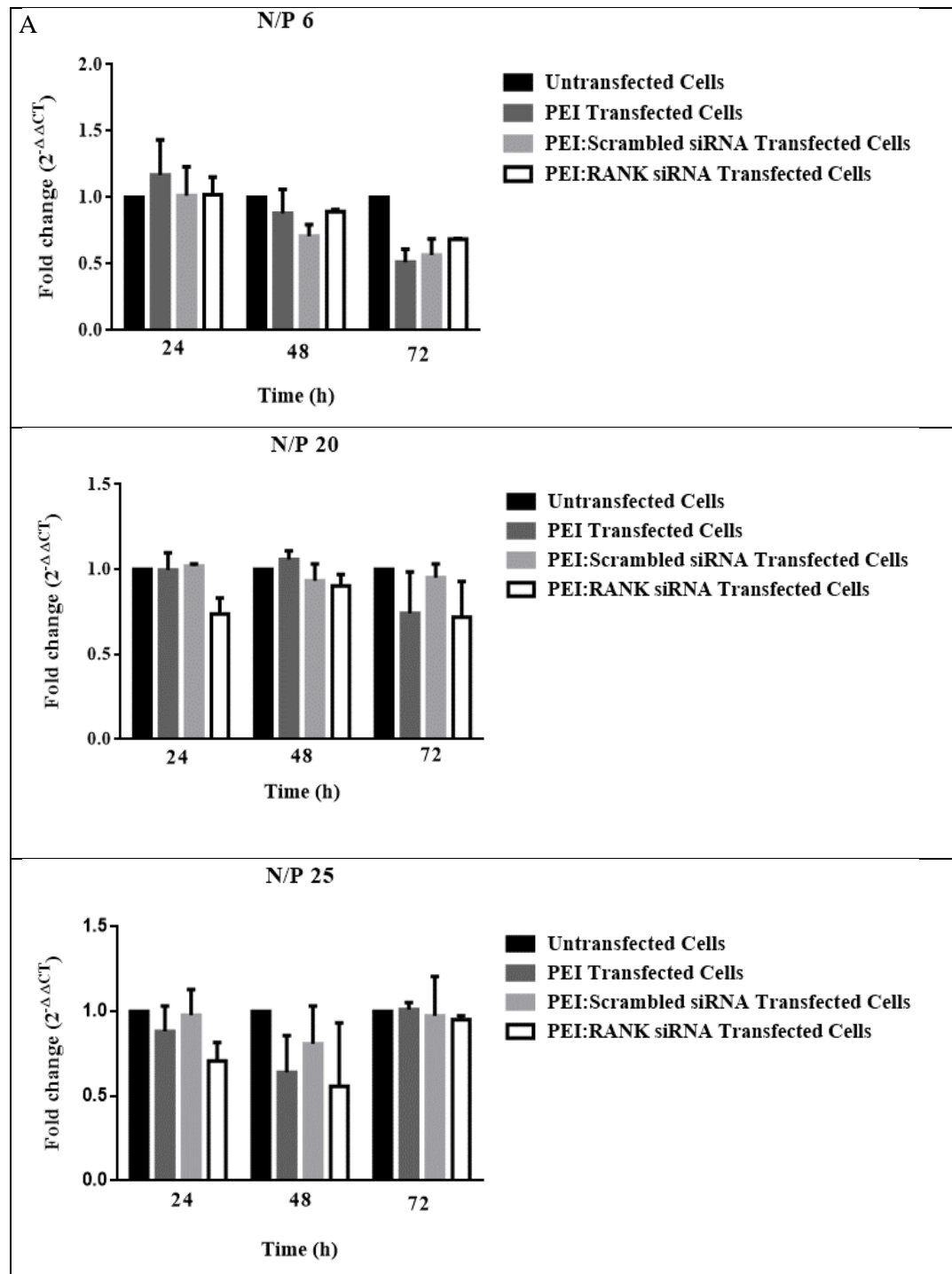


**Figure 24:** Fold change of RANK mRNA expression in mock (HiPerfect Transfection Reagent), scrambled, and RANK siRNA#2 transfected cells. The fold change of RANK expression is presented as mean  $\pm$  STDEV of three individual experiments.

### 3.4.2 Inhibition of RANK mRNA with Varying N/P Ratios

The inhibition studies with different N/P (6, 20, 25, 30, 60) were performed to determine the N/P that leads to the inhibition of the target gene and to eventually use that N/P complex in the following experiments. The qPCR results of the inhibition of RANK mRNA through transfection of cells with only the PEI:siRNA complexes (without entrapping the complexes into PLGA nanocapsules) are given in Figure 25. When N/P ratio of 6 is used for the transfection, no alteration in the RANK mRNA expression was observed. Also, 72 h post transfection, PEI showed an off-target effect on RANK mRNA fold change (Figure 25 dark gray bar-PEI transfected cells). N/P 20 led to 28% inhibition at 24 h post transfection, however, it was not statistically significant. During the transfection period, dead cells were observed with N/P 30 and 60 therefore, it was decided that they were very toxic to the cells. In addition, the N/P 25, 30 and 60 did not lead to significant inhibition and the PEI amount in those complexes seemed to have an off-target effect on RANK mRNA expression (Figure 25 dark gray bars-PEI transfected cells).

The PEI amount in the complex of N/P 20 did not lead to non-specific RANK mRNA inhibition in PEI transfected cells. When it was in a complex with RANK siRNA it led to 28 % inhibition, still insignificant, in the first 24 h.



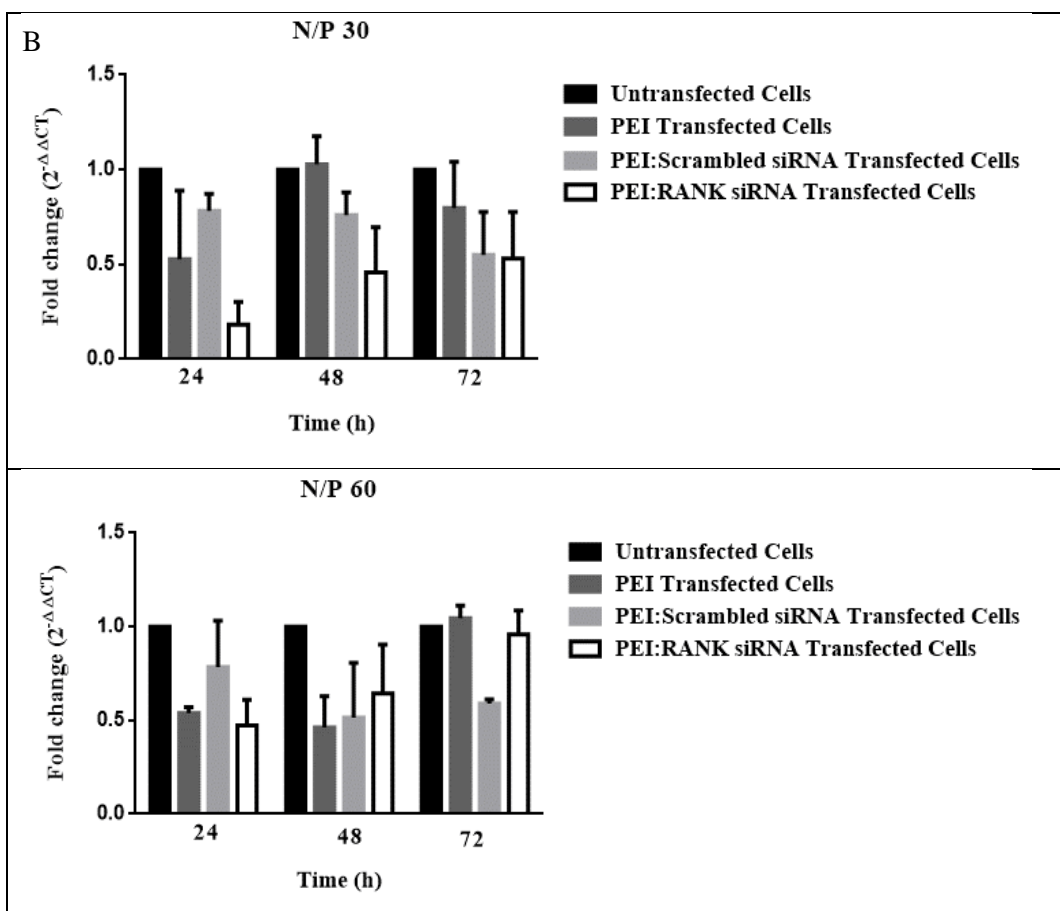


**Figure 25:** Inhibition of RANK mRNA expression with N/P ratios of 6, 20, 25, 30, 60 (A, B). The fold change of RANK expression is given as mean  $\pm$  STDEV of two individual studies.

It should be noted that in this study, the transfection of siRNA into the cells is only accomplished by PEI (in the absence of PLGA nanocapsules). The amount of PEI in the complex should be sufficient to both condense the siRNA and to transfer it into the cells. In addition, once in the cell, the amount of PEI should also allow the escape of the complex from the endosomes and release the siRNA into the cytoplasm. In order to escape from the endosomes, not only the PEI in PEI:siRNA complexes but also the free PEI plays an essential role. It is known that the protonated PEI in the endosomes expand volumetrically in order to reduce the electrostatic repulsion between the positive charges.

As a result of this expansion, it interacts with the endosomal membrane leading to lipid bilayer permeabilization and thus the release of the content of endosome into the cytoplasm (Neuberg and Kichler, 2014). The effect of different N/P on mRNA inhibition, although carrying the same siRNA amount is, therefore, also dependent on free PEI amount. The different efficiencies of RANK mRNA inhibition through transfection with different N/P might also be due to this phenomenon. There are more free PEI in the complex of N/P 20 than that of N/P 6 resulting in more endosomal escape capability and thus the efficacy. In the higher N/P, for instance the N/P of 30 and 60, the cytotoxicity and off-target effect of PEI on cells and RANK mRNA were observed. In the literature, the N/P of 20 was also chosen for mRNA knockdown in siRNA transfection studies with low cytotoxicity (Zhang et al., 2011; Wang et al., 2012). Based on the results obtained this study and the literature, N/P of 20 was chosen for use in the later experiments.

### **3.4.3 Inhibition of RANK mRNA in Nanocapsule Transfected Cells**

The efficacy of the PEI:RANK siRNA loaded PLGA nanocapsules on RANK mRNA inhibition was studied with qPCR (Figure 26). The expression of RANK mRNA normalized to that of housekeeping gene, GAPDH, and relative to control (the fold change of RANK) was calculated using the  $2^{-\Delta\Delta C_t}$ . The fold change in RANK mRNA was calculated by using the cells transfected with empty nanocapsules as the control group. On Day 3, a statistically significant reduction in RANK mRNA levels ( $0.53 \pm 0.10$ ) compared to the empty nanocapsule treated cells (47% inhibition) were observed. On Day 5, the inhibition was reduced ( $0.91 \pm 0.15$ ). The decrease in inhibition on Day 5 might be due to refreshing of the medium on Day 3. At this step, the nanoparticles were removed and therefore further inhibition was achieved only with the particles that were already taken up by the cells until Day 3. In addition to medium change, cell division decreases the amount of nanoparticles within each cell.

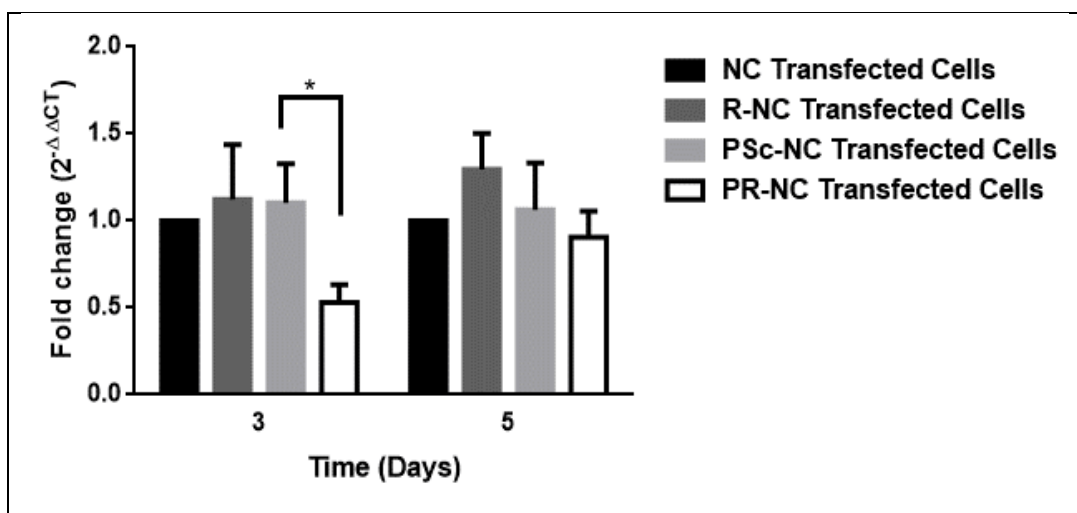


**Figure 26:** Fold change of RANK mRNA at 3 and 5 days post transfection with PLGA nanocapsules carrying different cargo (n=3). A statistically significant mRNA inhibition was observed on Day 3. Abbreviation Codes: NC: PLGA nanocapsule; R-NC: uncomplexed RANK siRNA loaded nanocapsules; PSc-NC: PEI:Scrambled siRNA loaded nanocapsules; PR-NC: PEI:RANK siRNA loaded PLGA nanocapsules.

As can be observed in Figure 26 the naked siRNA loaded nanocapsules (R-NC) did not lead to any RANK mRNA inhibition at either of the time points ( $1.12 \pm 0.32$  on Day 3, and  $1.30 \pm 0.21$  on Day 5). This result is also reported by other studies in the literature (Kim et al., 2008; Murata et al., 2008) and concluded to be due to absence of PEI. It was shown that although naked siRNA loaded PLGA microspheres caused inhibition in the first 12 hours, the level of this inhibition was reduced during the 8 days of culture. It was concluded that the addition of a cationic carrier such as PEI into the microspheres could achieve long lasting release of siRNA in the cells and thus silence the target, because the absence of PEI would allow the degradation of the siRNA in the lysosomes as naked siRNA is more prone to degradation by nucleases than that of its complexed form (with PEI) since complexation with PEI protects and leads siRNA escape from the lysosomes (Dominska and Dykxhoorn 2010).



Since no inhibition in RANK mRNA levels were observed with naked siRNA loaded PLGA nanocapsules, the group was not included in the later studies.

### **3.5 Inhibition of Osteoclast Differentiation and Activity**

The effect of PEI:RANK siRNA loaded nanocapsules were also studied to determine their efficacy on the inhibition of osteoclastogenesis and suppression of osteoclastic activity.

#### **3.5.1 Inhibition of Osteoclast Differentiation**

The efficacy of the delivery system in inhibiting the osteoclastic differentiation was studied by staining the enzyme Tartrate Resistant Acid Phosphatase (TRAP) by using Acid Phosphatase Leukocyte (TRAP) Kit (Sigma, Germany) according to manufacturer's protocol. TRAP is a phosphoprotein phosphatase (Oddie et al., 2000) that is found in the bone and TRAP staining is used as a histological marker for osteoclasts (Li et al. 1970). It has been shown that its main function in osteoclastic bone resorption is degradation of bone matrix phosphoproteins such as osteopontin (Ek-Rylander et al., 1994) and osteonectin (Andersson and Ek-Rylander, 1995). TRAP also causes the production of reactive oxygen species (ROS) in the resorption lacuna during bone resorption and help degrade collagen. It is also found in transcytotic vesicles which helps to further degrade the matrix degradation products that are transported from the resorption lacuna to the basolateral plasma membrane from where they are expelled (Hayman A., 2008).

In this study, RAW264.7 cells were transfected with empty nanocapsules, PEI:Scrambled siRNA or PEI:RANK siRNA loaded nanocapsules. The transfected cells were also differentiated into mature osteoclasts with RANKL and M-CSF for 5 days with a medium change on Day 3. On Days 3 and 5, the cells were fixed and TRAP staining was performed on TCPS slides. Representative images of the TCPS slides are given in Figure 27.

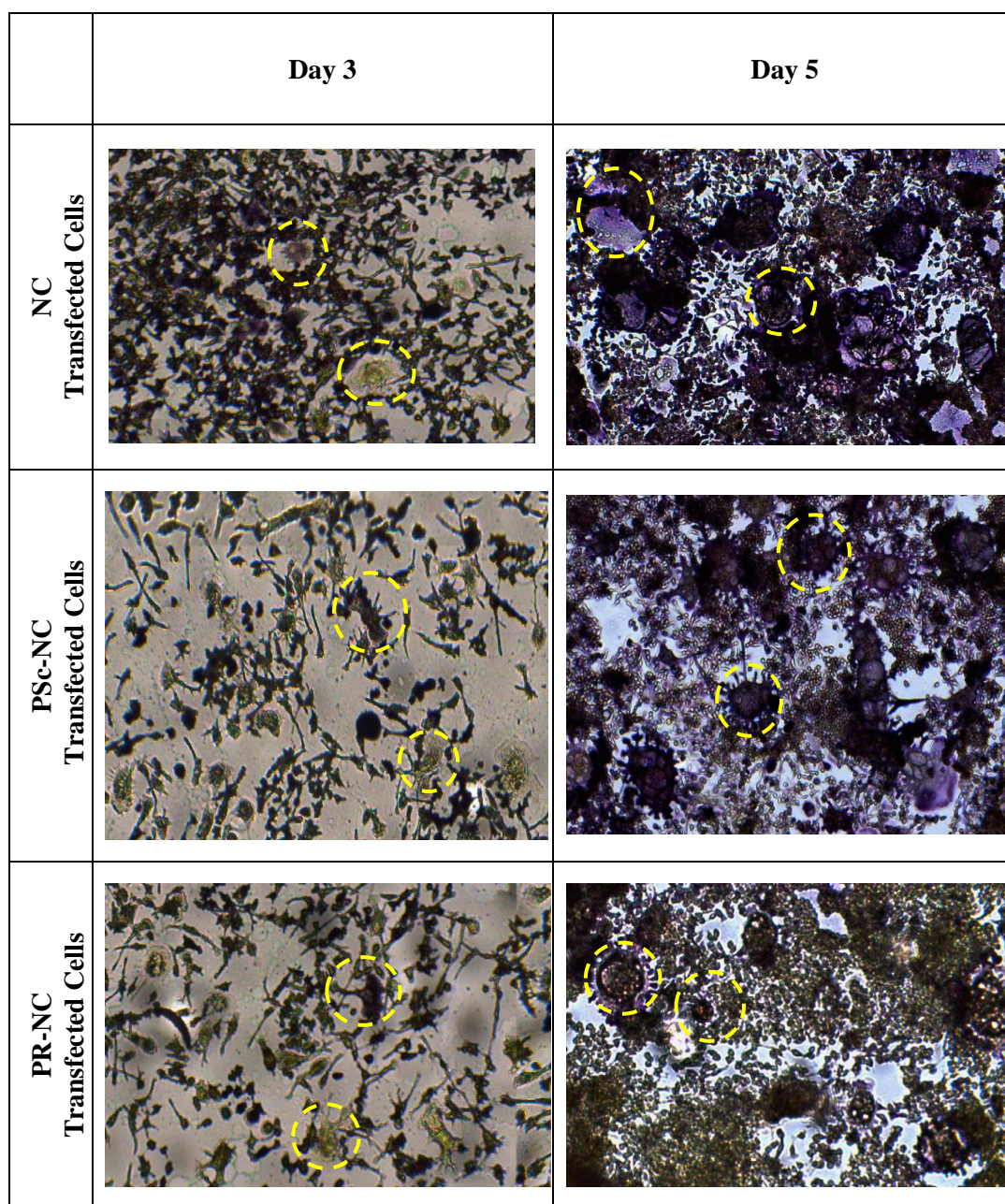


**Figure 27:** Representative images of staining of TRAP in differentiating RAW264.7 cells transfected with empty nanocapsules, PEI:Scrambled siRNA and PEI:RANK siRNA loaded PLGA nanocapsules. Dotted yellow circles are examples of the type of osteoclasts counted in each image. NC: PLGA nanocapsule, PSc-NC: PEI:Scrambled siRNA loaded, PR-NC: PEI:RANK siRNA loaded PLGA nanocapsule.

For the quantification of the number of osteoclastic cells, the whole area of the TCPS slides were counted for multinucleated TRAP (+) cells using Image J Analysis Software (NIH, USA). On Day 5, a statistically significant reduction in the number of TRAP (+) multinucleated cells were observed in PEI:RANK siRNA nanocapsule transfected cells compared to cells treated with empty nanocapsule or PEI:Scrambled siRNA loaded nanocapsule (Figure 28).

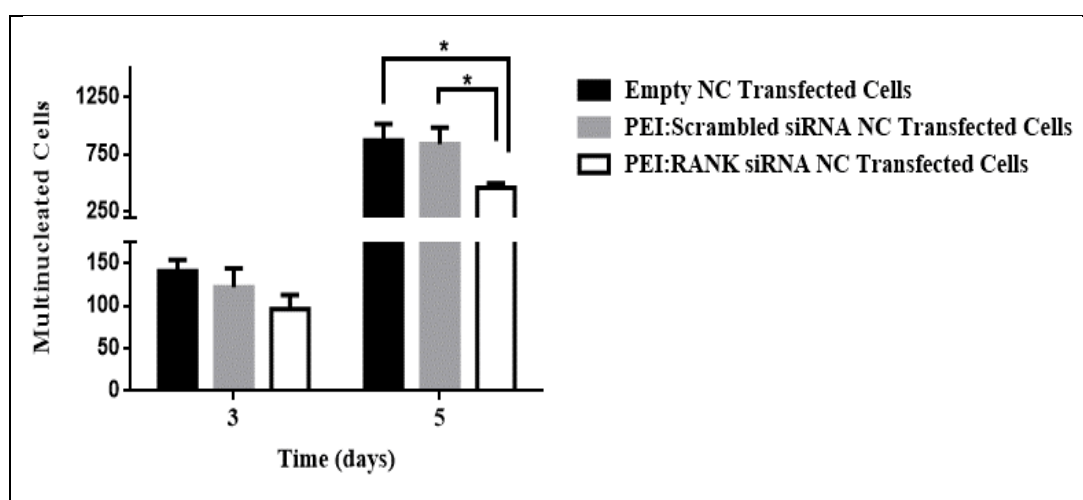


**Figure 28:** Inhibition of differentiation in empty nanocapsule, PEI:Scrambled and PEI:RANK siRNA loaded nanocapsule transfected cells. Data is expressed as mean  $\pm$  STDEV of three individual studies. NC: PLGA nanocapsule, PSc-NC: PEI:Scrambled siRNA loaded, PR-NC: PEI:RANK siRNA loaded PLGA nanocapsule.

Interestingly, on Day 3, larger cells, not stained positive for TRAP, were observed (Figure 27). The cell count on Day 3, therefore, was done based on their cell morphology. This result might be due to effect of PLGA nanocapsules on osteoclasts. A study performed by Cenni et al., revealed that pure PLGA nanocapsules cause actin ring disruption and inhibition of collagen degradation in differentiated human osteoclasts.

These functional properties are used in the determination of activity of mature osteoclasts (Cenni et al., 2012). Staining for TRAP is also a marker of osteoclast differentiation and function since it is responsible for degradation of bone matrix phosphoproteins and collagen due to ROS it produces (Halleen et al., 1999; Hayman A., 2008). It may, therefore, be possible that PLGA nanocapsules themselves have an inhibitory effect on TRAP activity in differentiating osteoclasts. It seems that after the removal of the capsules from the medium on Day 3 and with reduction in nanocapsule concentration endocytosed by cells with further cell division, the effect of the capsules on TRAP activity is reduced, and the cells could be stained for TRAP on Day 5.

### **3.5.2 Inhibition of Osteoclastic Activity**

It is known that when osteoclasts are cultured on bone or dentin slices, they excavate resorption lacuna or “pits” which are structures similar formed to those in *in vivo* environment during bone resorption (Charles and Aliprantis 2014). The number and size of those resorption pits are used as a quantification method for the osteoclastic activity. The osteoclastic activity was studied with pit formation assay by using the osteoassay surface 96-well plates (Corning, USA) which are plates coated with calcium phosphate and are used in functional assays of osteoclasts (Abe et al., 2012; Dou et al., 2014). The images presented in Figure 29 are the result of the batch analysis of 15 images obtained from each group (n=3).

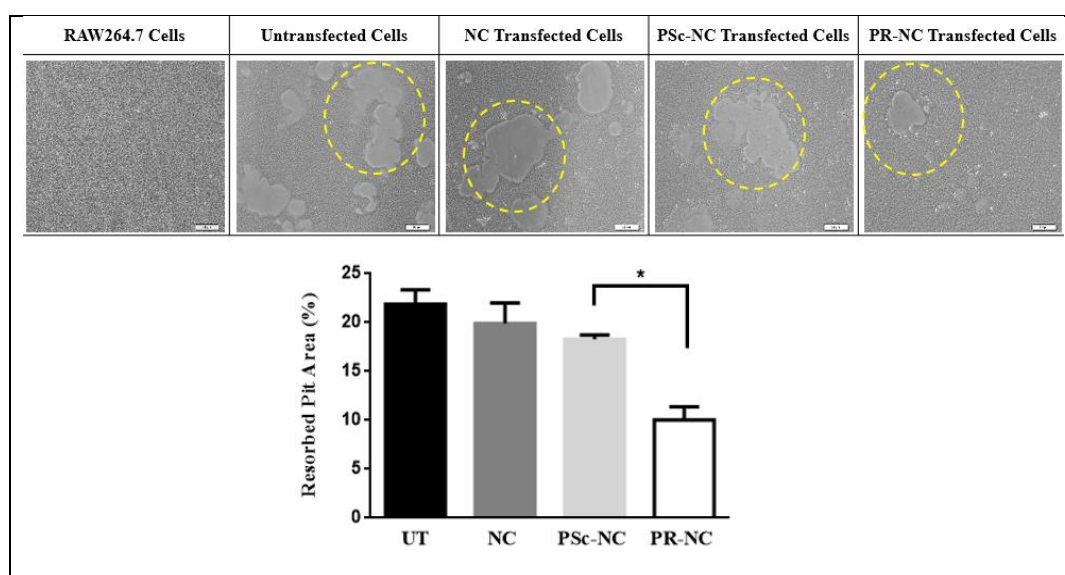


**Figure 29:** Osteoclastic activity determined by pit formation assay. Top panel: Representative images of areas resorbed by undifferentiated RAW264.7 cells, untransfected cells (UT) and differentiated RAW-OC cells transfected with PLGA nanocapsules carrying different cargo. NC: PLGA nanocapsule, PSc-NC: PEI:Scrambled siRNA loaded, PR-NC: PEI:RANK siRNA loaded PLGA nanocapsule. Bottom panel: Quantification of areas of resorbed pits (n=3). Dotted yellow circles show examples of resorbed pits in the micrographs. Scale Bar: 50  $\mu$ m

It is clearly observed that treatment of RAW264.7 cells with RANKL resulted in the formation of resorption pits (Figure 29, untransfected cells) supporting the role of RANKL dependent of osteoclast formation and function. The resorbed pit area was calculated to be  $21.9 \pm 1.5$  %. Treatment with empty nanocapsule or Scrambled siRNA loaded nanocapsules did not suppress the formation of pits ( $19.9 \pm 2.1$  % and  $18.3 \pm 0.4$  %, respectively). The treatment of cells with PEI:RANK siRNA loaded nanocapsules, however, resulted in a significant reduction in the formation of resorption pits ( $10.0 \pm 1.4$  %). It was concluded that the decrease in the formation of pits might be due to presence of fewer osteoclasts, as determined by TRAP enzyme staining, together with the reduction in the activity of differentiated osteoclasts caused by RANK inhibition.



## CHAPTER 4

### CONCLUSIONS

Osteoporosis is the most common bone disease characterized by low bone mass, elevation in bone fragility and susceptibility to fractures. Although being a major health problem, its effective treatment remains a challenge. Our motivation in this study was to develop an effective treatment strategy to achieve a systemic and bone targeted delivery of the therapeutic agent. siRNA was chosen as the therapeutic agent because of its specificity towards mRNA sequence. It was used in complex form with PEI to protect the siRNA in the extra- and intracellular environments. PLGA was used both to mask the toxicity of PEI and to carry the PEI:siRNA complex selectively to bone tissue. The increased bone affinity was imparted to the PLGA nanocapsules by coating the nanocapsules with a genetically engineered Elastin like recombinamer, ELR, carrying a sequence that has high affinity towards HAp.

The delivery system designed was characterized using SEM, TEM and XPS to show the efficiency in coating the ELR on the capsules. PEI:DNAoligo loaded PLGA nanocapsules were studied in terms of encapsulation efficiency and release kinetics. The efficacy of PEI:siRNA complex loaded nanocapsules were studied in osteoclast precursor cell line. The inhibition of mRNA through the action of delivered siRNA were studied along with the functional assays for differentiation of osteoclast precursors and activity of mature osteoclasts.

Experimental results indicated that, a high fraction of PEI:siRNA loaded and ELR coated PLGA nanocapsules had sizes smaller than 200 nm.

This makes the transport of these particles through the vasculature and extravasation theoretically possible, and it is likely that a fraction of the injected particles will be localized in bone tissue due to the interaction of ELR with the calcium phosphate of the bone. Once the nanoparticles are in the vicinity of the bone, the nanocapsules or the released siRNA complexes will be internalized by the bone cells where the siRNA would function. The encapsulation efficiency of PEI:siRNA complex was considered enough to release sufficient amount of PEI:siRNA complex. The delivery system was effective in inhibiting the mRNA levels of the target gene, RANK. It also suppressed the differentiation of osteoclast precursors to mature osteoclasts and the resorption of the osteoclasts. In summary, it is concluded that the delivery system designed has the capability to suppress bone resorption and decrease the incidence of osteoporosis.



## REFERENCES

- Abe, K., Yoshimura, Y., Deyama, Y., Kikuri, T., Hasegawa, T., Tei, K., Shinoda, H., Suzuki, K., Kitagawa, Y., 2012. Effects of bisphosphonates on osteoclastogenesis in RAW264.7 cells. *International journal of molecular medicine* 29, 1007-1015.
- Alshamsan, A., Haddadi, A., Hamdy, S., Samuel, J., El-Kadi, A.O.S., Uludağ, H., Lavasanifar, A., 2010. STAT3 Silencing in Dendritic Cells by siRNA Polyplexes Encapsulated in PLGA Nanoparticles for the Modulation of Anticancer Immune Response. *Molecular Pharmaceutics* 7, 1643-1654.
- Andersson, G., Ek-Rylander, B., 1995. The tartrate-resistant purple acid phosphatase of bone osteoclasts—a protein phosphatase with multivalent substrate specificity and regulation. *Acta Orthopaedica Scandinavica* 66, 189-194.
- Asafo-Adjei, T.A., Chen, A.J., Najarzadeh, A., Puleo, D.A., 2016. Advances in Controlled Drug Delivery for Treatment of Osteoporosis. *Curr Osteoporos Rep* 14, 226-238.
- Bannunah, A.M., Vllasaliu, D., Lord, J., Stolnik, S., 2014. Mechanisms of nanoparticle internalization and transport across an intestinal epithelial cell model: effect of size and surface charge. *Mol Pharm* 11, 4363-4373.
- Barbosa, J.S., Costa, R.R., Testera, A.M., Alonso, M., Rodríguez-Cabello, J.C., Mano, J.F., 2009. Multi-Layered Films Containing a Biomimetic Stimuli-Responsive Recombinant Protein. *Nanoscale Research Letters* 4, 1247.
- Barrett-Connor, E., Mosca, L., Collins, P., Geiger, M.J., Grady, D., Kornitzer, M., McNabb, M.A., Wenger, N.K., 2006. Effects of Raloxifene on Cardiovascular Events and Breast Cancer in Postmenopausal Women. *New England Journal of Medicine* 355, 125-137.

Barua, S., Mitragotri, S., 2014. Challenges associated with Penetration of Nanoparticles across Cell and Tissue Barriers: A Review of Current Status and Future Prospects. *Nano today* 9, 223-243.

Blair, H.C., Robinson, L.J., Huang, C.L., Sun, L., Friedman, P.A., Schlesinger, P.H., Zaidi, M., 2011. Calcium and bone disease. *BioFactors* (Oxford, England) 37, 159-167.

Bohr, A., Kristensen, J., Dyas, M., Edirisinghe, M., Stride, E., 2012. Release profile and characteristics of electrosprayed particles for oral delivery of a practically insoluble drug. *Journal of The Royal Society Interface* 9, 2437-2449.

Bone, H.G., Chapurlat, R., Brandi, M.L., Brown, J.P., Czerwinski, E., Krieg, M.A., Mellstrom, D., Radominski, S.C., Reginster, J.Y., Resch, H., Ivorra, J.A., Roux, C., Vittinghoff, E., Daizadeh, N.S., Wang, A., Bradley, M.N., Franchimont, N., Geller, M.L., Wagman, R.B., Cummings, S.R., Papapoulos, S., 2013. The effect of three or six years of denosumab exposure in women with postmenopausal osteoporosis: results from the FREEDOM extension. *J Clin Endocrinol Metab* 98, 4483-4492.

Bonnet, M.-E., Erbacher, P., Bolcato-Bellemin, A.-L., 2008. Systemic Delivery of DNA or siRNA Mediated by Linear Polyethylenimine (L-PEI) Does Not Induce an Inflammatory Response. *Pharmaceutical Research* 25, 2972.

Boyce, B.F., Xing, L., 2007. Biology of RANK, RANKL, and osteoprotegerin. *Arthritis research & therapy* 9 Suppl 1, S1.

Boyle, W.J., Simonet, W.S., Lacey, D.L., 2003. Osteoclast differentiation and activation. *Nature* 423, 337-342.

Brunner, T., Cohen, S., Monsonego, A., 2010. Silencing of proinflammatory genes targeted to peritoneal-residing macrophages using siRNA encapsulated in biodegradable microspheres. *Biomaterials* 31, 2627-2636.

Buckwalter, J.A., Glimcher, M.J., Cooper, R.R., Recker, R., 1995. Bone Biology. JBJS 77, 1256-1275.

Byler, D.M., Susi, H., 1986. Examination of the Secondary Structure of Proteins by Deconvolved FTIR Spectra. Biopolymers 25, 469-487.

Carthew, R.W., Sontheimer, E.J., 2009. Origins and Mechanisms of miRNAs and siRNAs. Cell 136, 642-655.

Cenni, E., Avnet, S., Granchi, D., Fotia, C., Salerno, M., Miceli, D., Sarpietro, M.G., Pignatello, R., Castelli, F., Baldini, N., 2012. The effect of poly(d,l-lactide-co-glycolide)-alendronate conjugate nanoparticles on human osteoclast precursors. Journal of biomaterials science. Polymer edition 23, 1285-1300.

Chan, C.K., Mason, A., Cooper, C., Dennison, E., 2016. Novel advances in the treatment of osteoporosis. British medical bulletin 119, 129-142.

Chang, W.H., Chang, Y., Lai, P.H., Sung, H.W., 2003. A genipin-crosslinked gelatin membrane as wound-dressing material: in vitro and in vivo studies. J Biomater Sci Polym Ed. 14, 481-495.

Chendrimada, T.P., Gregory, R.I., Kumaraswamy, E., Norman, J., Cooch, N., Nishikura, K., Shiekhattar, R., 2005. TRBP recruits the Dicer complex to Ago2 for microRNA processing and gene silencing. Nature 436, 740-744.

Cheng, H., Chawla, A., Yang, Y., Li, Y., Zhang, J., Jang, H.L., Khademhosseini, A., 2017. Development of nanomaterials for bone-targeted drug delivery. Drug Discovery Today 22, 1336-1350.

Choi, H.S., Liu, W., Misra, P., Tanaka, E., Zimmer, J.P., Ipe, B.I., Bawendi, M.G., Frangioni, J.V., 2007. Renal Clearance of Nanoparticles. Nature biotechnology 25, 1165-1170.

Collin-Osdoby, P., Yu, X., Zheng, B.S., Osdoby, P. 2012. RANKL-Mediated Osteoclast Formation from Murine RAW 264.7 Cells, In: H., H.M., Ralston S. H. (Eds.) *Methods in Molecular Medicine: Bone Research Protocols*. Humana Press, Totowa, N. J.

Cong, Y., Quan, C., Liu, M., Liu, J., Huang, G., Tong, G., Yin, Y., Zhang, C., Jiang, Q., 2015. Alendronate-decorated biodegradable polymeric micelles for potential bone-targeted delivery of vancomycin. *Journal of biomaterials science. Polymer edition* 26, 629-643.

Cun, D., Foged, C., Yang, M., Frøkjær, S., Nielsen, H.M., 2010. Preparation and characterization of poly(dl-lactide-co-glycolide) nanoparticles for siRNA delivery. *International Journal of Pharmaceutics* 390, 70-75.

Cun, D., Jensen, D.K., Maltesen, M.J., Bunker, M., Whiteside, P., Scurr, D., Foged, C., Nielsen, H.M., 2011. High loading efficiency and sustained release of siRNA encapsulated in PLGA nanoparticles: quality by design optimization and characterization. *European journal of pharmaceutics and biopharmaceutics : official journal of Arbeitsgemeinschaft fur Pharmazeutische Verfahrenstechnik e.V* 77, 26-35.

Dang, L., Liu, J., Li, F., Wang, L., Li, D., Guo, B., He, X., Jiang, F., Liang, C., Liu, B., Badshah, S.A., He, B., Lu, J., Lu, C., Lu, A., Zhang, G., 2016. Targeted Delivery Systems for Molecular Therapy in Skeletal Disorders. *International journal of molecular sciences* 17, 428.

Das, S., Crockett, J.C., 2013. Osteoporosis - a current view of pharmacological prevention and treatment. *Drug design, development and therapy* 7, 435-448.

Demadis, K.D., Paspalaki, M., Theodorou, J., 2011. Controlled Release of Bis(phosphonate) Pharmaceuticals from Cationic Biodegradable Polymeric Matrices. *Industrial & Engineering Chemistry Research* 50, 5873-5876.

Dempster, D.W., Shane, E., Horbert, W., Lindsay, R., 1986. A simple method for correlative light and scanning electron microscopy of human iliac crest bone biopsies: qualitative observations in normal and osteoporotic subjects. *J Bone Miner Res* 1, 15-21.

Dinarvand, R., Sepehri, N., Manoochehri, S., Rouhani, H., Atyabi, F., 2011. Polylactide-co-glycolide nanoparticles for controlled delivery of anticancer agents. *International Journal of Nanomedicine* 6, 877-895.

Dominska, M., Dykxhoorn, D.M., 2010. Breaking down the barriers: siRNA delivery and endosome escape. *Journal of Cell Science* 123.

Doschak, M.R., Kucharski, C.M., Wright, J.E., Zernicke, R.F., Uludag, H., 2009. Improved bone delivery of osteoprotegerin by bisphosphonate conjugation in a rat model of osteoarthritis. *Mol Pharm* 6, 634-640.

Dou, C., Zhang, C., Kang, F., Yang, X., Jiang, H., Bai, Y., Xiang, J., Xu, J., Dong, S., 2014. MiR-7b directly targets DC-STAMP causing suppression of NFATc1 and c-Fos signaling during osteoclast fusion and differentiation. *Biochim Biophys Acta* 1839, 1084-1096.

Dougall W. C., 2012. Molecular pathways: osteoclast-dependent and osteoclast-independent roles of the RANKL/RANK/OPG pathway in tumorigenesis and metastasis. *Clin Cancer Res* 18, 326-335.

Ducy, P., Zhang, R., Geoffroy, V., Ridall, A.L., Karsenty, G., 1997. *Osf2/Cbfa1*: A Transcriptional Activator of Osteoblast Differentiation. *Cell* 89, 747-754.

Eghbali-Fatourehchi, G., Khosla, S., Sanyal, A., Boyle, W.J., Lacey, D.L., Riggs, B.L., 2003. Role of RANK ligand in mediating increased bone resorption in early postmenopausal women. *J Clin Invest* 111, 1221-1230.

Ek-Rylander, B., Flores, M., Wendel, M., Heinegard, D., Andersson, G., 1994. Dephosphorylation of osteopontin and bone sialoprotein by osteoclastic tartrate-resistant acid phosphatase. Modulation of osteoclast adhesion in vitro. *J Biol Chem* 269, 14853-14856.

Eke, G., Goñi-de-Cerio, F., Suarez-Merino, B., Hasirci, N., Hasirci, V., 2015. Biocompatibility of Dead Sea Water and retinyl palmitate carrying poly(3-hydroxybutyrate-co-3-hydroxyvalerate) micro/nanoparticles designed for transdermal skin therapy. *Journal of Bioactive and Compatible Polymers* 30, 455-471.

Fahid, F.S., Jiang J., Zhu Q., Zhang C., E., Filbert E., K.E., S., 2008. Application of small interfering RNA for inhibition of lipopolysaccharide-induced osteoclast formation and cytokine stimulation. *J. Endod.* 37, 563–569.

Feng X., 2005. RANKing Intracellular Signalling in Osteoclasts. *Life* 57, 389-395.

Florencio-Silva, R., Sasso, G.R.d.S., Sasso-Cerri, E., Sim, M.J., Cerri, P.S., 2015. Biology of Bone Tissue: Structure, Function, and Factors That Influence Bone Cells. *BioMed Research International* 2015, 17.

Forlino, A., Marini, J.C., 2016. Osteogenesis imperfecta. *The Lancet* 387, 1657-1671.

Fröhlich E., 2012. The role of surface charge in cellular uptake and cytotoxicity of medical nanoparticles. *International Journal of Nanomedicine* 7, 5577-5591.

Gan, K., Yang, L., Xu, L., Feng, X., Zhang, Q., Wang, F., Tan, W., Zhang, M., 2016. Igaratimod (T-614) suppresses RANKL-induced osteoclast differentiation and migration in RAW264.7 cells via NF-kappaB and MAPK pathways. *International immunopharmacology* 35, 294-300.

Gratton, S.E.A., Ropp, P.A., Pohlhaus, P.D., Luft, J.C., Madden, V.J., Napier, M.E., DeSimone, J.M., 2008. The effect of particle design on cellular internalization pathways. *Proceedings of the National Academy of Sciences of the United States of America* 105, 11613-11618.

Hadjidakis, D.J., Androulakis, I.I., 2006. Bone remodeling. *Ann N Y Acad Sci* 1092, 385-396.

Hall, A., Larsen, A.K., Parhamifar, L., Meyle, K.D., Wu, L.P., Moghimi, S.M., 2013. High resolution respirometry analysis of polyethylenimine-mediated mitochondrial energy crisis and cellular stress: Mitochondrial proton leak and inhibition of the electron transport system. *Biochim Biophys Acta* 1827, 1213-1225.

Halleen, J.M., Raisanen, S., Salo, J.J., Reddy, S.V., Roodman, G.D., Hentunen, T.A., Lehenkari, P.P., Kaija, H., Vihko, P., Vaananen, H.K., 1999. Intracellular fragmentation of bone resorption products by reactive oxygen species generated by osteoclastic tartrate-resistant acid phosphatase. *J Biol Chem* 274, 22907-22910.

Hamdy N., A., 2009. Strontium ranelate improves bone microarchitecture in osteoporosis. *Rheumatology (Oxford, England)* 48 Suppl 4, iv9-13.

Hasan, W., Chu, K., Gullapalli, A., Dunn, S.S., Enlow, E.M., Luft, J.C., Tian, S., Napier, M.E., Pohlhaus, P.D., Rolland, J.P., DeSimone, J.M., 2012. Delivery of Multiple siRNAs Using Lipid-Coated PLGA Nanoparticles for Treatment of Prostate Cancer. *Nano Letters* 12, 287-292.

Hayman A., R., 2008. Tartrate-resistant acid phosphatase (TRAP) and the osteoclast/immune cell dichotomy. *Autoimmunity* 41, 218-223.

Hessle, L., Johnson, K.A., Anderson, H.C., Narisawa, S., Sali, A., Goding, J.W., Terkeltaub, R., Millan, J.L., 2002. Tissue-nonspecific alkaline phosphatase and plasma cell membrane glycoprotein-1 are central antagonistic regulators of bone mineralization. *Proc Natl Acad Sci U S A* 99, 9445-9449.

Holroyd, C., Cooper, C., Dennison, E., 2008. Epidemiology of osteoporosis. Best practice & research. Clinical endocrinology & metabolism 22, 671-685.

Hsu, H., Lacey, D.L., Dunstan, C.R., Solovyev, I., Colombero, A., Timms, E., Tan, H.L., Elliott, G., Kelley, M.J., Sarosi, I., Wang, L., Xia, X.Z., Elliott, R., Chiu, L., Black, T., Scully, S., Capparelli, C., Morony, S., Shimamoto, G., Bass, M.B., Boyle, W.J., 1999. Tumor necrosis factor receptor family member RANK mediates osteoclast differentiation and activation induced by osteoprotegerin ligand. Proc Natl Acad Sci U S A 96, 3540-3545.

Jiang, T., Yu, X., Carbone, E.J., Nelson, C., Kan, H.M., Lo, K.W.H., 2014. Poly aspartic acid peptide-linked PLGA based nanoscale particles: Potential for bone-targeting drug delivery applications. International Journal of Pharmaceutics 475, 547-557.

Jung, T.-S., Kwon, B.-S., Lee, H.-E., Kim, A.-Y., Lee, M.-J., Park, C.-R., Kang, H.-K., Kim, Y.-D., Lee, S.-K., Kang, J.-S., Choi, G.-J., 2009. Enhanced oral absorption of salmon calcitonin-encapsulated PLGA nanoparticles by adding organic substances. Korean Journal of Chemical Engineering 26, 131-135.

Kanis J. A., 2002. Diagnosis of osteoporosis and assessment of fracture risk. The Lancet 359, 1929-1936.

Kanis J. A., 2007. Assessment of Osteoporosis at the Primary Health Care Level. World Health Organization Scientific Group Technical Report University of Sheffield, UK: 66.

Kim, J.H., Kim, N., 2014. Regulation of NFATc1 in Osteoclast Differentiation. J Bone Metab 21, 233-241.

Kim, J.H., Kim, N., 2016. Signaling Pathways in Osteoclast Differentiation. Chonnam Med J 52, 12-17.



Kim, S.H., Jeong, J.H., Lee, S.H., Kim, S.W., Park, T.G., 2008. Local and systemic delivery of VEGF siRNA using polyelectrolyte complex micelles for effective treatment of cancer. *Journal of Controlled Release* 129, 107-116.

Kini, U., Nandeesh, B.N., 2012. Physiology of Bone Formation, Remodeling, and Metabolism. *Radionuclide and Hybrid Bone Imaging* DOI 10.1007/978-3-642-02400-9\_2.

Kong, J., Yu, S., 2007. Fourier transform infrared spectroscopic analysis of protein secondary structures. *Acta biochimica et biophysica Sinica* 39, 549-559.

Kumari, A., Yadav, S.K., Yadav, S.C., 2010. Biodegradable polymeric nanoparticles based drug delivery systems. *Colloids and Surfaces B: Biointerfaces* 75, 1-18.

Lajeunesse, D., Pelletier, J.P., Martel-Pelletier, J. 2010. Multiple connections: new concepts in bone health. In *Osteoporosis and osteoarthritis: bone is the common battleground*.

Lamoureux, F., Baud'huin, M., Duplomb, L., Heymann, D., Redini, F., 2007. Proteoglycans: key partners in bone cell biology. *BioEssays : news and reviews in molecular, cellular and developmental biology* 29, 758-771.

Lee, D., Heo, D.N., Kim, H.J., Ko, W.K., Lee, S.J., Heo, M., Bang, J.B., Lee, J.B., Hwang, D.S., Do, S.H., Kwon, I.K., 2016. Inhibition of Osteoclast Differentiation and Bone Resorption by Bisphosphonate-conjugated Gold Nanoparticles. *Sci Rep* 6, 27336.

Lerner U. H., 2006. Bone Remodeling in Post-menopausal Osteoporosis. *Journal of Dental Research* 85, 584-595.

Li, J., Bao, Q., Chen, S., Liu, H., Feng, J., Qin, H., Li, A., Liu, D., Shen, Y., Zhao, Y., Zong, Z., 2017. Different bone remodeling levels of trabecular and cortical bone in response to changes in Wnt/beta-catenin signaling in mice. *J Orthop Res* 35, 812-819.

Liang, C., Guo, B., Wu, H., Shao, N., Li, D., Liu, J., Dang, L., Wang, C., Li, H., Li, S., Lau, W.K., Cao, Y., Yang, Z., Lu, C., He, X., Au, D.W., Pan, X., Zhang, B.T., Lu, C., Zhang, H., Yue, K., Qian, A., Shang, P., Xu, J., Xiao, L., Bian, Z., Tan, W., Liang, Z., He, F., Zhang, L., Lu, A., Zhang, G., 2015. Aptamer-functionalized lipid nanoparticles targeting osteoblasts as a novel RNA interference-based bone anabolic strategy. *Nat Med* 21, 288-294.

Lips, P., van Schoor, N.M., 2011. The effect of vitamin D on bone and osteoporosis. *Best practice & research. Clinical endocrinology & metabolism* 25, 585-591.

Liu X., 2016. Bone site-specific delivery of siRNA. *J Biomed Res* 30, 264-271.

Lu, T., Ma, Y., Hu, H., Chen, Y., Zhao, W., Chen, T., 2011. Ethinylestradiol liposome preparation and its effects on ovariectomized rats' osteoporosis. *Drug Delivery* 18, 468-477.

Mailänder, V., Landfester, K., 2009. Interaction of Nanoparticles with Cells. *Biomacromolecules* 10, 2379-2400.

Makadia, H.H., Siegel, J.S., 2011. Poly Lactic-co-Glycolic Acid (PLGA) as Biodegradable Controlled Drug Delivery Carrier. *Polymers* 3.

Mao, Z., Fang Z., Yang Y., Chen X., Wang Y., Jian K., Qu X., Yuan W., K., D., 2017. Strontium ranelate-loaded PLGA porous microspheres enhancing the osteogenesis of MC3T3-E1 cells. *RSC Adv* 7, 24607-24615.

Miladi, K., Sfarb S., Fessia H. , A., E., 2013. Drug carriers in osteoporosis: Preparation, drug encapsulation and applications. *International Journal of Pharmaceutics* 445, 181-195.

Miller, F.A., Wilkins, C.H., 1952. Infrared Spectra and Characteristic Frequencies of Inorganic Ions. *Analytical Chemistry* 24, 1253-1294.

Mittal, G., Sahana, D.K., Bhardwaj, V., Ravi Kumar, M.N.V., 2007. Estradiol loaded PLGA nanoparticles for oral administration: Effect of polymer molecular weight and copolymer composition on release behavior in vitro and in vivo. *Journal of Controlled Release* 119, 77-85.

Mora-Raimundo, P., Manzano M., M., V.-R., 2017. Nanoparticles for the treatment of osteoporosis. *AIMS Bioengineering* 4, 259-274.

Morinobu, M., Ishijima, M., Rittling, S.R., Tsuji, K., Yamamoto, H., Nifuji, A., Denhardt, D.T., Noda, M., 2003. Osteopontin expression in osteoblasts and osteocytes during bone formation under mechanical stress in the calvarial suture in vivo. *J Bone Miner Res* 18, 1706-1715.

Murata, N., Takashima, Y., Toyoshima, K., Yamamoto, M., Okada, H., 2008. Anti-tumor effects of anti-VEGF siRNA encapsulated with PLGA microspheres in mice. *Journal of Controlled Release* 126, 246-254.

Nakagawa, N., Kinosaki, M., Yamaguchi, K., Shima, N., Yasuda, H., Yano, K., Morinaga, T., Higashio, K., 1998. RANK Is the Essential Signaling Receptor for Osteoclast Differentiation Factor in Osteoclastogenesis. *Biochemical and Biophysical Research Communications* 253, 395-400.

Nakamura H., 2007. Morphology, function, and differentiation of bone cells. *Journal of Hard Tissue Biology* 16, 15-22.

Narayanan, D., Anitha, A., Jayakumar, R., Chennazhi, K.P., 2013. In Vitro and in Vivo Evaluation of Osteoporosis Therapeutic Peptide PTH 1–34 Loaded PEGylated Chitosan Nanoparticles. *Molecular Pharmaceutics* 10, 4159-4167.

Neale, J.R., Richter, N.B., Merten, K.E., Grant Taylor, K., Singh, S., Waite, L.C., Emery, N.K., Smith, N.B., Cai, J., Pierce, W.M., 2009. Bone selective effect of an estradiol conjugate with a novel tetracycline-derived bone-targeting agent. *Bioorganic & medicinal chemistry letters* 19, 680-683.

Neuberg, P., Kichler, A., 2014. Recent developments in nucleic acid delivery with polyethylenimines. *Adv Genet* 88, 263-288.

Nguyen, M.K., Jeon, O., Krebs, M.D., Schapira, D., Alsberg, E., 2014. Sustained localized presentation of RNA interfering molecules from in situ forming hydrogels to guide stem cell osteogenic differentiation. *Biomaterials* 35, 6278-6286.

Oddie, G.W., Schenk, G., Angel, N.Z., Walsh, N., Guddat, L.W., de Jersey, J., Cassady, A.I., Hamilton, S.E., Hume, D.A., 2000. Structure, function, and regulation of tartrate-resistant acid phosphatase. *Bone* 27, 575-584.

Ohno, H., Kubo, K., Murooka, H., Kobayashi, Y., Nishitoba, T., Shibuya, M., Yoneda, T., Ise, T., 2006. A c-fms tyrosine kinase inhibitor, Ki20227, suppresses osteoclast differentiation and osteolytic bone destruction in a bone metastasis model. *Mol Cancer Ther* 5, 2634-2643.

Pantazis, P., Dimas, K., Wyche, J.H., Anant, S., Houchen, C.W., Panyam, J., Ramanujam, R.P., 2012. Preparation of siRNA-encapsulated PLGA nanoparticles for sustained release of siRNA and evaluation of encapsulation efficiency. *Methods Mol Biol* 906, 311-319.

Panyam, J., Zhou, W.Z., Prabha, S., Sahoo, S.K., Labhasetwar, V., 2002. Rapid endo-lysosomal escape of poly(DL-lactide-co-glycolide) nanoparticles: implications for drug and gene delivery. *Faseb j* 16, 1217-1226.

Panzavolta, S., Torricelli, P., Bracci, B., Fini, M., Bigi, A., 2010. Functionalization of biomimetic calcium phosphate bone cements with alendronate. *Journal of Inorganic Biochemistry* 104, 1099-1106.

Patil, Y., Panyam, J., 2009. Polymeric nanoparticles for siRNA delivery and gene silencing. *Int J Pharm* 367, 195-203.

Pisani, P., Renna, M.D., Conversano, F., Casciaro, E., Di Paola, M., Quarta, E., Muratore, M., Casciaro, S., 2016. Major osteoporotic fragility fractures: Risk factor updates and societal impact. *World Journal of Orthopedics* 7, 171-181.

Popescu, M.C., Vasile, C., Craciunescu, O., 2010. Structural analysis of some soluble elastins by means of FT-IR and 2D IR correlation spectroscopy. *Biopolymers*. 93, 1072-1084.

Pradhan, R., Poudel, B.K., Ramasamy, T., Choi, H.G., Yong, C.S., Kim, J.O., 2013. Docetaxel-loaded polylactic acid-co-glycolic acid nanoparticles: formulation, physicochemical characterization and cytotoxicity studies. *Journal of nanoscience and nanotechnology* 13, 5948-5956.

Raggatt, L.J., Partridge, N.C., 2010. Cellular and molecular mechanisms of bone remodeling. *J Biol Chem* 285, 25103-25108.

Ralston, S.H., Langston, A.L., Reid, I.R., 2008. Pathogenesis and management of Paget's disease of bone. *Lancet* 372, 155-163.

Rauch, F., Glorieux, F.H., 2004. Osteogenesis imperfecta. *The Lancet* 363, 1377-1385.

Ray, S., Shard, A.G., 2011. Quantitative analysis of adsorbed proteins by X-ray photoelectron spectroscopy. *Anal Chem* 83, 8659-8666.

Richards, G., Amy C., Doody, A.M., Putnam, D., 2006. Biophysical and Structural Characterization of Polyethylenimine-Mediated siRNA Delivery in Vitro. *Pharmaceutical Research* 23, 1868-1876.

Rodriguez-Cabello, J.C., Prieto, S., Reguera, J., Arias F. J., Riberio, A., 2007. Biofunctional design of elastin-like polymers for advanced applications in nanobiotechnology. *J. Biomater. Sci. Polymer Edn* 18, 269-286.

Roelofs, A.J., Thompson, K., Gordon, S., Rogers, M.J., 2006. Molecular mechanisms of action of bisphosphonates: current status. *Clin Cancer Res* 12, 6222s-6230s.

Saftig, P., Hunziker, E., Wehmeyer, O., Jones, S., Boyde, A., Rommerskirch, W., Moritz, J.D., Schu, P., von Figura, K., 1998. Impaired osteoclastic bone resorption leads to osteopetrosis in cathepsin-K-deficient mice. *Proc Natl Acad Sci U S A* 95, 13453-13458.

Sahana, H., Khajuria D. K., Razdan E., Mahapatra D. R., Bhat, M.R., Suresh S., Rao R. R., L., M., 2013. Improvement in Bone Properties by Using Risedronate Adsorbed Hydroxyapatite Novel Nanoparticle Based Formulation in a Rat Model of Osteoporosis. *Journal of biomedical nanotechnology* 9, 193-201.

Saini, D., Fazil, M., Ali, M.M., Baboota, S., Ali, J., 2015. Formulation, development and optimization of raloxifene-loaded chitosan nanoparticles for treatment of osteoporosis. *Drug Deliv* 22, 823-836.

Sakagami, H., Kishino, K., Amano, O., Kanda, Y., Kunii, S., Yokote, Y., Oizumi, H., Oizumi, T., 2009. Cell death induced by nutritional starvation in mouse macrophage-like RAW264.7 cells. *Anticancer Res* 29, 343-347.

Samadi Moghaddam, M., Heiny, M., Shastri, V.P., 2015. Enhanced cellular uptake of nanoparticles by increasing the hydrophobicity of poly(lactic acid) through copolymerization with cell-membrane-lipid components. *Chem Commun (Camb)* 51, 14605-14608.

Sekido, T., Sakura, N., Higashi, Y., Miya, K., Nitta, Y., Nomura, M., Sawanishi, H., Morito, K., Masamune, Y., Kasugai, S., Yokogawa, K., Miyamoto, K., 2001. Novel drug delivery system to bone using acidic oligopeptide: pharmacokinetic characteristics and pharmacological potential. *J Drug Target* 9, 111-121.

Shen, Y., Wang, J., Li, Y., Tian, Y., Sun, H., Ammar, O., Tu, J., Wang, B., Sun, C., 2015. Co-delivery of siRNA and paclitaxel into cancer cells by hyaluronic acid modified redox-sensitive disulfide-crosslinked PLGA-PEI nanoparticles. *RSC Advances* 5, 46464-46479.

Singh, H., Laibinis, P.E., Hatton, T.A., 2005. Rigid, Superparamagnetic Chains of Permanently Linked Beads Coated with Magnetic Nanoparticles. Synthesis and Rotational Dynamics under Applied Magnetic Fields. *Langmuir* 21, 11500-11509.

Singh, R., Lillard, J.W., 2009. Nanoparticle-based targeted drug delivery. *Experimental and molecular pathology* 86, 215-223.

Sobacchi, C., Schulz, A., Coxon, F.P., Villa, A., Helfrich, M.H., 2013. Osteopetrosis: genetics, treatment and new insights into osteoclast function. *Nat Rev Endocrinol* 9, 522-536.

Soutschek, J., Akinc, A., Bramlage, B., Charisse, K., Constien, R., Donoghue, M., Elbashir, S., Geick, A., Hadwiger, P., Harborth, J., John, M., Kesavan, V., Lavine, G., Pandey, R.K., Racie, T., Rajeev, K.G., Rohl, I., Toudjarska, I., Wang, G., Wuschko, S., Bumcrot, D., Koteliansky, V., Limmer, S., Manoharan, M., Vornlocher, H.P., 2004. Therapeutic silencing of an endogenous gene by systemic administration of modified siRNAs. *Nature* 432, 173-178.

Soysa, N.S., Alles, N., Aoki, K., Ohya, K., 2012. Osteoclast formation and differentiation: an overview. *J Med Dent Sci* 59, 65-74.

Sun, Y., Ye, X., Cai, M., Liu, X., Xiao, J., Zhang, C., Wang, Y., Yang, L., Liu, J., Li, S., Kang, C., Zhang, B., Zhang, Q., Wang, Z., Hong, A., Wang, X., 2016. Osteoblast-Targeting-Peptide Modified Nanoparticle for siRNA/microRNA Delivery. *ACS Nano* 10, 5759-5768.

Sze, A., Erickson, D., Ren, L., Li, D., 2003. Zeta-potential measurement using the Smoluchowski equation and the slope of the current–time relationship in electroosmotic flow. *Journal of Colloid and Interface Science* 261, 402-410.

Takahashi, N., Udagawa, N., Suda, T., 2014. Vitamin D endocrine system and osteoclasts. *Bonekey Rep* 3, 495.

Takayanagi H., 2005. Mechanistic insight into osteoclast differentiation in osteoimmunology. *Journal of molecular medicine (Berlin, Germany)* 83, 170-179.

Takeuchi, I., Fukuda, K., Kobayashi, S., Makino, K., 2016. Transdermal delivery of estradiol-loaded PLGA nanoparticles using iontophoresis for treatment of osteoporosis. *Bio-medical materials and engineering* 27, 475-483.

Tanaka, T., Takei, Y., Zaima, N., Moriyama, T., Yamanouchi, D., 2017. Hyperglycemia Suppresses RANKL-Induced Osteoclast Differentiation through LXRbeta Expression in RAW264.7 Cells. *Journal of nutritional science and vitaminology* 63, 28-34.

Tejeda-Montes, E., Smith, K.H., Rebollo, E., Gómez, R., Alonso, M., Rodriguez-Cabello, J.C., Engel, E., Mata, A., 2014. Bioactive membranes for bone regeneration applications: Effect of physical and biomolecular signals on mesenchymal stem cell behavior. *Acta Biomaterialia* 10, 134-141.

Teti, A., Rucci, N., 2010. The unexpected links between bone and immune system. *Medicographia* 32, 341-348.

Theoleyre, S., Wittrant, Y., Couillaud, S., Vusio, P., Berreur, M., Dunstan, C., Blanchard, F., Rédini, F., Heymann, D., 2004. Cellular activity and signaling induced by osteoprotegerin in osteoclasts: involvement of receptor activator of nuclear factor  $\kappa$ B ligand and MAPK. *Biochimica et Biophysica Acta (BBA) - Molecular Cell Research* 1644, 1-7.



Udagawa, N., Takahashi, N., Akatsu, T., Tanaka, H., Sasaki, T., Nishihara, T., Koga, T., Martin, T.J., Suda, T., 1990. Origin of osteoclasts: mature monocytes and macrophages are capable of differentiating into osteoclasts under a suitable microenvironment prepared by bone marrow-derived stromal cells. *Proceedings of the National Academy of Sciences of the United States of America* 87, 7260-7264.

Utsuno, K., Uludag, H., 2010. Thermodynamics of Polyethylenimine-DNA Binding and DNA Condensation. *Biophysical Journal* 99, 201-207.

Vasir, J.K., Labhasetwar, V., 2007. Biodegradable nanoparticles for cytosolic delivery of therapeutics. *Advanced Drug Delivery Reviews* 59, 718-728.

Wada T., Nakashima T., Hiroshi N., M., P.J., 2006. RANKL–RANK signaling in osteoclastogenesis and bone disease. *Trends in Molecular Medicine* 12, 17-25.

Wagner, M., Rinkenauer, A.C., Schallon, A., Schubert, U.S., 2013. Opposites attract: influence of the molar mass of branched poly(ethylene imine) on biophysical characteristics of siRNA-based polyplexes. *RSC Advances* 3, 12774-12785.

Wang, H., Liu, J., Tao, S., Chai, G., Wang, J., Hu, F.-Q., Yuan, H., 2015. Tetracycline-grafted PLGA nanoparticles as bone-targeting drug delivery system. *International Journal of Nanomedicine* 10, 5671-5685.

Wang, Y., Grainger, D.W., 2010. siRNA Knock-Down of RANK Signaling to Control Osteoclast-Mediated Bone Resorption. *Pharmaceutical research* 27, 1273-1284.

Wang, Y., Grainger, D.W., 2012. RNA therapeutics targeting osteoclast-mediated excessive bone resorption. *Adv. Drug Deliv. Rev.* 64, 1341-1357.

Wang, Y., Tran, K.K., Shen, H., Grainger, D.W., 2012. Selective local delivery of RANK siRNA to bone phagocytes using bone augmentation biomaterials. *Biomaterials* 33, 8540-8547.

Wei, D., Jung, J., Yang, H., Stout, D.A., Yang, L., 2016. Nanotechnology Treatment Options for Osteoporosis and Its Corresponding Consequences. *Curr Osteoporos Rep* 14, 239-247.

Whitehead, K.A., Langer R., Anderson D. G., 2009. Knocking down barriers: advances in siRNA delivery. *Nature Reviews: Drug discovery* 8, 129-139.

Willson, T., Nelson, S.D., Newbold, J., Nelson, R.E., LaFleur, J., 2015. The clinical epidemiology of male osteoporosis: a review of the recent literature. *Clinical Epidemiology* 7, 65-76.

Yu, B., Wang, C.T., 2016. Osteoporosis, a Result of an “Aged” Bone Microenvironment. *Trends in molecular medicine* 22, 641-644.

Zeng, X.-z., He, L.-g., Wang, S., Wang, K., Zhang, Y.-y., Tao, L., Li, X.-j., Liu, S.-w., 2016. Aconine inhibits RANKL-induced osteoclast differentiation in RAW264.7 cells by suppressing NF- $\kappa$ B and NFATc1 activation and DC-STAMP expression. *Acta Pharmacologica Sinica* 37, 255-263.

Zhang, G., Guo, B., Wu, H., Tang, T., Zhang, B.-T., Zheng, L., He, Y., Yang, Z., Pan, X., Chow, H., To, K., Li, Y., Li, D., Wang, X., Wang, Y., Lee, K., Hou, Z., Dong, N., Li, G., Leung, K., Hung, L., He, F., Zhang, L., Qin, L., 2012. A delivery system targeting bone formation surfaces to facilitate RNAi-based anabolic therapy. *Nat Med* 18, 307-314.

Zhang, L., Lu, Z., Zhao, Q., Huang, J., Shen, H., Zhang, Z., 2011. Enhanced Chemotherapy Efficacy by Sequential Delivery of siRNA and Anticancer Drugs Using PEI-Grafted Graphene Oxide. *Small* 7, 460-464.

Zhang, Y., Dusad, A., Ren, K., 2014. Drug Delivery Strategies for Treating Osteoporosis. . *Orthopedic Muscul Sys* S2:003, doi:10.4172/2161-0533.S4172-4003.

Zhang, Y., Wei, L., Miron, R.J., Shi, B., Bian, Z., 2015. Anabolic bone formation via a site-specific bone-targeting delivery system by interfering with semaphorin 4D expression. *J Bone Miner Res* 30, 286-296.

Zhang, Y., Wei, L., Miron, R.J., Shi, B., Bian, Z., 2016. Bone scaffolds loaded with siRNA-Semaphorin4d for the treatment of osteoporosis related bone defects. *6*, 26925.



## **APPENDIX A**

### **OPTIMIZATION OF QUANTITATIVE REAL TIME POLYMERASE CHAIN REACTION (qRT-PCR)**

#### **RNA Isolation**

RNA isolation was performed by using RNeasy Micro Kit (Qiagen, Germany) according to manufacturer's protocol. Briefly, cells were disrupted with buffer RLT (350  $\mu$ L) by vortexing and was added into QIAshredder spin column for homogenization and centrifuged (14000 rpm, 2 min). Ethanol (70%, 350  $\mu$ L) was added and suspension was transferred to an RNeasy MinElute spin column and centrifuged (10000 g, 15 s). The spin column was washed with RW1 buffer (700  $\mu$ L), RPE buffer (500  $\mu$ L), ethanol (80%, 500  $\mu$ L). RNA was eluted from the membrane by centrifugation (14000 rpm, min) with nuclease free water (22  $\mu$ L). Finally, the RNA sample was incubated at 65<sup>0</sup>C for 10 min and treated with DNase I to clean the contaminating DNA.

#### **DNase I Treatment**

DNase I treatment was performed using DNA-free<sup>TM</sup> kit (Ambion, Invitrogen, Germany). Briefly, RNA solution contaminated with DNA (20  $\mu$ L) was incubated with DNase I buffer (2  $\mu$ L) and rDNase I (1  $\mu$ L) at 37<sup>0</sup>C for 30 min. Then DNase inactivation reagent (2  $\mu$ L) was added to the solution and incubated for 2 min at room temperature, mixing occasionally during the incubation. Lastly, the solution was centrifuged (10000 g, 5 min) and the supernatant was taken into a DEPC treated tube and stored at -80<sup>0</sup>C until used.

### First Strand cDNA Synthesis

First strand cDNA synthesis was performed by using RevertAid First Strand cDNA Synthesis Kit (Invitrogen, Germany). The following reagents were added into a sterile, DEPC treated tube:

Reagent	Volume
Total RNA	1 µg
Oligo (dT) <sub>18</sub> primer	1 µL
Nuclease Free Water	Complete to 12 µL
<b>Total Volume</b>	<b>12 µL</b>

This solution was incubated at 65<sup>0</sup>C for 5 min and chilled on ice. Then the following components were added in the following order:

Reagent	Volume (µL)
5X Reaction Buffer	4
Ribolock RNase inhibitor (20 u/µL)	1
10 mM dNTP mix	2
Revertaid M-MulV Reverse Transcriptase (200 u/µL)	1
<b>Total Volume</b>	<b>20</b>

The solution was incubated at 42<sup>0</sup>C for 60 min in a thermal cycler and the reaction was terminated by heating at 70<sup>0</sup>C for 5 min.

## Optimization of Primers for qRT-PCR

Reaction mixtures of 100, 10, 1, 0.1 and 0.01 ng cDNA samples were prepared and qRT-PCR was performed. The amplification (Figure 30 and Figure 33 ), melt (Figure 31 and Figure 34) and standard curves (Figure 32 and Figure 35) of each primer pair were plotted to determine the reaction efficiency.

### *RANK Primer*

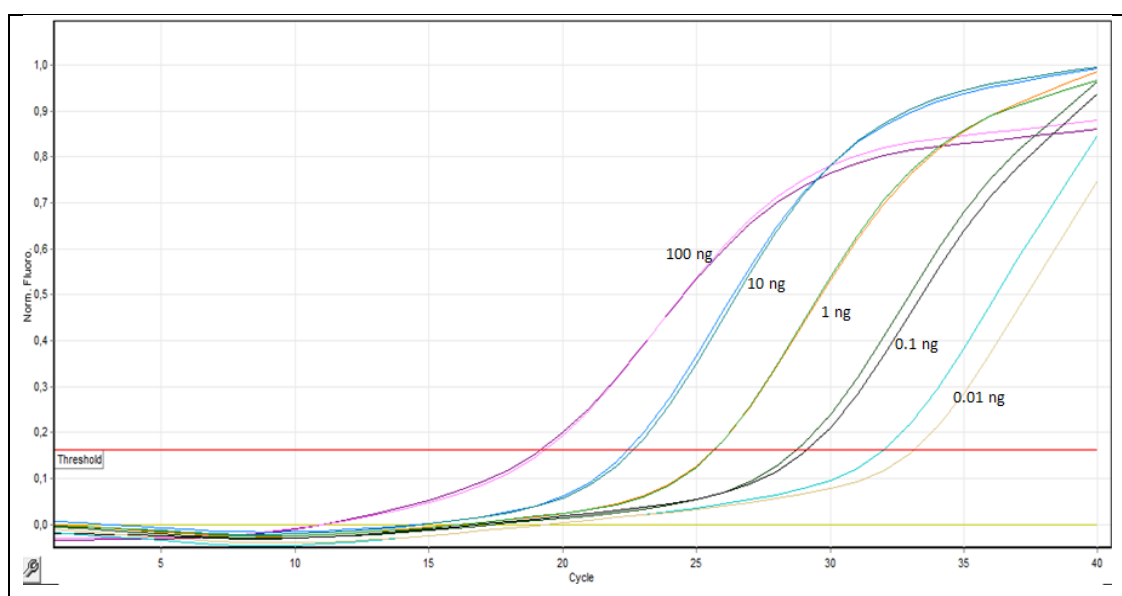


**Figure 30:** The amplification of RANK amplicon (yellow line: Non-template control).

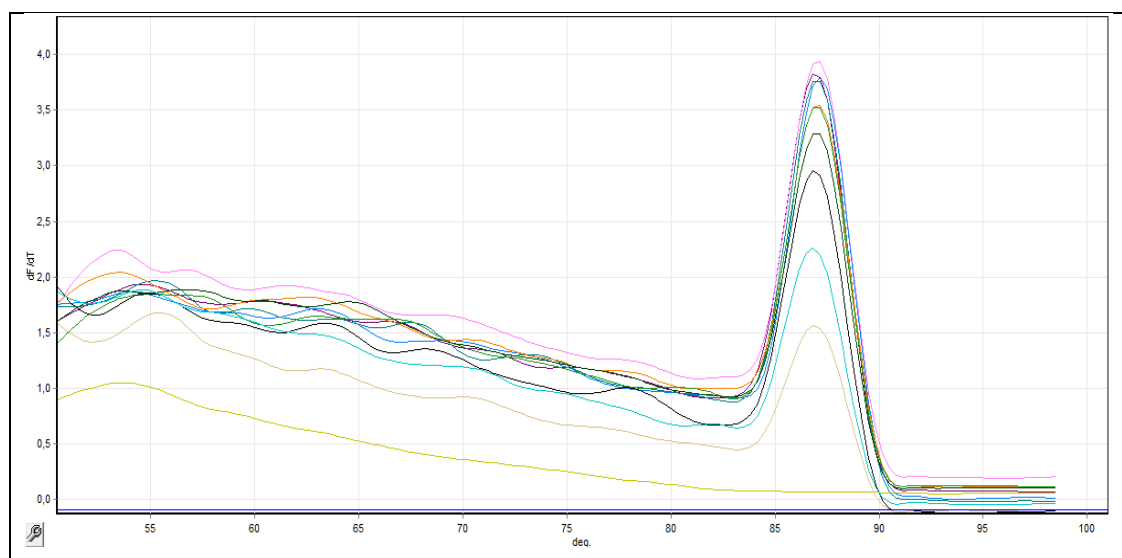


**Figure 31:** The melt curve of RANK amplicons (yellow line: Non-template control).

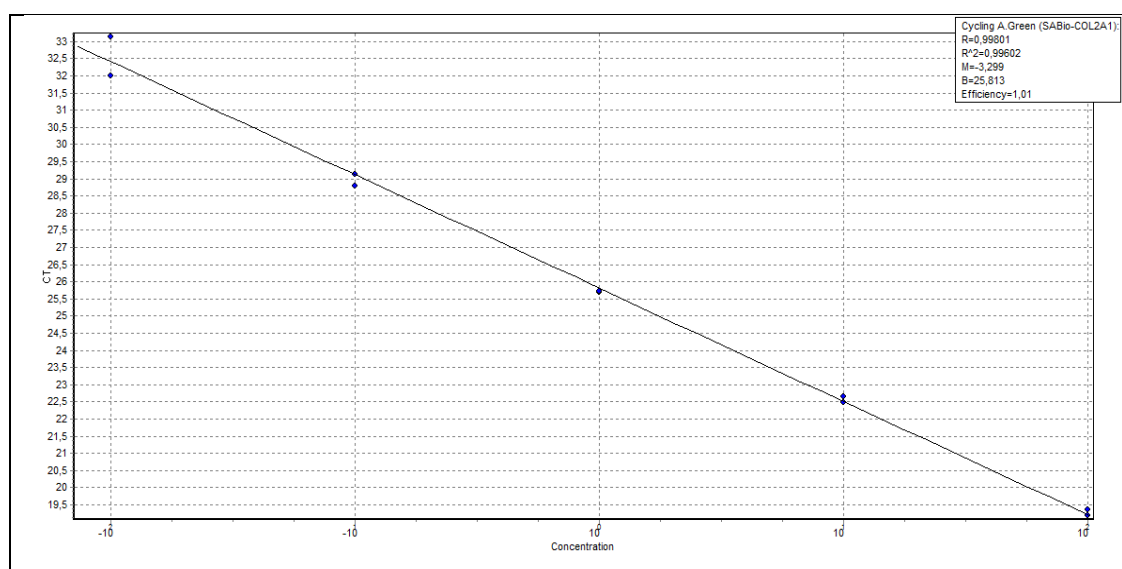


**Figure 32:** The standard curve of RANK primer.



### ***GAPDH Primer***

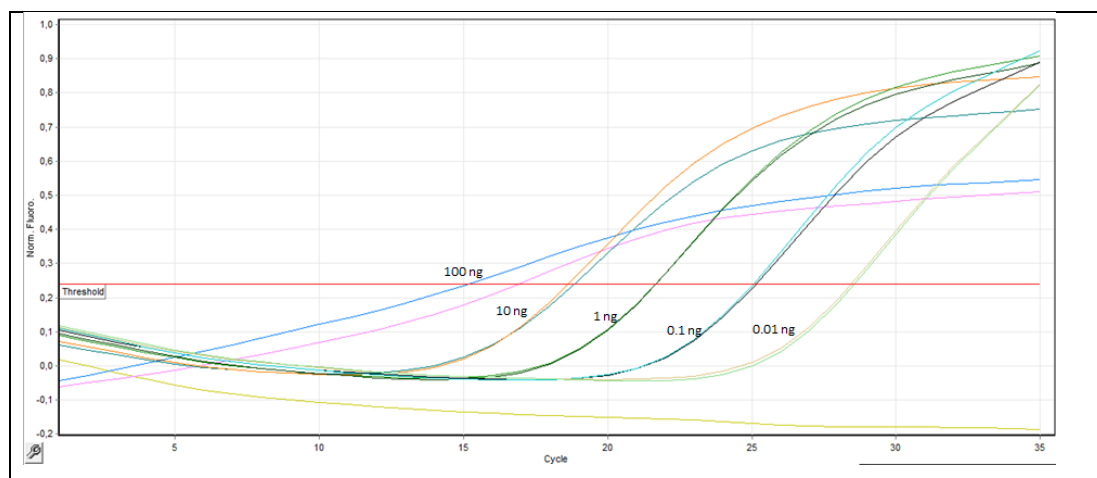


**Figure 33:** The amplification of GAPDH amplicons (yellow line: Non-template control).

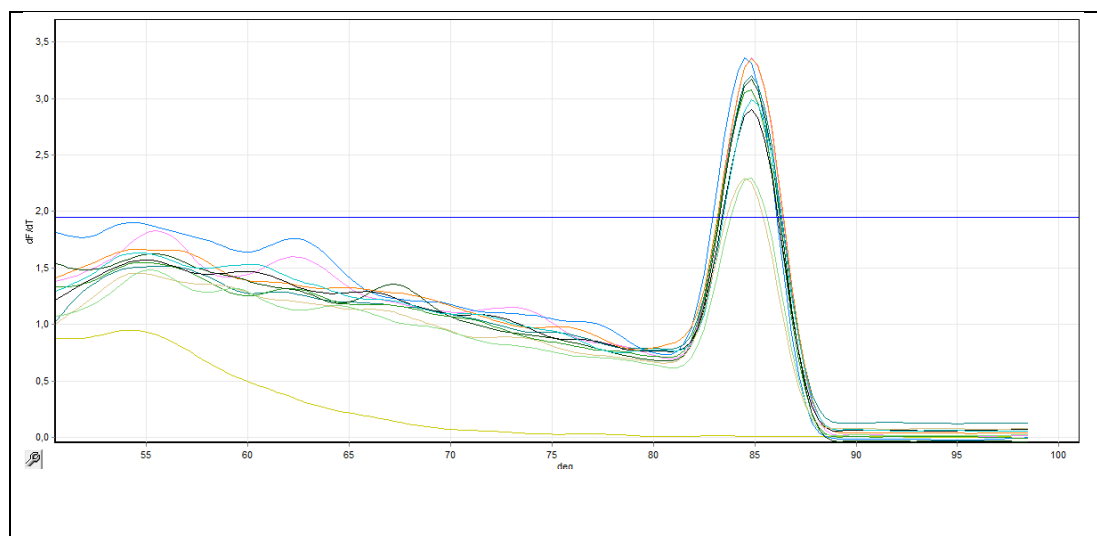


**Figure 34:** The melt curve of GAPDH amplicons (yellow line: Non-template control).

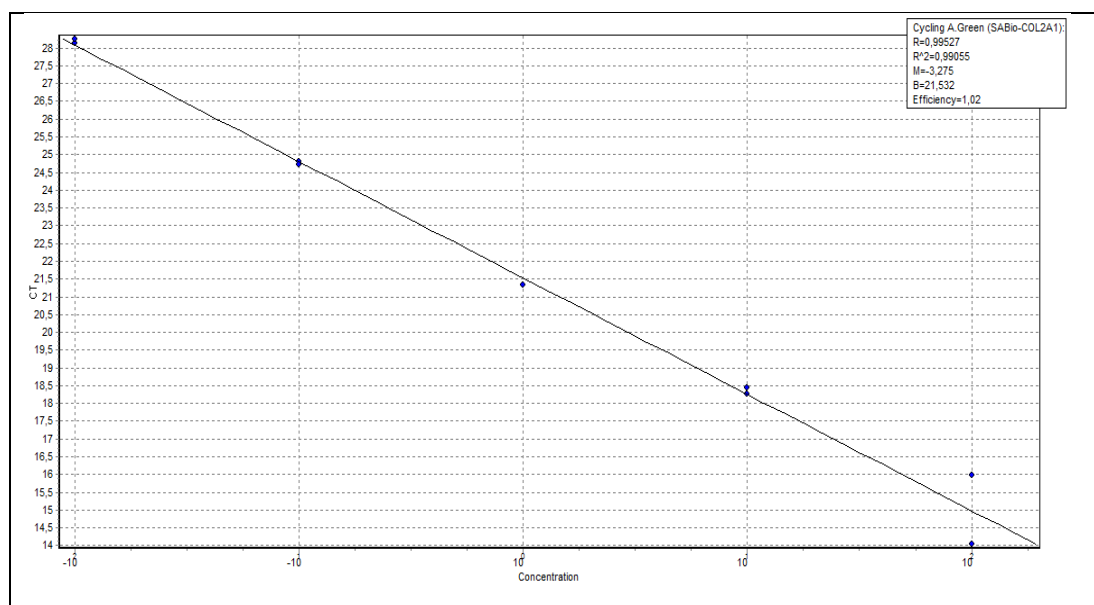


**Figure 35:** The standard curve of GAPDH primer.

The PCR products were also checked with agarose gel electrophoresis (Figure 36). Products around expected sizes were observed. The amplicon sizes of RANK and GAPDH are represented in Table 2.

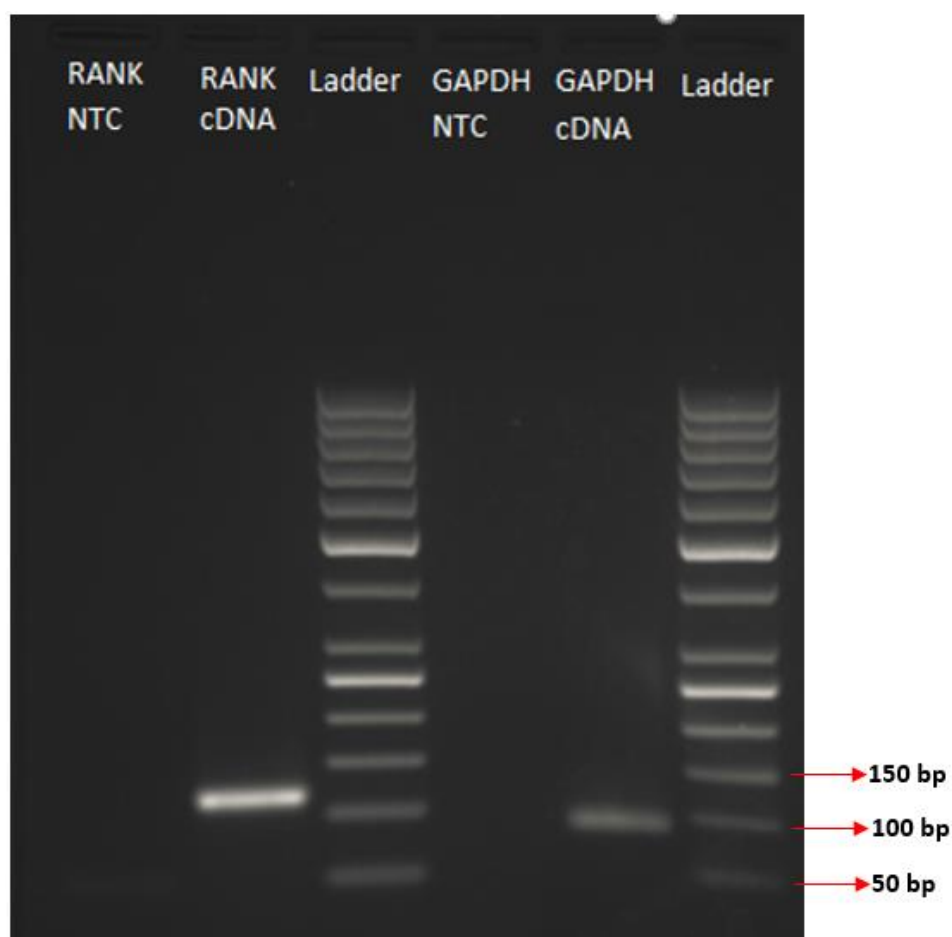


**Figure 36:** Agarose gel electrophoresis of PCR products. NTC: non-template control

The isolated RNA samples were also checked for DNA contamination via PCR without using reverse transcriptase enzyme and no product was observed (Figure 37 and Figure 38).

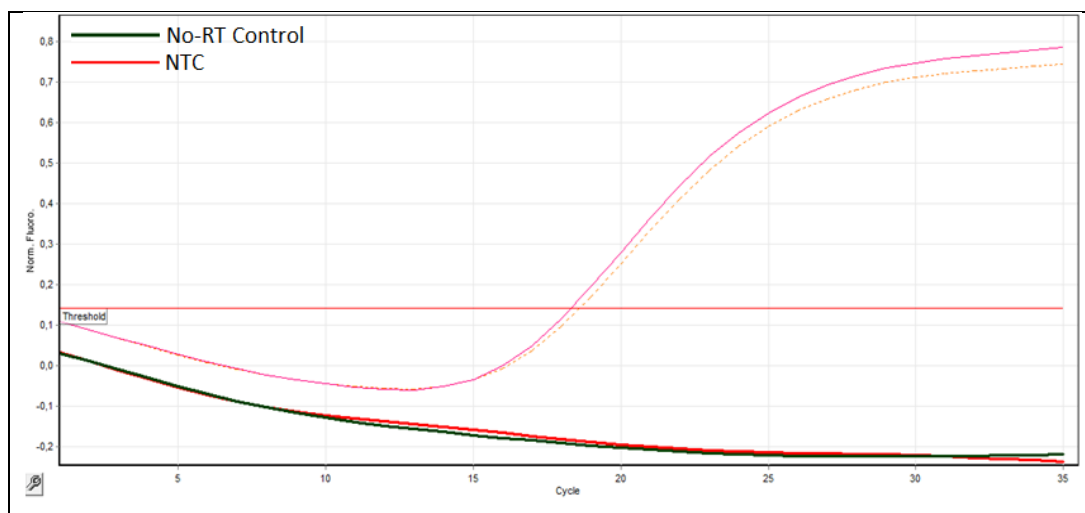


**Figure 37:** Amplification of DNaseI treated RNA sample (No-RT control) and NTC (No-Template Control). No amplification was observed in No-RT and NTC.

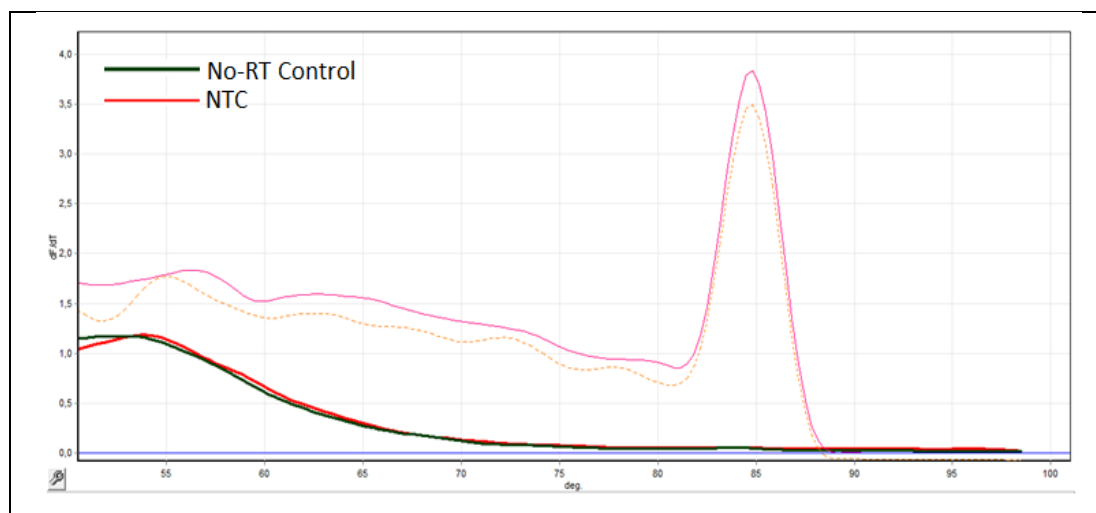


**Figure 38:** Melt Curves of No-RT control or NTC. Melt curves did not indicate any product since there was no amplification during PCR.

## APPENDIX B

### RAW 264.7 PRE-OSTEOCLAST CELL LINE ALAMAR BLUE CALIBRATION CURVE

Cell Number	Percent Reduced
10000	0.463
25000	3.227
50000	9.027
75000	14.959
100000	19.487
250000	46.697

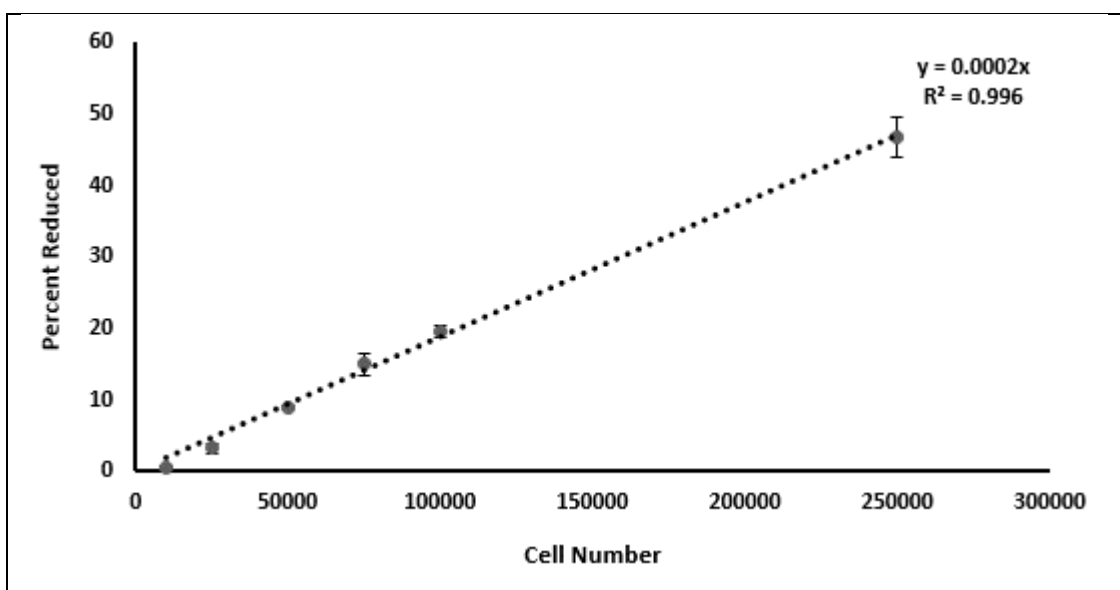


**Figure 39:** Alamar Blue calibration curve of RAW264.7 preosteoclast cell line.



## APPENDIX C

### PEI:FAM-LABELLED DNAOLIGO FLUORESCENCE INTENSITY CALIBRATION CURVE

DNAoligo ( $\mu\text{g}$ )	Average FI
0.8	214.28
0.6	157.08
0.4	124.77
0.2	46.65
0.1	22.07
0	0.00

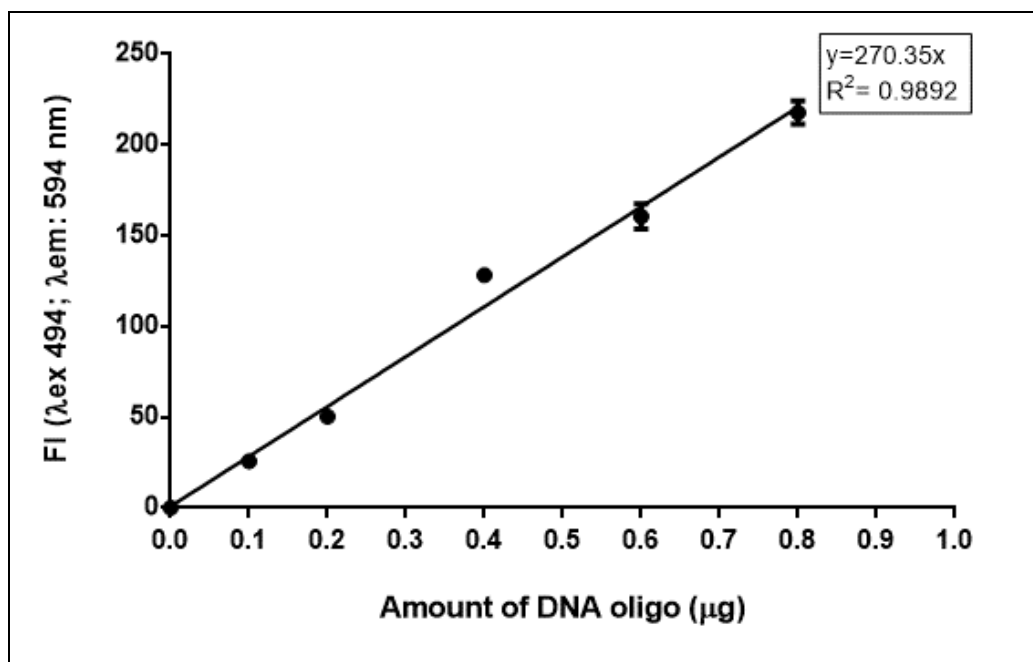


**Figure 40:** Calibration curve of PEI:FAM labelled DNAoligo complex





## CURRICULUM VITAE

### PERSONAL INFORMATION

Surname, Name: Sezlev Bilecen, Deniz  
Nationality: Turkish (T.C.)  
Date and Place of Birth: 01 October 1985, Ankara  
Marital Status: Married  
Phone: +905418275800  
Email: dsezlev@gmail.com

### EDUCATION

Degree	Institution	Year of Graduation
MS	METU, Biological Sciences	2012
BS	Hacettepe University, Biology	2008
High School	Nermin Mehmet Cekic Anatolian High School	2002

### WORK EXPERIENCE

Year	Place	Enrollment
2007	Biochemistry and Hormone Laboratory, Bilgi Hospital, Ankara, Turkey	Intern
2006	Involved in a field survey of Caretta caretta in Dalyan, Turkey	Intern

### FOREIGN LANGUAGES

English (Fluent)  
French (Basic)

## **PUBLICATIONS**

- 1) Sezlev Bilecen D., Uludag H., Hasirci V. Development of PEI-RANK siRNA Complex Loaded PLGA Nanocapsules for the Treatment of Osteoporosis. Tissue Engineering Part A. 2018.
- 2) Sezlev Bilecen D, Rodriguez-Cabello JC, Uludag H, Hasirci V. Construction of a PLGA based, targeted siRNA delivery system for treatment of osteoporosis. Journal of Biomaterials Science, Polymer Edition. 2017;28:1859-73.
- 3) Sezlev Bilecen D, Ak M, Yanik T. Dysregulation of hypothalamic modulation in olanzapine treated male rats. Progress in Neuro-Psychopharmacology and Biological Psychiatry. 2016;71:103-7.
- 4) Ak M, Sezlev D, Sutçigil L, Akarsu S, Özgen F, Yanik T. The investigation of leptin and hypothalamic neuropeptides role in first attack psychotic male patients: olanzapine monotherapy. Psychoneuroendocrinology. 2013;38:341-7.

## **POSTERS AND PRESENTATIONS**

- 1) Sezlev Bilecen D., Uludag H., Hasirci H. (2015). Use of Hydroxyapatite Specific Elastin-like Polypeptide in Targeting of PLGA Nanocapsules to Bone Tissue. (Poster Presentation in BIOMED 2015).
- 2) Sezlev Bilecen D., Rodriguez-Cabello JC, Uludag H, Hasirci V. (2017) Targeted Delivery of PEI:DNAoligo Complexes with PLGA Nanocapsules to Bone Tissue (Oral Presentation in BIOMED 2017).